SPACE SCIENCES LABORATORY

THE POSSIBLE EFFECTS OF LUNAR MASCONS ON LUNAR MAGNETIC AND ELECTROMAGNETIC EXPERIMENTS

By
W. E. Glenn, and S. H. Ward

Final Report on
NAS Contract NAS2-5078
Item 309A

June 1970

Space Sciences Laboratory Series 11 Issue 54
UNIVERSITY OF CALIFORNIA, BERKELEY

THE POSSIBLE EFFECTS OF LUNAR MASCONS ON LUNAR MAGNETIC AND ELECTROMAGNETIC EXPERIMENTS

By

W. E. Glenn
S. H. Ward

NASA Contract NAS2-5078

Final Report on Item 309A

Space Sciences Laboratory Series 11 Issue 54

June 1970

The Possible Effects of Lunar Mascons on Lunar Magnetic and Electromagnetic Experiments

by

W. E. Glenn
S. H. Ward

ABSTRACT

The electromagnetic and magnetic response of lunar mascons is studied. Electromagnetic models, including spherical, disk-shaped, and two-layered models, are examined for a range of values of the electromagnetic parameters, frequency, magnetic permeability, conductivity, and dielectric constant. The geometry and electromagnetic properties of the various models used were based on the shapes and geological properties of the gravity models proposed in the literature.

A two-dimensional Fourier analysis of the available gravity data for the near-side of the moon and Poisson's relation between gravity and magnetics are utilized to predict associated static magnetic fields of the lunar mascons for an assumed 10 γ interplanetary inducing field and for a range of magnetic susceptibilities compatible with the mascon geological materials proposed in the literature.

Using the results presented here, several electromagnetic and magnetometer experiments are discussed which could be used to determine, quantitatively and qualitatively, some of the geological and physical aspects of the lunar mascons.

ACKNOWLEDGEMENTS

We would like to express our thanks to Dr. P. M. Muller and Dr. W. L. Sjogren for making available to us their gravity data for the near side of the moon. The helpful discussions with Dr. W. I. Linlor and Mr. G. R. Jiracek are appreciated. Also we wish to thank our draughtswoman and typists for their invaluable assistance. This work was sponsored by NASA Contract NAS2-5078.

The Possible Effects of Lunar Mascons on Lunar Magnetic and Electromagnetic Experiments

by

W. E. Glenn
S. H. Ward

I. Introduction

Sill and Blank (1968) suggested that the presence of lunar mass concentrations, delineated from gravimetric measurements by Muller and Sjogren (1968), may significantly affect future magnetic measurements at or near the lunar surface. Ward (1968) proposed that a study be made of the electromagnetic response of these mascons in static and low-frequency magnetic fields and we have made this the object of our present study.

For the static case, Poisson's relation between gravity and magnetic potentials is utilized to predict a possible magnetic anomaly map of the near side of the moon. We have made the tacit assumption that the inducing field is a 10γ solar wind which is vertically incident, uniform and non time-varying. No remanent magnetization is considered. A range of magnetic permeabilities has been used to cover all probable material compositions of the disturbing masses.

The rigorous boundary value problems pertinent to the time-varying case either do not lend themselves to easy solutions or are impossible to solve. Using the various models of mascons that have been proposed in the literature we will investigate the electromagnetic scattering from: (1) a plane-layered, half-space model in a normally incident plane electromagnetic wave; (2) an infinitely-conductive, thin disk excited by a uniform, time-varying, normally-incident magnetic field and (3) a homogeneous, highly permeable sphere in a uniform, time varying magnetic field.

Models having various electromagnetic parameters, selected to be compatible with the respective gravity models, are examined in each case.

2. History of the Moon and its Bearing on Possible Origins of Lunar Mascons

2.1 Origin

Any theory proposed to date which attempts to explain the origin and subsequent development of the moon and, in particular, the earth-moon system has many inherent weaknesses. Although many hypotheses have been suggested in the literature, the current cycle of scientific opinion gives credence to the following three possibilities:

1. The moon was formed by the accumulation of solid particles in some orbit around the primitive sun removed from the earth and was later captured in a direct or retograde orbit by the earth;
2. The moon was formed by the accumulation of solid particles in the vicinity of the earth at about the same time as the earth's formation and;
3. The moon was spawned from a molten earth when the earth became dynamically unstable.

Any lunar hypotheses must account for: (1) The lower mean density of the moon relative to the earth which implies a different bulk composition for the moon; (2) The relatively uniform density which is in marked contrast with the earth's radially-dependent density; (3) The surface topography and geology of the moon; (4) The triaxial shape of the moon; (5) The presence of mascons which imply a rigid moon; (5) The orbital dynamics of the earth-moon system, and (7) The age of the lunar surface material. Of the three "Orgin of the Moon Postulates", listed above, the one which

presents fewest contradictions is the first one. It lends a certain continuity to the formation of not only the earth-moon system but also to the solar system. Urey (1968) and Baldwin (1968) among others have favoured this theory.

The present consensus of scientific opinion would seem to favour a moon formed by a similar process envisioned for the earth; that is, it formed cold by a coalensence of planetesimals at the time the solar nebula was being differentiated into the sun and the planets. Its initial temperature could not have been much above several hundred degrees Kelvin (Kopal, 1962) and its orbit was such that it was probably captured by the earth 1.75 billion years ago (Hibbs, 1967). Lyttleton (1967) discusses the conditions for moon capture. Urey et al. (1959) suggested the moon was formed by 10^4 to 10^5 objects of various sizes and densities. MacDonald (1965) revised the number to about 10^3. Gold (1956) suggests the moon's surface may illustrate how it was built up over time by the continual bombardment of interplanetary debris. A formation of the moon in this manner can easily explain the moon's shape, surface features, density, and any inhomogeneities such as mascons. Urey (1968) has indicated that the maria and the associated mascons are of meteoritic origin. He also suggests that there may be a layer of Fe-Ni accumulation in the moon's surface built up over time by the bombardment of metallic meteorites. The striking differences between the earth's surface and the moon's is easily explained by an absence of (1) an atmosphere or a hydrosphere and (2) large scale tectonism on the moon. The lower mean density of the moon can be attributed to its formation in a differentiated solar nebula. Numerous postulates on the formation of the solar system do argue credulously for differentiation

of the material that was the primordial solar matter. The fractionation found in meteorites, in the form of chondrules, and in the Widmanstaten figures of iron-nickle meteorites is good evidence for this process. Also, the inner, terrestrial planets show a higher concentration of heavier elements, notably iron, than do the outer planets. The moon, then, was formed in a part of the nebular cloud consistent with its mean composition. However, if the moon should be of the same mean composition as the earth then it must have an anomalous concentration of lighter substances such as carbon (10%) or water (2-3%), (Kopal, 1962).

Opik (1955, 1961), Ruskal (1960), MacDonald (1964) and Ringwood (1966), among others, have argued for the formation of the moon as part of the earth's formation either as a many-moon theory or as a coagulation of a sediment ring, a cloud of debris encircling the earth. The fission theory dates back to Darwin (1898) and although refuted by Jeffreys (1930) it has support in a modern approach to the same idea by Ringwood (1960), Wise (1963, 1969), Cameron (1963), and O'Keefe (1969). Although plausible, these latter two theories appear less attractive than the first one discussed and the interested reader may consult the cited references if more information is desired.

2.2 Thermal Considerations and Lunar Compositions

Presupposing a particular origin of the moon does not begin to simplify the many unanswered questions about the moon. To construct a geologic history of the moon and to predict its present geologic state requires an assumption of its composition. The radioactive element content which determines the heat generated within the moon is comcomitant with this

assumption. The tidal effects of the earth and sun, the surface bombardment by space debris and the solar wind, among others are factors that must be considered.

Choosing a composition for the moon is the most important initial assumption and several investigators, for example, have done this in order to construct thermal histories for the moon. Lee (1968) has examined both a chondritic moon and a terrestrial moon. His work, Kopal's (1966) and others suggest that the moon may not have melted throughout as has the earth but a partially molten interior past and/or present is most likely.

The moon should, initially at least, posses a heterogeniety inherent in its formation. The accumulation of numerous particles of various sizes and densities would ensure this, if they were not subsequently mixed by the melting of the moon. The discovery of mascons tends to substantiate this view. O'Leary et al. (1969) have shown that the apparent correlation of maria and mascons is not unique to the moon. Hence this phenomenon may belie the very formation of the planets by accumulation. Subsequent isostatic adjustments and igneous processes would soon dissipate any such inhomogeneities in the earth.

Nakamura and Latham (1969) have presented a most detailed analysis of the internal constitution of the moon. Among their many conclusions they state that "(1) There must be a concentration of lighter material near the surface of the moon, and (2) The deep interior of the moon is more likely to be chemically heterogeneous than to be homogeneous throughout, although the possibility of chemical homogeneity cannot be ruled out judging from the current range of uncertainty of the moment of inertia of the moon." They considered several models from homogeneous to two and three layer models.

They show that a liquid iron core and a 20Km basaltic crystal layer are compatible with the moment of inertia calculations.

Van Dorn (1969) considered a hypothetical thermal model for the moon, at the time of mare formation, comprised of a molten interior below 200 Km overlain by a 100 Km eclogite plastic layer wherein the temperatures were low enough and the pressures high enough to inhibit phase transition to basalt and a 50 Km elastic basalt layer warm enough to permit slow recrystallization by diffusion and a 50 Km unconsolidated, low density, basaltic surface layer thoroughly turned into rubble by an extensive impact history. He states that his model is compatible with those of Anderson and Phinney (1967) and Levin (1966). It also appears compatible with the work of Nakamura and Latham (1969).

Kovach and Anderson (1965) have concluded that the moon must differ in composition from the earth but can have a metallic core constituting as much as 8.5% of its total mass. Internal melting and differentiation in the moon have been postulated by Fricker et al. (1967), MacDonald (1963), Lowman (1963) and others. Kopal (1962) suggests that convection within an internally melted moon may have occurred and indicates that small craters of the Claires or Schichard type, or that the small circular maria such Mares Crisium or Humorum, may be relic surface expressions of the tops of convection cells.

Hence, either with or without a composition similar to the earth, there is substantial mathematical basis that both supports and precludes a melted moon and/or radial differentiation. Whether differentiation processes have been operative on the moon or are now taking place is crucial to the argument for ingneous processes giving rise to mascons.

2.3 Igneous Processes in Support of Mascon Theories

The surface geological evidence supporting igneous activity on the moon and subsequently explaining mascons as a result is essentially the flatness of the maria, the "basaltic" composition of the surface material (Turkevich et al., 1967, 1968; Gault et al. 1968), the presence of calderas on the moon's surface (Smith, 1966; Shoemaker, 1962; Baldwin, 1963; and others), and the igneous aspect of many of the rock samples returned by Apollo II (The Lunar Sample Preliminary Examination Team (I), 1969).

The flatness of the maria has led many, headed by Baldwin (1963, 1968) to suggest that lava flows have filled the maria. Hence the mascons could be a concentration of lava in crater bottoms (Baldwin, 1968) or a result of a differentiated igneous crust (Kaula, 1969). Urey (1960, 1965) has always opposed the idea of a melted moon and any large scale lave flows out onto the surface. Muller and Sjogren (1969) believe, on the basis of work by Kaula (1969) and Urey (1968), among others, that the mascons are incompatible with any simple lava flows into and out of the ringed seas. They envision a need for a more complex multiple-step process to produce mascons by large scale lava flows. Using the work of Conel and Holstrum (1968) as a basis, Kaula (1969) gives a thickness for the differentiated crust as 25 Km, and a density differential of 0.5 gm/cc. This density is compatible with Baldwin's (1968) density differential of 0.4 gm/cc but both ideas would require a moon which has heated up to produce magmas at the present time or sometime in the past. Some thermal models may preclude this. Lee (1968) states that if the moon's initial temperature had been 0°C the moon would never have heated to the fusion curve of basalt and as a result would not have fractionated. He also shows that for an unfractionated

moon the present temperature would be 600°C lower than for a fractionated moon.

Stipe (1968) also suggests a magmatic origin for the mascons but his hypothesis is that the magma was generated by pressure releases at depth due to penetrations of iron-nickel meteorites to depths as great as 450-670 Km for Mare Imbrium. Although he bases his calculations on his experimental work of shooting steel balls into concrete he may be overextending his extrapolation. Van Dorn (1969, p. 693) has a similar idea: "The lunar maria are considered to have evolved as homogeneous, transient, gravity-wave systems from larger impact craters on a crustal layer 50 Km. thick, fluidized from beneath by prompt, shock-induced melting inside an initially hot moon". The mathematical consistency of his observations gives considerable merit to his conclusions.

Igneous activity has been used to explain the origin of various other surface phenomena on the moon.

Karlstrom et al. (1967) suggest that rilles and ridges are evidence of crustal stretching and radial compression or folding, or the rise of magma along fractures. Domes are presumed to be laccoliths. The ideas of Baldwin (1963) and Kopal (1962) would tend to support this hypothesis. Cameron (1964) suggests sinuous rilles such as Schroters Valley were eroded by nuee ardentes. However, a cause other than igneous activity has been cited to explain these features. For example, Gilvarry (1964) and Lingenfelter et al. (1968) explain rilles as river erosion. Lunar domes may be lunar "hydrolaccoliths",(Kopal, 1962) or the result of mineral phase changes or the result of outgassing of the moon, (Baldwin, 1963), (Kuiper, 1966).

Although igneous activity on the moon draws considerable support from the scientific community there are a few who support it with some reservation, (Urey, 1960, 1965), (Kaula, 1968). They feel it is difficult to accept the idea of volcanism in a small body such as the moon. Craters that are thought to be volcanic may be collapse structures formed by the gradual withdrawal of water due to outgassing of the moon (Kuiper, 1966). Oberbeck and Quaide (1967) and Gold (1956) submit hypotheses of crater formation which give rise to assorted morphologies that do not require volcanism. Gilvarry (1964) suggests that crater morphology indicates the former presence of water on the moon's surface.

O'Keefe and Cammeron (1962), Cammeron (1964), Karlstrom et al. (1967), Kuiper (1959), Baldwin (1963), Kaula (1969), El-Baz (1970), and many more argue in favour of volcanism on the moon. O'Keefe and Adams (1965) have suggested the source of tektites may be lunar volcanic activity. The low gravity of the moon would permit ejecta to escape the moon and be captured by the earth.

2.4 Other Mascon Theories

Gilvarry (1960, 1964) has proposed that the flat maria and various other surface phenomena owe their character to the erosional force of water on the moon and that the mascons are simply isostatically uncompensated sediments lying in maria basins (Gilvarry, 1969).

Urey (1968) postulated a meteorite origin for the mascons. Urey (1967) has shown a suitable mechanism for mass concentrations to form in the circular maria and his discussion (Urey, 1968) as the their composition is compatible with this idea.

Alternatively it may be that volcanic flows triggered by meteorite impact are the cause of the mass concentrations as has been suggested by Stipe (1968) and Van Dorn (1969).

2.5 Discussion and Summary

It becomes apparent from the previous discussions that if one wishes to favour a particular hypothesis for explaining the lunar surface features and interpreting past events on the moon he may find much circumstantial evidence to support his theory and that the same evidence may be used to sustain more than one theory.

It seems reasonable to believe that the lunar surface is very old and may date back to the early stages of the formation of the solar system, for the age determinations on several Apollo II samples yielded dates of 3×10^9 to 4×10^9 years (Lunar Sample Preliminary Examination Team (1), 1969). It is felt that the dates may even be lower than the true values. The mascons, significantly, seem to be intimately related to existence of the circular maria on the moon and may have been formed as a direct result, or certainly in conjunction with, the maria formation. Apparently then, one could be justified in saying that the large mass concentrations have been in existence within the moon's crust for most of the moon's history. This implies that the moon has not been molten or even sufficiently plastic over this time to allow isostatic adjustments to occur, a conclusion also reached by Kopal (1962), Caputo (1965) and Urey (1968). This fact would preclude tectonism and volcanism on the scale witnessed on the earth.

Gilvarry's (1969) idea of having uncompensated aqueous sediment filling the maria may be generalized to say that, given any other erosional

and depositional mechanism on the moon, the mascons could be any kind of sediments. Such other processes have been proposed by Gold (1956) and others but it is difficult to accept that any sedimentary process, other than mass transport by water, could result in such a levelling of the maria floors.

The complex character of the breccia and the amount of glass found in the rocks and soil on the lunar surface (The Lunar Sample Preliminary Examination Team (1), 1969) suggests that much of the surface material of the moon may owe its origin to a mixture of impact debris and borken up lunar bedrock material. A long history of impacting on the surface could significantly "weather" the moon's surface and smooth it by infilling. It was pointed out earlier that this eveness of the maria bottoms has been cited as evidence that the material in the maria consisted of basalt flows. However, it is difficult to envision lava flows on such a large scale occurring on the moon. If flows occurred they must have been early in the moon's history, possibly in the later stages of cooling of an initially melted moon. The age of the mascons, coupled with the thermal histories postulated for the moon suggest that the moon may never have melted (Urey, 1968; O'Leary et al., 1969).

To sum up, the theories for the origin of the maria and consequently the mascons may be grouped into five postulates:

(1) the magmatic infilling of meteorite craters as a consequence of impact, or much later, or

(2) meteorite craters filled with lunar soil and/or meteorite material, or

(3) old sea floors, or

(4) crustal differentiates, or

(5) a complex combination of (1) and (2).

There is certainly much left to be learned before truly definite conclusions can be drawn about the origin of the moon and its unique characteristics. The exploration of the moon by the Apollo crews will certainly resolve many of the problems; yet, undoubtedly, it will reveal still further interesting enigmas to explain.

3. Ranges of Possible Physical Properties of Mascons

Lunar mass concentrations as delineated by the work of Muller and Sjogren (1968) appear to be localized mass excesses associated with the circular maria of the moon. Mascons proposed by Muller and Sjogren (1969) are listed in Table 1. The mascons associated with Mares Marginis and Orientale have since been discounted, Gottlieb et al. (1969). O'Leary et al. (1969), on the basis of a spherical harmonic analysis of the gravity data predicted further mascons, including a large one located on the backside of the moon, which they have proposed should be called Mare Occultum.

The lesser anomalies, between 4 and 50 milligals, do not correlate with visible surface features. No attempt, as yet, has been made to fit them into a pattern. Muller and Sjogren (1969) have confidence in their results for the area bounded by $\pm$ 50° latitude and $\pm$ 110° longitude and for anomaly values greater than 20 milligals, though the values are approximate.

When the results of Muller and Sjogren became known, several scientists suggested various physical models compatible both with intuition concerning the geological state of the moon and with the gravity data. The gravity models proposed for the mascons are shown in Table 2.

Any one or all of the proposed mascons could give rise to anomalies in surface magnetic or orbital electromagnetic experiments, depending upon the physical properties, size, and depth of each mascon. To assess the possible range of sizes of such magnetic and electromagnetic anomalies requires careful consideration of their possible origins. It is not our purpose to postulate physical models for the mascons but to use the ones proposed by others in the literature, and repeated in Table 2, to effect a choice of suitable magnetic and electromagnetic model parameters.

The gravity models are either based on basaltic or iron-nickel meteorite materials and the shapes vary from disks to spheres.

4. Selection of Models of Mascons

To predict the static field using Poisson's relation between gravity and magnetic fields requires no model but simply one of the field components defined over some surface. However, it is necessary to assume a range of magnetic susceptibilities. For iron meteorite material the relative magnetic permeability μ/μ_o might range as high as 100 (Ward, 1968), whereas for materials of basaltic composition it may be as low as 1.001. In light of the measurements made on the Apollo 11 samples (The Lunar Sample Preliminary Examination Team (1), 1969), the range 1.1 to 1.5 may be most realistic. This range should ensure a coverage of all possible materials that may comprise the mascons. Admittedly the upper limit of the range is not too probable in reality, but it ensures that no reasonable possibilities will be overlooked.

The time-varying problems, if one were to try simply to predict the electromagnetic anomalies for the preferred gravity models, would nearly

all be impossible to solve given the present state of the art. However, we can begin by reducing each problem to a geometry that can be handled, while maintaining realism, and use boundary and inducing field conditions appropriate to each model which can be mathematically treated. The simplifying assumptions which will be made in each case will be justified and the consequence of these assumptions on the end results will be discussed with the purpose of interpolating a more accurate picture of the determined results.

If we assume a mascon was formed by a sphere of iron-nickel meteorite (Muller and Sjogren, 1968; Stipe, 1968), its conductivity, relative magnetic permeability, and dielectric constant would reasonably be (Ward, 1968):

$$10^4 < \sigma < 10^7 \quad \text{mhos/m}$$

$$5 < \mu/\mu_0 < 100$$

$$\varepsilon \approx \varepsilon_0$$

Because the conductivity is high, one may neglect displacement currents and find the solution for a sphere in a non-dissipative whole space in which secondary fields are assumed to be zero. Since the conductivity of the lunar subsurface to depths of order 100 km, at zero frequency, is unlikely to be greater than 10^{-4} mhos/m (Ward, 1968), this solution should be a valid one. The resulting model would establish an upper limit on conductivity and magnetic permeability for a homogeneous spherical mascon. We can infer from the results the effects which will be generated by allowing the conductivity of the half-space to increase and, in particular, we may estimate the response when the parameters of the sphere approach those of the half space.

Conel and Holstrum (1968) and Kane (1969) have concluded that plate models best fit the gravity data of Muller and Sjogren (1968). We have developed the theory of Ward et al. (1968) for magnetic the field scattered from an infinitely conductive, thin disk in a uniform time-varying magnetic field, in a non-reacting whole space. The disk-shaped mascons of Urey (1968) composed of Fe-Ni meteorite or H-type meteorite material which have thickness-diameter ratios less than 0.04 and may have conductivities as high as 10 mhos/m should be suited to the infinitely conductive, thin disk approximation. The disks of Conel and Holstrum (1968), however, are composed of basaltic material and the approximation discussed above would no longer pertain. However, using suggestions made by Ward et al. (1968) we may suitably predict fields for finitely conductive disks and, as with the sphere, we may interpolate the effects on the fields due to a dissipative half-space. In a further approach to the disk models, we treat them, locally, as a layered half-space. The disk radii may be as large as 300 km for Serenitatis (Conel and Holstrum, 1968) and if one is close to the moon's surface, (relative to the diameter of the mascon) a half-space approximation should hold near the center of the disk. This approach should give us an intuitive understanding for field changes due to changing values of conductivity, relative permeability and dielectric constant.

In Table 3 we list the mascon models selected for study and the various electromagnetic parameters attached to them. The electromagnetic parameters are based on figures given in Ward, Jiracek and Linlor (1968, 1969), Ward, (1969) and Jiracek and Ward (1970).

5. Static Magnetic Field Anomalies

5.1 Introduction

A contoured gravity map of the terrestrial side of the moon has been obtained by Muller and Sjogren (1969). This map shows that the gravity anomalies are associated with the circular maria of the moon. The area covered by this map is between latitudes $\pm$ 50° and longitudes $\pm$ 110°. In this area there are 13 mascons yielding anomalies of more than 20 mgals correlated with circular maria.

Mathematically the static magnetic field anomaly of a body with certain magnetization is proportional to the first order directional derivative of the gravity field anomaly of that body. The directional derivative is taken along the direction of magnetization of that body. This relationship has been known since Poisson's time. This mathematical operation has been applied to three of the thirteen mascons (Serenitatis, Crisium, and Nectaris) to compute the range of magnetic anomalies, which we would expect to find associated with these mascons, under various assumptions of the contrast in density and susceptibility between mascon and the remainder of the moon.

5.2 The Lunar Gravity Data

The gravipotential map of the lunar nearside presented by Muller and Sjogren (1968) is actually a map of the normalized spacecraft acceleration in the spacecraft-earth direction. Muller and Sjogren (1968) explained the procedures of obtaining the gravity map in detail.

The Lunar Orbiter V spacecraft was tracked by the Deep Space Network with an earth-based radio transmission at 2300 Mhz. The shift (in terms of mm/sec.) between the transmitted and received signal is accumulated in a

doppler cycle counter and sampled every minute, every 30-seconds, or every 10 seconds. The raw data covers ± 100° in longitude and from pole to pole in latitude.

The Lunar Orbiter spacecraft was tracked continuously for 80 consecutive orbits in a 10-day period. The orbit of the spacecraft has the following characteristics: semimajor axis 2636 Km, eccentricity 0.27, inclination to the lunar equator, 85° and orbital period of the spacecraft 3 hrs. 11 min. The closest approach to the lunar surface was 100 km at 2° N latitude.

The raw doppler data were then processed through the following steps: (a) The doppler shift caused by the primary motions was substracted from the raw data by using least square fitting techniques. The primary motion includes the motions of the earth, the moon, and any planetary perturbations. (b) The residuals were then fitted to a smooth curve which could be differentiated to provide line-of-sight accelerations. These acceleration data contain the local gravity effects. (c) The acceleration data were then normalized to a constant elevation above the lunar surface; 100 km was chosen as a normalized altitude. Under the assumption that the typical mascons were at a depth of 50 km below the surface, a normalization formula has been used (after Muller and Sjogren, 1968).

$$A_n = A_c (H + 50)^2 / (150)^2 \qquad 5\text{-}1$$

Where An is the normalized acceleration, A_c is the computed acceleration, and H is the local orbital altitude in kilometers. (d) The normalized acceleration data were then coded and countured on a Mercator projection of the lunar earthside hemisphere.

5.3 Poisson's Relation Between Gravity and Magnetostatic Field Anomalies

Since a gravity field is conservative it is derivable from a scalar potential. For a point mass m, the gravity field is

$$\vec{F} = -G\frac{M}{|\vec{r}|^3}\vec{r} = -\nabla\phi \qquad 5\text{-}2$$

where G is the universal constant of gravitation and has the value of 6.67×10^{-8}, $\vec{r}$ is the position vector from the point mass to a unit testing mass, and ϕ is a scalar gravity potential. Equation 5-2 can be written as

$$\phi = -G\frac{m}{r} \qquad 5\text{-}3$$

If the material is a uniformly distributed mass with density ρ, then the gravity potential exterior to the mass is

$$\phi' = -\int_M G\frac{dm}{|\vec{r}-\vec{r}_o|} = -\int_V \frac{G\rho\, dv}{|\vec{r}-\vec{r}_o|} \qquad 5\text{-}4$$

where $\vec{r}$ and $\vec{r}_o$ are the position vectors of an observation point and of an element of mass respectively. V is the volume of the mass distribution and d_v is an element of volume.

Similarly, the magnetostatic field can be written as the gradient of a scalar magnetic potential

$$\vec{H} = -\nabla\Psi \qquad 5\text{-}5$$

where ψ is a scalar magnetic potential of a magnetic dipole. Following Grant and West (1965), p. 213

$$\psi = -\bar{X} \cdot \nabla\left(\frac{1}{r}\right) \qquad 5\text{-}6$$

in which $\bar{X}$ is the magnetization vector, defined by

$$\bar{X} = k_m \vec{H}_o \cdot \hat{a} \qquad 5\text{-}7$$

where $\vec{H}_o$ is the primary magnetostatic field, and $\hat{a}$ is a unit vector in the direction of magnetization, and k_m is the magnetic susceptibility of the magnetized material. If we assume that $\vec{H}_o$ and $\hat{a}$ are in the same direction then

$$\bar{X} = k_m H_o \hat{a} \qquad 5\text{-}8$$

Hence (5-6) can be written as

$$\psi = -k_m H_o \hat{a} \cdot \nabla\left(\frac{1}{r}\right) \qquad 5\text{-}9$$

and the magnetic potential of a body with uniformly distributed magnetic dipoles is

$$\psi' = -\int_v k_m H_o \hat{a} \cdot \nabla\left(\frac{1}{|\bar{r}-\bar{r}_o|}\right) dv$$

$$= -k_m H_o \hat{a} \cdot \nabla \int_v \frac{1}{(\bar{r}-\bar{r}_o)} dv \qquad 5\text{-}10$$

From 5-4 and 5-10 we find

$$\psi' = \frac{k_m H_o}{G\rho}\,\hat{a}\cdot\nabla\phi' = \frac{k_m H_o}{G\rho}\,\frac{\partial}{\partial\hat{a}}(\phi') \qquad 5\text{-}11$$

Differentiating 5-11 with respect to Z

$$\frac{\partial\psi'}{\partial z} = H_z = \frac{k_m H_o}{G\rho}\,\frac{\partial}{\partial z}\frac{\partial}{\partial\hat{a}}(\phi') \qquad 5\text{-}12$$

$$= \frac{k_m H_o}{\rho G}\,\frac{\partial}{\partial\hat{a}}(\Delta g)$$

where H_z is the vertical component of the magnetic field, and Δg is the vertical component of the gravity field, which is usually called the gravity anomaly.

In this study we shall assume for simplicity that the direction of magnetization of the mascon material is vertical, then

$$H_z = \frac{k_m H_o}{G\rho}\,\frac{\partial}{\partial z}(\Delta g) \qquad 5\text{-}13$$

From equation 5-13 we can calculate a magnetic anomaly from the gravity anomaly and this calculation is simplified by using Fourier Transform techniques.

5.4 Fourier Transformation and its Application to this Problem

We know from basic Fourier Transform theory that a differentiation in the space domain becomes a simple multiplication in the frequency domain

(e.g. Bracewell, 1965). When we Fourier transform 5-13, we obtain

$$H_z' = \frac{k_m H_c}{G\rho} (-j 2\pi k_z) (\Delta G') \qquad 5\text{-}14$$

where H_z' and $\Delta G'$ are the Fourier transformations of H_z and Δg respectively. K_z is the frequency in the vertical, Z, direction and $j = \sqrt{-1}$.

In a region without sources we find,

$$\nabla^2 (\Delta g) = 0 \qquad 5\text{-}15$$

Upon Fourier transforming 5-15 to the frequency domain, we obtain

$$4\pi^2 (k_x^2 + k_y^2 + k_z^2) \Delta G' = 0 \qquad 5\text{-}16$$

Hence

$$-(k_x^2 + k_y^2) = k_z^2 \qquad 5\text{-}17$$

or

$$k_z = \pm j (k_x^2 + k_y^2)^{1/2} \qquad 5\text{-}18$$

where K_x and K_y are the frequency spectra in the x and y directions respectively.

Substituting 5-18 into 5-14 we obtain

$$H_z' = \frac{k_m \vec{H}_o}{G\rho} (\pm) 2\pi (k_x^2 + k_y^2)^{1/2} (\Delta G') \qquad 5\text{-}19$$

Signs in 5-19 are determined by the direction of $\vec{H}_o$. If $\vec{H}_o$ has the same direction as the gravity field (vertically downward) the plus sign is used or, if oppositely directed, the minus sign is used.

The gravity data of these mascons (Crisium, Nectaris, and Serenitatis) have been selected from the coded gravity map obtained by Muller and Sjogren (1969), Figure 1. In order to avoid the influence of any nearby mascons we have chosen 16 x 16 data points for each mascon. Figures 2, 3, and 4 show the countoured raw gravity map of Crisium, Serenitatis, and Nectaris mascons, respectively.

The edges of each gravity map have been smoothed by a Hanning smoothing function. Hence the error introduced by data truncation is reduced. The smoothed gravity data of these mascons are shown in Figures 5, 6, and 7.

The smoothed gravity data were then operated on using a computer program developed on the basis of the Fast Fourier Transform Algorithm of Cooley and Tukey (1965). $\vec{H}_o$ in 5-19 is assumed to be a z-directed uniform constant magnetic field which we assume is an interplanetary field of approximately 10γ, ($1\gamma = 10^{-5}$ Oersted). The relative susceptibilities and densities of the mascons used are shown in Table 4 (assume $k_m = 0$, and $\rho = 2.60$ gm/c.c. for the lunar surface material).

After performing the calculation of 5-19 on the gravity data in the frequency domain we inverse transform H_z' to H_z in the space domain.

5.5 The High Frequency Noise Effect

Figure 8 shows the magnetic field anomaly, transformed directly from the smoothed gravity field anomaly of the Crisium mascon by assuming that $H_o = 10\,\gamma$, $k_m = 1.00$, and $\Delta\rho = 2.60$ gm/cc. We can see that the magnetic field is dominated by a lot of high frequency noise. It does not look like a dipole field, as a uniform $\vec{H}$ magnetization body should have. Obviously the magnetic field shown in Figure 8 is due to topographic variation, some small bodies buried at shallow depth, and also the noise introduced by digitizing.

A low-pass two-dimensional rectangular filter with filter bandwidth equal to 2/5 of the total frequency band is applied to the smoothed gravity data. Figure 9 shows the smoothed and filtered gravity anomaly of the Crisium mascon. The magnetic field anomaly, transformed from the smoothed and filtered gravity data, is shown in Figure 10. A clear dipole pattern is shown.

5.6 Results

Five models with relative susceptibility and density shown in section 5.5 have been set up for each mascon. Figures 10, 11, and 12 are the contoured magnetic field anomaly of Crisium, Serenitatis, and Nectaris mascons respectively with $k_m = 1.0$ and $\Delta\rho = 2.60$ gm/cc. Both the susceptibility and the density of a mascon will affect the amplitude of its magnetic anomaly, however the field pattern would not be changed by a different choice of susceptibility or density. Figure 13 contains plots of the peak magnetic field anomaly, in gammas, of Crisium, Serenitatis, and Nectaris mascons versus the ratio $k_m/\Delta\rho$, which is a linear factor in equation 5-19. From Figure

13 we can see the slope of the curve depends on the gravity anomaly of the mascon.

5.7 Discussion

As described above, the magnetic field anomaly of three mascons have been predicted for an elevation of 100 km above the lunar surface. If we assume that the mascon is a spherical body with radius 50 km and with its center buried 50 km below the lunar surface then we would expect a magnetic anomaly on the lunar surface with amplitude 27 times the values shown in Figure 12.

The position of the magnetic peak may be correlated to the gravity high for each mascon, as expected. The magnetic field is obtained by taking the first order vertical derivative of the gravity field so that the sign of the magnetic field should change when the gravity field changes sign. The negative gravity anomalies shown in Figures 5, 6, and 7 are related to the datum on the gravity anomaly data. If we change the datum to assure a positive gravity anomaly everywhere then the negative magnetic peaks would be eliminated and a more uniform negative magnetic anomaly surrounding the positive magnetic high would be expected. However, the magnetic anomaly depends upon the gradient of the gravity anomaly too.

If we assume that the mascons are composed of magnetite, we could expect to measure a magnetic field strength of about 0.82 γ for Serenitatis, 0.66 γ for Nectaris, and 0.58 γ for Crisium at an elevation of 100 km above the lunar surface.

The assumption that the density of the lunar surface material equals 2.60 gm/cc. is quite arbitrary. But the density contrasts between the

mascons and the surrounding medium, $\Delta\rho$, are based on the suggestions made by Urey (1968), Baldwin (1968) etc.

6. Reflection from a Plane-Layered Lunar Mascon Model

6.1 Introduction

We shall examine two-layered lunar models in which the first layer is presumed to be the mascon and the second layer is assumed to be a homogeneous moon composed of some "dry" rock for all models. The object is to investigate the reflections of electromagnetic waves from mascon materials suggested by Urey (1968) and Conel and Holstrum (1968).

The theory developed by Jiracek and Ward (1970) is used to obtain the reflection coefficient and phase for the various models chosen. The selection of the distribution of electromagnetic parameters in the moon for each model was based on curves which may be found in Ward, Jiracek and Linlor (1968, 1969), Ward (1969a) and Jiracek and Ward (1970). Variations of conductivity and dielectric constant with frequency are used following Jiracek and Ward (1970). Also we shall only consider the case of normal incidence since the effects of changing angles of incidence and the direction of polarization are examined in detail in Jiracek and Ward (1970).

The plane layered model requires certain assumptions: (1) that the fields are observed at a point where the edge of the mascon has negligible effect; (2) that the wave-length in the media is much less than the curvature of the moon such that the planar model is a good representation of the real case; (3) that the two layers are homogeneous throughout such that no discrete scattering centers exist within the layers, and (4) that a surface debris

layer can be neglected without serious consequences. Hence we are using the simplest case for our study with respect to both the exciting field and the physical models.

6.2 Mathematical Basis

One can write for the amplitude reflection coefficient R, for normal incidence, from Ward et al. (1968) for example, as

$$R = (Z_a - Z_o) / (Z_a + Z_o) \qquad 6\text{-}1$$

where Z_o is the plane wave impedance of free space and where Z_a is the impedance of a layered structure. The reflection coefficient is, in general, complex and can be written in polar form

$$R = |R| e^{i\phi_R} \qquad 6\text{-}2$$

Using the recursive relation for impedance over an n-layered structure, Wait (1958), we can write the impedance Z_a for the two layered moon as

$$Z_a = Z_1 \frac{\hat{Z}_2 + Z_1 \tan \gamma_1 h_1}{Z_1 + \hat{Z}_2 \tan \gamma_1 h_1} , \qquad 6\text{-}3$$

in which

$$\hat{Z}_2 = i \mu_2 \omega / \gamma_2 , \qquad 6\text{-}4$$

and in which

$$\gamma_j^2 = i\omega\mu_j(\sigma_j + i\omega\varepsilon_j), \quad j = 0, 1, 2, \ldots \qquad 6\text{-}5$$

The subscript j refers to the layer considered. Upon substitution of the various parameters into equations 6-4 and 6-5, and using 6-1 and 6-3, the values for the reflection coefficient can be calculated.

6.3 Presentation of Results

Figures 14a through 21b show Cal Comp plots of the modulus and phase of the reflection coefficient for the eight layered mascon models detailed in Table 5.

The phase of the reflection coefficient should be relative to π but because of the nature of the computer library function all phase plots are relative to zero.

6.4 Discussion

The first five models are meant to represent the H-type or Fe-Ni meteorite mascons proposed by Urey (1968) and the last three models are for the basaltic mascons proposed by Conel and Holstrum (1968).

The mascon models of Urey (1968) were given relatively high values of conductivity because the conductivity of iron and nickel is high and, as expected, the reflected coefficients are near unity for the lower frequencies examined and they decrease at the higher frequencies (Figures 14-19). The basaltic mascons, having a much lower conductivity, have reflection coefficient of 0.5 or less and show little variation with frequency.

An increase in magnetic permeability will cause a decrease in $|R|$ for $\mu/\mu_0 < \varepsilon/\varepsilon_0$ at normal incidence (Jiracek and Ward, 1970). This effect is noticeable between models 4 and 5 and between models 6, 7, and 8 where the only parameter change is magnetic permeability. In the other models, where the magnetic permeability also changes, the lowering effect is masked, at the higher frequecies, by an increased conductivity which tends to increase $|R|$. This effect is particularly noticeable between models 1 and 2. The significance of this effect is that if the moon is essentially homogeneous, with magnetic permeability variations expected, then one could conceivably map the magnetic variation of the lunar surface rocks. Whether the rock material is a conductor, or a lossy dielectric can be ascertained from the amplitude and phase curves.

For the first five models, where-in the conductivity is high and the reflection coefficient near unity, the phase, as expected, is near 180°. At the higher frequencies where the displacement currents begin to become significant and the mascon begins to behave as a lossy dielectric, the reflection coefficient decreases and the phase departs from 180°. The last three models behave in reverse fashion. At the lower frequencies the mascons appear to be lossy dielectrics with a phase near 180° but at the higher frequencies the displacement currents dominate and the phase approaches 180° as the medium begins to look like a lossless dielectric. Taken together, the phase and the modulus of the reflection coefficient can be diagnostic of the electromagnetic properties of layered mascon models but either one alone would be insufficient.

One consequence of a higher conductive layer at or near the lunar surface is that it would mask the layer or layers below. Skin depths would be much

less than the thickness of proposed gravity models such that little reflection could be expected from any underlying layer.

Layering can lead to oscillations in the curves of the modulus and phase of the reflection coefficient versus frequency as illustrated by Ward, Jiracek and Linlor (1968, 1969). Interference between surface and second layer reflections, for frequencies where the thickness of the first layer is one quarter the wave length of the field inside the medium, causes this oscillatory behaviour. For the basaltic mascon layers these oscillations would occur near 10^4 Hz but should be of small amplitude due to the large thicknesses assumed for the mascon layer. The calculated curves of reflection coefficient versus frequency, for these models, bear this out. The meteorite models examined are sufficiently conductive to mask the contribution from the second layer for the model depths chosen. Mascons of greater thickness but of similar conductivity would not completely inhibit detection of reflections from the second layer and one might expect to see oscillations in the phase and amplitude curves.

7. Electromagnetic Reflection from a Thin Disk Model of a Mascon

7.1 Introduction

The theoretical development of Ward et al. (1968) for the magnetic fields scattered by the thin disk in a natural field is modified slightly to model the electromagnetic characteristics of a thin-disk representation of a mascon. The electromagnetic properties of the mascon models have been selected to conform to the physical descriptions of disk-shaped mascons proposed by Urey (1968). The disk as treated in Ward et al. (1968) is assumed to be in a whole space and both the conductive and displacement currents

of the whole space are neglected. To justify this assumption, the conductivity of the disk must be appreciably higher than that of the whole space. Of course, the assurance of a realistic approximation would deteriorate as the conductivity of the disk approaches that of the main lunar bedrock. Hence the approach taken here could not be appropriately applied to disks of lesser conductivity such as would be the case if the disk models of Conel and Holstrum (1968) were studied.

7.2 Mathematical Basis

To simplify the mathematics (without detracting from the solution in any way) the exciting field is chosen to be a uniform, time-varying magnetic field, $H_o e^{-i\omega t}$ applied normal to the disk in the negative z direction (see Figure 22).

The object is to find the magnetic fields scattered by the disk. We shall utilize the Schelkunoff vector potential $\vec{G}$, arising in electric sources (Schelkunoff, 1943) from which the fields may be derived via

$$\vec{H} = \nabla \times \vec{G} \qquad 7\text{-}1$$

and

$$\vec{E} = i\mu\omega \vec{G} + \frac{1}{\sigma - i\varepsilon\omega} \nabla \cdot (\rho G) \qquad 7\text{-}2$$

Following the development of Ward et al. (1968) we can write for regions containing no sources

$$(\nabla^2 + k^2) G^2 = 0, \quad k^2 = \mu\varepsilon\omega + i\mu\sigma\omega, \qquad 7\text{-}3$$

which is the homogeneous vector wave equation applicable to the region occupied by the disk.

By neglecting displacement and conduction currents outside the disk, 7-3 becomes

$$\nabla^2 \vec{G} = 0 \qquad 7\text{-}4$$

for the region exterior to the disk.

It is intuitively obvious that a mgnetic field normally incident on a conductive disk will generate only a θ component of the electric field E (and therefore only a θ component of G according to 7-2). The equation for the cross-product in cylindrical co-ordinates is

$$\nabla \times \vec{A} = \hat{e}_r \left[\frac{1}{r} \frac{\partial A_z}{\partial \theta} - \frac{\partial A_\theta}{\partial z} \right] + \hat{e}_\theta \left[\frac{\partial A_r}{\partial z} - \frac{\partial A_z}{\partial r} \right] - \hat{e}_z \left[\frac{1}{r} \frac{\partial (r A_\theta)}{\partial r} - \frac{1}{r} \frac{\partial A_r}{\partial \theta} \right] \qquad 7\text{-}5$$

which becomes

$$\nabla \times \vec{G} = - \frac{\partial G_\theta}{\partial z} \hat{e}_r + \left[\frac{1}{r} \frac{\partial}{\partial r} (r G_\theta) \right] \hat{e}_z \qquad 7\text{-}6$$

Therefore 7-1 and 7-2 reduce to

$$\vec{H} = \frac{1}{r} \frac{\partial}{\partial r} (r G_\theta) \hat{e}_z - \frac{\partial G_\theta}{\partial z} \hat{e}_r \qquad 7\text{-}7$$

and

$$\vec{E} = i\mu\omega G_\theta \hat{e}_\theta \qquad 7\text{-}8$$

From Morse and Feshback (1953, p. 116) we can write for 7-4

$$\nabla^2 G_\theta = \frac{G_\theta}{r^2} \,, \qquad 7\text{-}9$$

or

$$\frac{1}{r}\frac{\partial}{\partial r}(r G_\theta^s) + \frac{\partial^2 G_\theta^s}{\partial z^2} = \frac{G_\theta^s}{r^2} \,, \qquad 7\text{-}10$$

in which G_θ^s is the secondary potential exterior to the disk. The uniform, inducing field has no gradient in the z-direction. Therefore, it may be derived from a primary potential

$$G_\theta^p = -\frac{H_0 r}{2} \qquad 7\text{-}11$$

In accordance with 7-7 the negative sign in 7-11 is introduced because the primary field is directed in the negative z direction.

Equation 7-10 has the solution

$$G_\theta^s = \int_0^\infty g(\lambda)\, e^{-\lambda|z|}\, J_1(\lambda r)\, d\lambda \,, \qquad 7\text{-}12$$

where $g(\lambda)$ is an eigenfunction to be evaluated via applying appropriate boundary conditions.

From 7-7 we can write

$$\frac{1}{r}\frac{\partial}{\partial r}(rG_\theta^P) + \frac{1}{r}\frac{\partial}{\partial r}(rG_\theta^S) = 0 \qquad 7\text{-}13$$

applicable when $z = 0$, $0 \leq r < A$, since H_z must vanish on the surface of the infinitely conducting disk. Upon integrating 7-13 we get

$$G_\theta^S = -G_\theta^P + \frac{c}{r} \quad ; \quad z = 0, \quad 0 \leq r < A. \qquad 7\text{-}14$$

Since a singularity cannot exist at $r = 0$, then $c = 0$ and

$$G_\theta^S = -G_\theta^P = \frac{H_0 r}{2} = \int_0^\infty g(\lambda) J_1(\lambda r)\, d\lambda \quad , \qquad 7\text{-}15$$

under the constraint $z = 0$, $0 \leq r < A$.

However, we still need a solution on the $z = 0$ plane for

$$A < r \leq \infty \quad . \qquad 7\text{-}16$$

Since, by symmetry, the induced electric field is purely toroidal, the secondary magnetic field must be poloidal and symmetric about the $z = 0$ plane as must be the resultant field. Therefore we may assert that $H_r = 0$

provided $z = 0$, $A < r < \infty$. 7-17

From 7-7 we see that

$$H_r = -\frac{\partial G_\theta^S}{\partial z} \qquad 7\text{-}18$$

so that from 7-12 we obtain

$$\int_0^\infty \lambda\, g(\lambda)\, \bar{J}_1(\lambda r)\, d\lambda = 0 \qquad 7\text{-}19$$

provided,

$$z = 0, \quad A < r \leq \infty \,.$$

Hence we have a complete solution except at $r = A$ which poses no problem.

The dual integral equation 7-15 and 7-19 can be solved as in Titchmarch (1937) to yield

$$g(\lambda) = \left(\frac{2}{\pi\lambda}\right)^{1/2} J_{3/2}(\lambda A)\, A^{3/2} H_0 \,. \qquad 7\text{-}20$$

Therefore 7-12 can be rewritten as

$$G_\theta^s = \left(\frac{2A^3}{\pi}\right)^{1/2} H_0 \int_0^\infty \lambda^{-1/2} J_{3/2}(\lambda A) J_1(\lambda r) e^{-\lambda|z|}\, d\lambda \,, \qquad 7\text{-}21$$

which can be reduced to a finite integral by a transformation due to Gegenbauer (1884) as quoted in Watson (1952, p. 390, no. (4)), as follows

$$G_\theta^s = \frac{4 r^3 H_0}{2\pi} \int_0^\pi \frac{\sin^3\theta\, d\theta}{\left[(z + iA\cos\theta)^2 + r^2\right]^{3/2}} \qquad 7\text{-}22$$

The total potential is then

$$G_\theta = G_\theta^s + G_\theta^p \qquad 7\text{-}23$$

Using 7-7 the components of the magnetic field exterior to the disk may be found. We can write

$$H_r = -\frac{\partial G_\theta}{\partial z} \quad , \qquad 7\text{-}24$$

$$H_z = \frac{1}{r}\frac{\partial}{\partial r}(r G_\theta) \quad . \qquad 7\text{-}25$$

Therefore we conclude that

$$H_r = \frac{3A^3 r H_0}{2\pi}\int_0^{\pi} \frac{\sin^3\theta (z + iA\cos\theta)\, d\theta}{\left[(z+iA\cos\theta)^2 + r^2\right]^{5/2}} \quad , \qquad 7\text{-}26$$

and that

$$H_z = \frac{A^3 H_0}{\pi}\left\{\int_0^{\pi} \frac{\sin^3\theta\, d\theta}{\left[(z+iA\cos\theta)^2 + r^2\right]^{3/2}} - \frac{3r^2}{2}\int_0^{\pi} \frac{\sin^3\theta\, d\theta}{\left[(z+iA\cos\theta)^2 + r^2\right]^{5/2}}\right\} - H_0 \qquad 7\text{-}27$$

We shall for convenience normalize the field components of the inducing field and z and r to the radius A. Equations 7-26 and 7-27 become

$$\frac{H_r}{H_0} = \frac{3}{2\pi}\int_0^{\pi} \frac{\sin^3\theta \left(\frac{z}{A} + i\cos\theta\right) d\theta}{\left[\left(\frac{z}{A} + i\cos\theta\right)^2 + r^2\right]^{5/2}} \quad , \qquad 7\text{-}28$$

and

$$\frac{H_z}{H_0} = \frac{1}{\pi}\left\{\int_0^{\pi} \frac{\sin^3\theta\, d\theta}{\left[\left(z/A + i\cos\theta\right)^2 + \left(r/A\right)^2\right]^{3/2}} - \int_0^{\pi} \frac{\left(r/A\right)^2 \sin^3\theta\, d\theta}{\left[\left(z/A + i\cos\theta\right)^2 + \left(r/A\right)^2\right]^{5/2}}\right\} - 1 \qquad 7\text{-}29$$

In general, the resultant magnetic field in the vicinity of a imperfectly conducting body will be elliptically polarized. Ward (1967) gives equations to calculate the inclination to the horizontal of the major axis of an ellipse of polarization as

$$\alpha = \tan^{-1} \frac{-B \pm \sqrt{B^2 - 4AC}}{2A}, \qquad 7\text{-}30$$

where

$$\left.\begin{aligned} A &= 2H_r\left(H_z + H_0\cos\phi\right) \\ B &= 2\left(H_z^2 + H_0^2 - H_r^2 + 2H_0H_z\cos\phi\right), \end{aligned}\right\} \qquad 7\text{-}31$$

and

$$C = -A$$

Angle ϕ is the phase of the response of a subsurface conductor measured relative to the phase of the inducing field. Ward (1967) states that for all $\phi < 45°$ the cos ϕ term can be set equal to unity without introducing serious error. Then equation 7-30 becomes

$$\left.\begin{aligned} \tan\alpha &= H_r/H_z \\ \text{or} \quad \tan\alpha &= H_r/H_o \,/\, H_z/H_o \end{aligned}\right\} \qquad 7\text{-}32$$

Ward et al. (1968, p. 626) suggest that the fields near a disk of finite conductivity can be expressed by

$$H(\omega) = \frac{2}{3}\,\frac{A^3 H_o}{\pi}\left[X - iY\right] GF \qquad 7\text{-}33$$

The quantity GF is the spatial variation of the field components and can be obtained from equations 7-28 and 7-29. Ward et al. (1968) further state that the physical property factor X-iY is separated from the geometric factor by making the tacit assumption that the current distribution in the disk is independent of the induction number, and that the phase of the secondary field is independent of position in space. They give some justification for doing this. Figure 23 shows the estimated in-phase X and quadrature Y response of a disk in a uniform field as a function of the induction number θ (Ward et al., 1968).

7.3 Presentation of Results

Figures 24 and 25 show the vertical and horizontal components of the magnetic field scattered by disks of various sizes as a function of

observation elevation. These results pertain to disks for which $\theta > 30$ such that eddy current saturation has been reached. The reflection fields exhibit maximum values of in-phase component (X=1) and zero values of quadrature component (Y=0) once eddy current saturation has been reached, (Figure 23).

As can be expected from drawing an analogy between the fields about a conductive disk and about current loops, the vertical component of the secondary magnetic field is a maximum over the center of the disk, passes through zero near its edge, and then becomes opposite in sign beyond the disk. The radial component varies from zero at the center to a maximum near the edge of the disk whereupon it falls off with distance.

The tilt angles of Figure 26 offer a further field parameter that exhibits sufficient variation to be measurable.

A further aspect to consider, which is fully described by Ward et al. (1968), is the effect of varying the angle of incidence of the inducing field. The result, as seen in Figure 27, would be the introduction of asymmetry in the radial component as well as increasing its magnitude at the expense of the vertical component. In the limit of zero incidence, no secondary components are generated.

7.4 Discussion

As pointed out in 7.3 the results obtained here pertain to disks for which $\theta > 30$. For example, if we substitute the physical parameters for one of our models outlined in Table 3 into the induction number,

$$\theta = (\sigma \mu \omega t A)^{1/2} \qquad 7\text{-}34$$

we can determine for what range of conductivity and frequency our model curves pertain. Selecting a radius $A = 100$ km, a thickness $t = 3.75$ km and $\mu = \mu_0 = 4\pi \times 10^{-7}$ MKS we find that θ has the value $\theta \geq 22.2 (\sigma\omega)^{1/2}$. Hence, the quantity $(\sigma\omega)^{1/2}$ must be $(\sigma\omega)^{1/2} \leq 1.33$ or $\sigma\omega \geq 1.82$ in order to maintain the assumption $\theta > 30$. If we assume that a lunar EM sounder experiment were to employ frequencies f, ($\omega = 2\pi f$), we would impose a condition

$$10^4 \text{ Hz} \leq f \leq 10^{10} \text{ Hz} \qquad 7\text{-}35$$

such that, 0.3×10^{-4} mhos/m $\geq \sigma \geq 0.3 \times 10^{-10}$ mhos/m. Therefore, if one were to probe the lunar surface with the wide range of frequencies indicated a good response could be anticipated for any conductivity over the range calculated above. Comparing these conductivities with those used in this paper (c.f. Tables 3 and 5) and suggested elsewhere Ward (1969a), Ward et al. (1968, 1969), and Jiracek and Ward (1970) for lunar materials we find they represent a fairly realistic range of conductivities. One point, however, is that we assumed here that the disks were in a non-dissipative whole space, by comparison, and as a result, if one is dealing with disks having conductivities of 10^{-6} mhos/m or lower then this assumption

is no longer valid and one should consider the effect of the whole space. For an active, lunar orbital electromagnetic experiment in which frequencies in the band 10^4 to 10^{10} Hz would be used, then the disk model quantitatively discussed above would respond at eddy current saturation; that is, a maximum in-phase and zero quadrature response would occur.

As another approach we could estimate the size of disk shaped mascons appropriate to our assumptions of eddy current saturation. Since the disk should be more conductive than the host rock it would be appropriate to use a conductivity of 10^{-4} mhos/m for the disk. Substituting this value for conductivity into the induction number and setting $\mu = \mu_0$, as before, we get for the two extremes of our frequency range that the conditions imposed on the radius thickness product At is

$$\left.\begin{aligned} f = 10^{10}\,Hz &, \quad At \geq 112\ m^2, \\ f = 10^{4}\,Hz &, \quad At \geq 1.12 \times 10^{6}\ m^2. \end{aligned}\right\} \qquad 7\text{-}36$$

As two extreme examples, for illustrative purposes, inequalities 7-36 suggest that we could expect eddy current saturation in a disk having a radius of 112 m and a thickness of 1 m ($f = 10^{10}$ Hz) or in a disk having a radius of 10 Km and a thickness of 112 m ($f = 10^4$ Hz). Reslistically these two examples might be manifested by a high percentage of Fe-Ni meteorite material distribution in the lunar surface in an area of meteorite impact. Such areas would be expected to show up as anomalies in any electromagnetic survey, either orbital or on-surface.

8. A Conducting Sphere in a Whole Space

8.1 Introduction

If the mascons are interpreted as spherical bodies of iron-nickel meteorite impacted and penetrated into the moon, then the conductivity of the mascon could be as high as 10 mho/m (Verhoogen and Evernden, 1956).

The purpose of this part of our study is to investigate the electromagnetic reflection from such an object. A uniform alternating magnetic field is used to simulate the interplanetary field which is incident upon the moon. The mascon is assumed to be embedded in an electrically homogeneous infinite medium, such that a conducting sphere in a whole space is a suitable model. Using this model we may calculate the reflection coefficient of the magnetic field on the lunar surface over a buried sphere.

8.2 Theoretical Development

Analytical solutions of a conducting sphere in a uniform alternating magnetic field have been obtained by Wait (1951) and Ward (1967). Figure 28 shows the geometrical configuration of a sphere, with radius R, in a whole space. A uniform alternating magnetic field with time dependence $e^{-j\omega t}$

$$\vec{H} = \vec{H}_0 \, e^{-j\omega t} \qquad 8\text{-}1$$

is applied in the X-direction, where ω is the angular frequency of the primary field and H_0 is its amplitude ($t=0$).

The propagation constant of the primary field in the infinite medium with conductivity σ_1, magnetic permeability μ_1, and dielectric permitivity ε_1, is defined as

$$k_1 = \left[\mu_1 \varepsilon_1 \omega^2 + j \sigma_1 \mu_1 \omega \right]^{1/2} \qquad 8\text{-}2$$

Similarly, the propagation constant for the medium of the sphere, with parameters σ_2, μ_2, and ε_2 is

$$k_2 = \left[\mu_2 \varepsilon_2 \omega^2 + j \sigma_2 \mu_2 \omega \right]^{1/2} \qquad 8\text{-}3$$

$|k_1 R| << 1$ is required to assure that the field is uniform in the vicinity of the sphere. Since we know that

$$k_1 = 2\pi / \lambda_1 \qquad 8\text{-}4$$

where λ_1 is the wave length of the primary field in the finite medium, then the condition $|k_1 R| << 1$ implies that the radius of the sphere has to be much smaller than the wave length λ_1.

Following Ward's (1967, p. 74) development, the three components of the total magnetic field outside the sphere can be represented by the following formulas:

$$\left.\begin{aligned} H_x &= R^3 H_0 (M - jN) \frac{2x^2 - y^2 - z^2}{r^5} + H_0 \\ H_y &= R^3 H_0 (M - jN) \frac{3xy}{r^5} \\ H_z &= R^3 H_0 (M - jN) \frac{3xz}{r^5} \end{aligned}\right\} \qquad 8\text{-}5$$

where

$$(M - jN) = \left[\frac{2\mu_2 (\tan\alpha - \alpha) - \mu_1 (\alpha - \tan\alpha + \alpha^2 \tan\alpha)}{2\mu_2 (\tan\alpha - \alpha) + 2\mu_1 (1 - \tan\alpha + \alpha^2 \tan\alpha)} \right] \qquad 8\text{-}6$$

$$\alpha = k_2 R = \left[\mu_2 \varepsilon_2 \omega^2 + j\sigma_2 \mu_2 \omega\right]^{1/2} R \qquad 8\text{-}7$$

and

$$r = (x^2 + y^2 + z^2)^{1/2}$$

The reflection coefficient is the ratio of the amplitude of the reflected magnetic field to that of the primary field

$$\left.\begin{aligned} R_x &= \frac{R^3 H_0 (M - jN)(2x^2 - y^2 - z^2)/r^5}{H_0} \\ &= R^3 (M - jN)(2x^2 - y^2 - z^2)/r^5 \\ R_y &= R^3 (M - jN)\ 3xy/r^5 \\ R_z &= R^3 (M - jN)\ \frac{3xz}{r^5} \end{aligned}\right\} \qquad 8\text{-}8$$

8.3 Calculation and Results

By applying the condition of $R \ll \lambda$, to assure that the field is uniform we have made the reflection of magnetic field independent of the electromagnetic parameters of the infinite medium. It is clearly shown in equations 8-5, 8-6, and 8-7. Then for the calculation of the reflection coefficients, only the parameters of the sphere, σ_2, μ_2, and ε_2 are considered.

As mentioned in Section 8.1 we assumed that the mascon is composed of very conductive material, $\sigma_2 = 10$ mhos/m. For such a highly

conductive body it is fairly reasonable to neglect the displacement current, i.e. $\mu_2 \epsilon_2 \omega \approx 0$ provided that the frequency is not very high. The relative permeability, μ_2/μ_1, range is chosen to vary from 1 (free space) to 100, the highest limit suggested by Ward (1968). We also assume that the mascon is a sphere with radius 25 km and the position of its center 50 km below the lunar surface.

In choosing the frequency of the primary field we considered two different cases of application: (1) for the magnetometer experiments, we assumed $f \leq 1$ Hz, and (2) for the electromagnetic sounder experiment, 10^5 Hz $\leq f \leq 10^7$ Hz (Ward, 1969b).

Figure 29 shows the in-phase component of the reflection coefficient at the lunar surface immediately aobve the mascon, plotted versus $\theta = (\sigma_2 \mu_2 \omega)^{1/2} R$. Figure 30 shows the out-of-phase component of the reflection coefficient at the same position.

8.4 Discussion

If we assume that the primary magnetic field is applied along the z-direction, then at any position along the z-axis there is no field components in the z and y directions. The coordinate system is arbitrary; as long as we can determine the direction of the primary field, the only measurement needed is of the total field in the direction of the primary field.

For a given permeability, at very low frequencies, $\theta \ll 1$, the out-of-phase part of the reflection coefficient is near zero, and the in-phase part approaches a constant. This in-phase component of the secondary field is due to the magnetostatic response of the body. A magnetometer may be used to measure

the magnetic field strength and the relative magnetic permeability of the sphere may be estimated. The resolution power of this estimation is smaller when the relative permeability is high.

At high frequencies, $\theta > 2 \times 10^3$, the out-of-phase part of the secondary field goes to zero, and the in-phase part saturates to a constant value which is independent of the relative permeability of the body.

At frequencies higher than 10^5 Hz $|k_1 R|$ is no longer smaller than unity and for such models equation 8-25 would no longer be valid (even though the whole space is assumed to be free space, i.e. $\sigma_1 = 0$, $\mu_1 = \mu_0$, $\varepsilon_1 = \varepsilon_0$). In the low frequency range, the range for magnetometer experiment, $|k_2 R|$ is always much less than unity.

The amplitude of the reflection coefficient of this model is about 0.06 for the high frequency saturation, and is about 0.11 for highly permeable material at zero frequency.

9. Summary and Conclusion

9.1 Summary

We have attempted to obtain some rational measure of the effect lunar mascons might have on any lunar magnetic or electromagnetic surveys. We have examined plane-layered, disk-shaped and spherical mascon models in uniform harmonically varying plane wave electromagnetic fields and have estimated a maximum induced static magnetic field for three mascons by applying Poisson's relation to the known lunar gravity data.

We have shown that a static field induced by an interplanetary field on the order of 10 γ could produce an anomaly of 0.82 γ for Serenities 100 km

above the surface, which would be approximately 22 γ on the surface. The smaller mascons, Crisium and Nectaris, give slightly smaller anomalies but still within measureable range.

Results presented here indicate that a lunar orbital electromagnetic sounder using frequencies from 10^4 Hz to 10^{10} Hz could detect any mascons of the type proposed as gravity models in the literature from highly conductive, permeable Fe-Ni meteorite spheres to relatively low conductive layered mascons. An analysis of an infinitesimally thin, infintely conductive disk suggest eddy current saturation is possible for conductivities as low as 10^{-4}mhos/m. Also disks as small as 10 km wide and 100 meters thick could be easily detected.

9.2 Conclusions

Our results indicate that a lunar orbiting electromagnetic experiment could readily distinguish anomalous inhomogeneities in the lunar near-surface such as the lunar mascons as described by gravity models proposed in the literature. The results indicate a 100 km orbit would be satisfactory but possibly near the limit of good signal to noise discrimination. This is only a good guess at best since noise levels, particularly geological noise levels, would be hard to predict.

Further, a magnetometer with sensitivity of 0.1 γ should easily pick up, even in a 100 km orbit, any induced magnetic anomalies associated with the lunar mascons, assuming an interplanetary inducing field of 10 γ's and an μ/μ_o ratio possibly as low as 1.01.

Appendix I

The values of dielectric constant and conductivity of postulated lunar mascon materials for frequencies of 1 Hz and 10^7 Hz respectively are given in Table 3. The change of dielectric constant and conductivity with frequency is presumed to obey a power function of the form

$$p = a f^{b} \tag{1}$$

where

$$p = \begin{cases} \sigma \\ k_e \end{cases}$$

and both a and b are constants such that a = p at 1 Hz and b is the slope of the function on a log-log plot; for example,

$$b = \frac{\log \sigma_{10^7} - \log \sigma_1}{\log 10^7 - \log 1} = \frac{\log \sigma_{10^7} - \log \sigma_1}{7} \tag{2}$$

A similar equation results for k_e when k_e is substituted for σ.

The functional variation used here is arbitrary but it closely approximates the variation of these parameters given in Ward, Jiracek and Linlor (1968, 1969) and Ward (1969a). Above 10^7 Hz both σ and k_e are taken to be constant with frequency.

List of Tables

List of Figures

Figure 15a Amplitude of reflection coefficient over two-layered lunar mascon models incident with an interplanetary plane wave source, Model II.

Figure 15b Phase of reflection coefficient over two-layered lunar mascon model incident with an interplanetary plane wave source, Model II.

Figure 16a Amplitude of reflection coefficient over two-layered lunar mascon models incident with an interplanetary plane wave source, Model III.

Figure 16b Phase of reflection coefficient over two-layered lunar mascon models incident with an interplanetary plane wave source, Model III.

Figure 17a Amplitude of reflection coefficient over two-layered lunar mascon models incident with an interplanetary plane wave source, Model IV.

Figure 17b Phase of reflection coefficient over two-layered lunar mascon models incident with an interplanetary plane wave source, Model IV.

Figure 18a Amplitude of reflection coefficient over two-layered lunar mascon models incident with an interplanetary plane wave source, Model V.

Figure 18b Phase of reflection coefficient over two-layered lunar mascon models incident with an interplanetary plan wave source, Model V.

Figure 19a Amplitude of reflection coefficient over two-layered lunar mascon models incident with an interplanetary plane wave source, Model VI.

Figure 19b Phase of reflection coefficient over two-layered lunar mascon models incident with an interplanetary plane wave source, Model VI.

Figure 20a Amplitdue of reflection coefficient over two-layered lunar mascon models incident with an interplanetary plane wave source, Model VII.

Figure 20b Phase of reflection coefficient over two-layered lunar mascon models incident with an interplanetary plane wave source, Model VII.

Figure 21a Amplitude of reflection coefficient over two-layered lunar mascon models incident with an interplanetary plane wave source, Model VIII.

Figure 21b Phase of reflection coefficient over two-layered lunar mascon models incident with an interplanetary plane wave source, Model VIII.

Figure 22 A perfectly conducting infinitesimally thin disk of radius A In a uniform harmonically varying field, frequency ω , $r^2 = x^2 + y^2$.

Figure 23 Estimated in-phase X and quadrature Y response of a disk in a uniform field as functions of the induction number θ.

Figure 24 Field components H_z/H_o and H_r/H_o over horizontal disks as percent of normally incident primary field.

Figure 25 Secondary vertical magnetic field as percent of inducing field. Z/A is vertical observation distance normalized to disk radius and X/A is normalized traverse distance.

Figure 26 Tilt angle profiles over horizontal disk in normally incident primary field.

TABLE I*

Mascon Name	Lat.	Long.	ACC.(mgals)	Mass (20×10^{-6} lunar masses)
Imbrium	+38	-18	170	20
Serenitatis	+28	+18	170	20
Crisium	+16	+58	100	10
Nectaris	-16	+34	90	9
Aestuum	+10	-8	60	6
Humorum	-25	-40	50	5
Humboltianum	+57	+82	40	4
Orientale	-20	-95	40	4
Smythii	-4	+85	40	4
Unnamed	-7	+27	40	4
Unnamed	-17	+70	30	3
Grimaldi	-6	-68	20	2
Iridum	+45	-31	-70	-7

* From Muller and Sjogren, (1969), Table 3

TABLE 2

Gravity Model of Mascon

Shape and Location	Material	Reference
Trough-like mass excess distribution, 50 x 200 km, running east-west Mare Imbrium and Serenitatis		Muller and Sjogren, 1968
Flat circular plates 1. (a) 3.75 km thick, at surface (b) 6.6 km thick at 50 km depth diameters = 200 km 2. 3.8 km thick, at surface, diameter = 50 km Mare Imbrium	Ni-Fe meteorite Material, $\Delta\rho$ = 5 H-type metorite material in basalt	Urey, 1968
Spheres mare — dia. — depth (km) Imbrium 61.2 450-670 Serenitatis 36.7 270-400 Crisium 27.2 200-300 Humorum 21.3 155-233 Nectaris 16.0 116-175 Ptolemaius 10.0 93-109	Iron metorites mass x 10^{15} kg 930 200 82 39 17 4	Stipe, 1968
Mare Serenitatis 1. Disc model (a) r_1 = 210 km r_2 = 265 km r_3 = 150 km r_4 = 50 km total thickness = 14 km (b) r = 300 km thickness = 8 km. 2. Sphere (a) buried 200 km. (b) buried 50 km.	$\Delta\rho$ = 1.1 gm/cc. (If $\Delta\rho$ = 0.5, thickness = 30.8 km) $\Delta\rho$ = 1.0	Conel and Holstrum, 1968
Mare Imbrium Parabolic shape r = 3.38 x 10 cm. d = 82 km.	$\Delta\rho$ = 0.4 basalt	Baldwin, 1968

TABLE 3: ELECTROMAGNETIC MODELS FOR LUNAR MASCONS

Model No.	*Shape	Size	Density Contrast	**Conductivity mho/m	Relative Magnetic Permeability	**Dielectric Constant
I.	Sphere	50 km. Dia.	5	10 to 15	5.0	1.0
II.	Disk (a)	200 km. Dia.	5	Infinite	—	—
	(b)	300 km. Dia.	1.1	Infinite	—	—
III.	Top Layer of Half Space	4-6 km. thick	(a) 5		1.1 - 5.0	6.0 - 11.0
		8 km. thick	(b) 1.1 to 1.4	10^{-5} to 10^{-8}	1.001 - 1.05	6.0 - 11.0

* For model III the second layer extends to infinity and has electrical parameters identical to the mascon layer of each model.

** For model III the conductivity and dielectric constant are given for frequencies of 1.0 Hz and 10^7 Hz, and a power function variation is assumed for the intermediate frequencies and the values become constant above 10^7 Hz, (Appendix I).

TABLE 4

SUSCEPTIBILITIES AND DENSITIES OF LUNAR MASCONS

USED IN POISSON'S EQUATION

k_m	0.001 (Mafic effusive rock)	0.013 (Periodotite)	0.125 (Pyrrhotite)	0.3 (Magnetite rock)	1.0 (Magnetite)
ρ_0 (gm/c.c)	0.24	0.5	2.0	2.2	2.6

TABLE 5: TWO-LAYERED MASCON MODELS

Mascon Parameters							Gravity Model
Model No.	Conductivity, mhos/m		Dielectric Constant		Magnetic Permeability	Thickness, Meters	
	1Hz	10^7Hz	1Hz	10^7Hz			
1.	1.0×10^{-2}	1.0	11.0	6.0	2.0	4000	Urey (1968)
2.	1.0×10^{-2}	10.0	11.0	6.0	5.0	4000	H - type or
3.	1.0×10^{-3}	0.1	11.0	6.0	1.1	6000	Fe-Ni Meteorite
4.	1.0×10^{-3}	1.0	11.0	6.0	1.5	6000	Material
5.	1.0×10^{-3}	1.0	11.0	6.0	5.0	6000	
6.	1.0×10^{-8}	1.0×10^{-4}	11.0	6.0	1.001	8000	Conel and
7.	1.0×10^{-8}	1.0×10^{-4}	11.0	6.0	1.01	8000	Holstrum (1968)
8.	1.0×10^{-8}	1.0×10^{-4}	11.0	6.0	1.05	8000	"Basaltic" Material
"Dry" Rock Substratum Same for all Models							
	1.0×10^{-10}	1.0×10^{-4}	11.0	6.0	1.0	∞	

References

Anderson, D. L., and R. A. Pinney, 1967, Early thermal history of the terrestical planets: in mantles of the Earth and Terrestical Planets, ed. S. K. Runcorn, Interscience Publishers, pp. 113-126.

Baldwin, R. B., 1963, The measure of the moon, University of Chicago Press, Chicago.

Baldwin, R. B., 1966, On the origin of the moon, Jour. Geophys. Res., vol. 71, pp. 1936-1937.

Baldwin, R. B., 1968, Lunar Mascons: Another interpretation, Science 162, pp. 1407-1408.

Bracewell, R., 1965, The fourier transform and its applications, McGraw Hill Book Co., New York, pp. 381.

Cameron, A. S. W., 1963, The origin of the atmospheres of Venus and the Earth, Icarus 2, pp. 249-257.

Caputo, M., 1965, On the shape, gravity field, and strength of the moon, Jour. Geophys. Res., v. 70, no. 16, pp. 3993-4003.

Conel, J. E., and G. B. Holstrum, 1968, Lunar mascons: a near-surface interpretation, Science 162, pp. 1403-1405.

Cooley, J. W., and J. W. Tukey, 1965, An algorithm for the machine calculation of complex fourier series, Math. of Comp., v. 19, p. 297-301.

Darwin, G. H., 1898, The tides, Houghton Mifflin Co., New York.

El-Baz, Farouk, 1967, Lunar igneous intrusions, Science 167, pp. 49-50.

Fielder, G., 1967, Evidence for volcanism and faulting on the moon; in Mantles of the Earth and Terrestrial Planets, ed. S. K. Runcom, Interscience Publishers, pp. 461-472.

Fricker, P. E., R. T. Reynolds, and A. L. Summers, 1967, On the thermal history of the moon, Jour. Geophys. Res., v. 72, no. 10, pp. 2649-2662.

Gault, D. E., et al., 1968, Lunar theory and processes, Jour. Geophys. Res., v. 73, no. 12, pp. 4115-4131.

Gegenbauer, L., 1884, Uber die Bessel'schen Funktionen, Wiener Sitzungsberichte, v. 88, no. 2, pp. 995.

Gilvarry, J. J., 1960, Origin and nature of lunar surface features, Nature 188, pp. 886-891.

Gilvarry, J. J., 1964, Evidence of the pristine presence of a lunar hydrosphere, Publ. Astron. Soc. Pacific 76, pp. 245-253.

Gilvarry, J. J., 1969, Nature of the lunar mascons, Nature 221, pp: 732-735.

Gold, T., 1956, The lunar surface, Monthly Notices of R.A.S., v. 115, pp. 585-604.

Gottlieb, P. O., M. Muller, and W. L. Sjogren, 1969, Nonexistence of Large Mascons at Mare Marginis and Mare Orientale, Science 166, pp. 1145-1147.

Grant, F. S., and G. F. West, 1965, Interpretation theory in applied geophysics, McGraw Hill Book Co., New York, pp. 584.

Hibbs, A. R., 1967, Surface of the moon, Scientific American, March, pp. 60-72.

Jefferys, H., 1930. The resonant theory of the origin of the moon, Mon. Not. Roy. Astron. Soc., 91, pp. 169-173.

Jiracek, G. R., and S. H. Ward, 1970, Oblique electromagnetic reflection from layered lunar models, (in press).

Kane, M. F., 1969, Doppler Gravity, a new method, Jour. Geophys. Res., v. 74, no. 27, pp. 6579-6582.

Karlstrom, Thor, N. V., et al., 1967, U. S. G. S. Position Paper, Geology Working Group, NASA 1967 Summer Conference on Lunar Exploration and Science.

Kaula, W. M., 1968, An introduction to Planetary Physics; the terrestrial Planets, John Wiley and Sons, Inc., New York, p. 490.

Kaula, W. M., 1969, Interpretation of Lunar Mass Concentrations, Phys. Earth Planet. Inter. vol. 2, no. 2, pp. 123-137.

Kopal, Zdenek, 1962, The internal constitution of the moon, Planet Space Science, 9, pp. 625-638.

Kopal, Zdenek, 1966, An introduction to the study of the moon, D. Reidel Pub. Co., Dordrecht-Holland, p. 464.

Kovach, R. L., and D. L. Anderson, 1965, The interiors of the terrestrial planets, Jour. Geophys. Res., v. 70, no. 12.

Kuiper, G. P., 1959, The Moon, Jour. Geophys. Res., v. 64, no. 11, pp. 1713-1719.

Kuiper, G. P., 1966, Interpretation of the ranger records, in H. Brown, G. J. Stanley, D. O. Muhleman, and G. Munch Eds., Proc. Caltec - JPL Lunar and Planetary Conf., Sept. 13-18, 1965, pp. 24-29.

Lee, W. H. K., 1968, Effects of selective fusion on the thermal history of the moon, Mars, and Venus, Earth and Planetary Science Letters, North Holland Pub. Co., Amsterdam, pp. 277-283.

Levin, B. J., 1966, Thermal history of the moon and the development of its surface; in the nature of the lunar surface; eds. W. N. Hess, D. H. Menzel, J. A. O'Keefe, John Hopkins Press, Baltimore, pp. 267-273.

Lingenfelter, R. E., S. J. Peale, and G. Schubert, 1968, Lunar Rivers, Science 161, pp. 266-269.

Lowman, D. D., Jr., 1963, The relation of tektites to lunar igneous activity, Icarus, 2, pp. 1-35.

Lunar Sample Preliminary Examination Team, 1969, A physical, chemical, mineralogical, and biological analysis of 22 kilograms of lunar rocks and fines, Science 165, pp. 1211-1227.

Lyttleton, R. A., 1967, Dynamical capture of the moon by the earth, Proc. Roy. Soc. London, A., 296, pp. 285-292.

MacDonald, G. J. F., 1963, The internal constitution of the inner planets and moon, Space Science Review 2, pp. 473-557.

MacDonald, G. J. F., 1965, On the internal constitution and origin of the moon in Proc. Caltech - JPL Lunar and Planetary Conf., Pasadena, pp. 77-83.

Morse, P. M., and H. Feshback, 1953, Methods of theoretical physics, Pt.I, New York, McGraw-Hill Book Co., Inc.

Muller, P. M., and W. L. Sjogren, 1968, Mascons. lunar mass concentrations, Science 161, pp. 680-684.

Muller, P. M., 1969, Lunar gravimetrics, Unpublished.

Nakamura, Y., and G. V. Latham, 1969, Internal constitution of the moon: Is the lunar interior chemically homogeneous?, Jour. Geophys. Res., v. 74, no. 15, pp. 3771-3780.

Oberbeck, V. R., and W. L. Quaide, 1967, Estimated thickness of a fragmental surface of oceanus procellarum, Jour. Geophys. Res., v. 72, no. 18.

O'Keefe, J. A., 1969, Origin of the moon, Jour. Geophys. Res., v. 74, no. 10, p. 2758-2767.

O'Keefe, J. A., and E. W. Adams, 1965, Tektite structure and lunar ash flows, Jour. Geophys. res., v. 70, no. 16.

O'Keefe, J. A., and W. S. Cameron, 1962, Evidence from the moon's surface features of the production of lunar gravities, Icarus, 1-3, pp. 281-284.

O'Leary, B. T., M. J. Campbell, and C. Sagan, 1969, Moon: Two new mascon basins, Science, 164, pp. 1273-1275.

Opik, E. J., 1955, The origin of the moon, Irish Astron. Jour., 3, pp. 245-248.

Opik, E. J., 1961, Tidal deformation and the origin of the moon, Astro. Jour., 66, pp. 60-67.

Ringwood, A. E., 1960, Some aspects of the thermal evolution of the earth, Geochim. Cosmochim Acta 20, pp. 241-259.

Ringwood, A. E., 1966, Chemical evolution of the terrestrial planets, Geochimica et. Cosmochimica Acta 30, pp. 41-104.

Ruskal, E. L., 1960, The origin of the moon, Sov. Astron. AJ, 4, pp. 657-668.

Schelkunoff, S. A., 1943, Electromagnetic waves, Van Nostrand Co., New York.

Shoemaker, E. M., 1962, Interpretation of Lunar Craters in Physics and Astronomy of the moon, ed. by Z. Kopal, pp. 327, Academic Press, New York.

Sill, W. R., and J. L. Blank, 1968, Lunar response to the time varying interplanetary magnetic field and application to the alsep magnetometer experiment, Bellcom Inc., Rpt. under NASA Contract NASW-417.

Smith, R. L., 1966, Terrestrial calderas, associated pyroclastic deposits and possible lunar applications, in W. N. Hess, D. H. Manzel, and J. A. Baltimore, pp. 241-257.

Stipe, J. G., 1968, Mascons Interpreted, Science, 162, pp. 1402-1403.

Turkevich, A. L., E. J. Franzgrote, and J. H. Patterson, 1967, Chemical analysis of the Moon at the Surveyor v landing site, Science, 158,pp.635-637.

Turkevich, A. L., J. H. Patterson, and E. J. Franzgrote, 1968, The chemical analysis of the lunar surface, Am. Scientist, 56, (4), pp. 312-343.

Urey, H. C., 1960, Criticism of the melted Moon theory, Jour Geophys. Res., v. 65, no. 1, pp. 358-359.

Urey, H. C., 1965, Meteorites and the Moon, Science, 147, pp. 1262-1265.

Urey, H. C., 1967, The origin of the Moon, Ch. 5 of Mantles of the Earth and Terrestrial Planets, ed. by S. K. Runcorn, Interscience Publishers, London.

Urey, H. C., 1968, Mascons and the history of the Moon, Science, 162, pp. 1408-1410.

Urey, H. C., Elasser, W. N., and Rochester, M. G., 1959, Note on the internal structure of the Moon, Astrophys. Jour., v. 129, pp. 842-848.

Van Dorn, W. G., 1969, Lunar maria: Structure and evolution, Science, v. 165, pp. 693-695.

Verhoogen, J., and J. F. Evernden, 1956, Electrical resistivity of meteorites, Nature, v. 178, pp. 106.

Wait, J. R., 1951, A conducting sphere in a time-varying magnetic field, Geophysics, v. 16, no. 4, pp. 666.

Wait, J. R., 1958, Transmission and reflection of electromagnetic waves in the presence of stratified media, Jour. Res., NBS, 61, (3), pp. 205.

Ward, S. H., 1967, Electromagnetic theory for geophysical applications, in Soc. Expl. Geophys. Mining Geophys. vol. II. Theory, Compiled and Edited by the SEG Mining Geophys., v. Ed. Committee, Soc. Expl. Geophys., Tulsa, Oklahoma.

Ward, S. H., 1968, Electromagnetic responses of mascons, Proposal UCBSSL No. 309, Space Sciences Lab., Univ. of Calif., Berkeley, California.

Ward, S. H., 1969a, Gross estimates of the conductivity, dielectric constant, and magnetic permeability distributions in the Moon, Radio Sci., 4, 2, p. 117.

Ward, S. H., 1969b, personal communication.

Ward, S. H., G. R. Jiracek, and W. I. Linlor, 1968, Electromagnetic reflection from a plane-layered lunar model, Jour. Geophys. Res., v. 73, no. 4, pp. 1355-1372.

Ward, S. H., G. R. Jiracek, and W. I. Linlor, 1969, Some factors affecting electromagnetic detection of lunar subsurface water, IEEE Trnas., Geosci. Elect., GE-7, 1, p. 19.

Ward, S. H., D. P. O'Brien, J. R. Parry, and B. K. McKnight, 1968, AGMAG - Interpretation, Geophysics, v. 33, no. 4, pp. 621-644.

Watson, G. N., 1952, Theory of Bessel functions, Cambridge, The University Press.

Wise, D. U., 1963, An origin of the Moon by rotational fission during formation of the Earth's core, Jour. Geophys. Res., v. 68, pp. 1547-1554.

Wise, D. U., 1969, Origin of the Moon from the Earth: Some new mechanisms and comparisons, Jour. Geophys. Res., v. 74, no. 25, pp. 6034-6045.

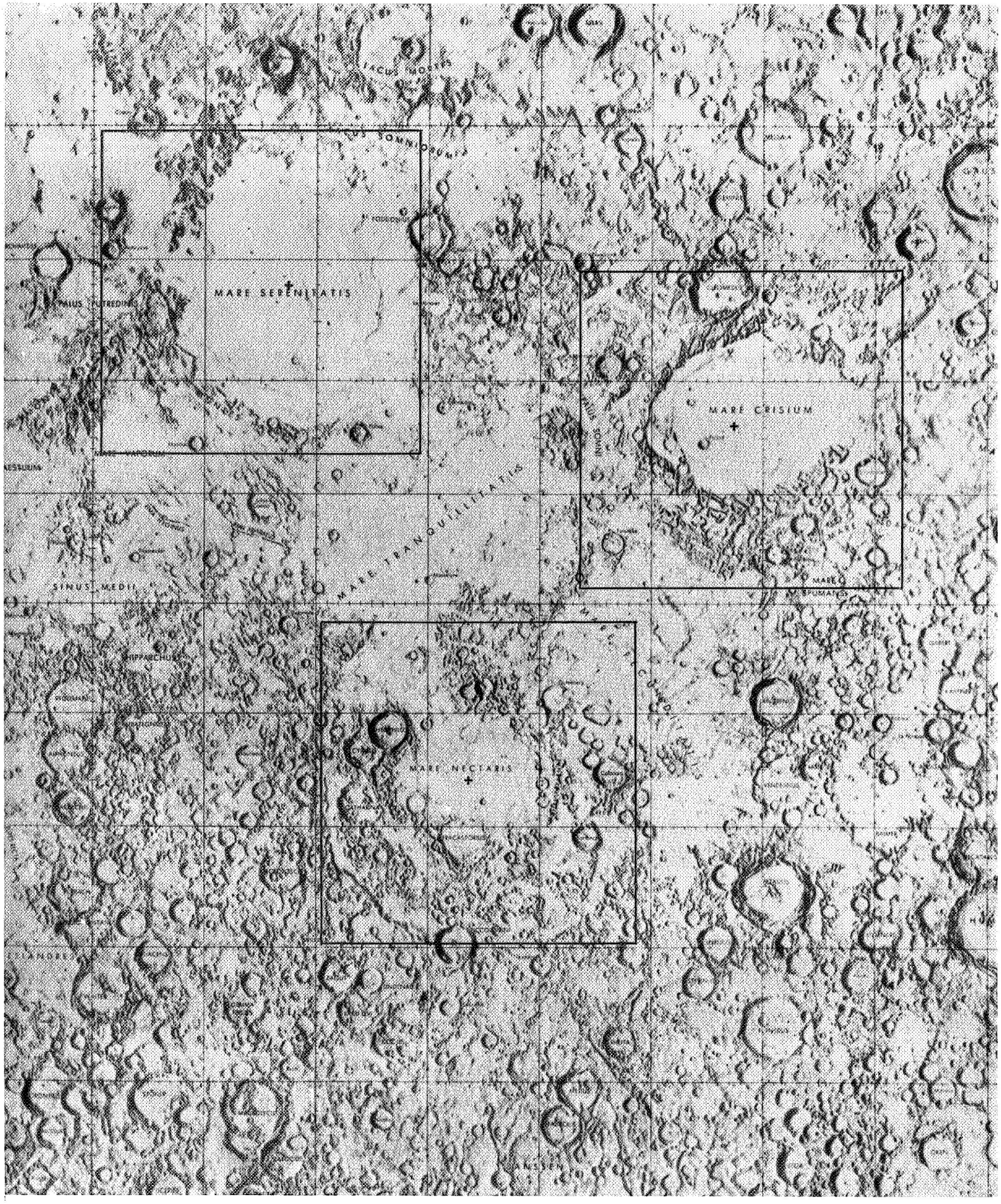
LACUS SOMNIORUM
MARE SERENITATIS
MARE CRISIUM
MARE TRANQUILLITATIS
SINUS MEDII
MARE NECTARIS

FIG. 1

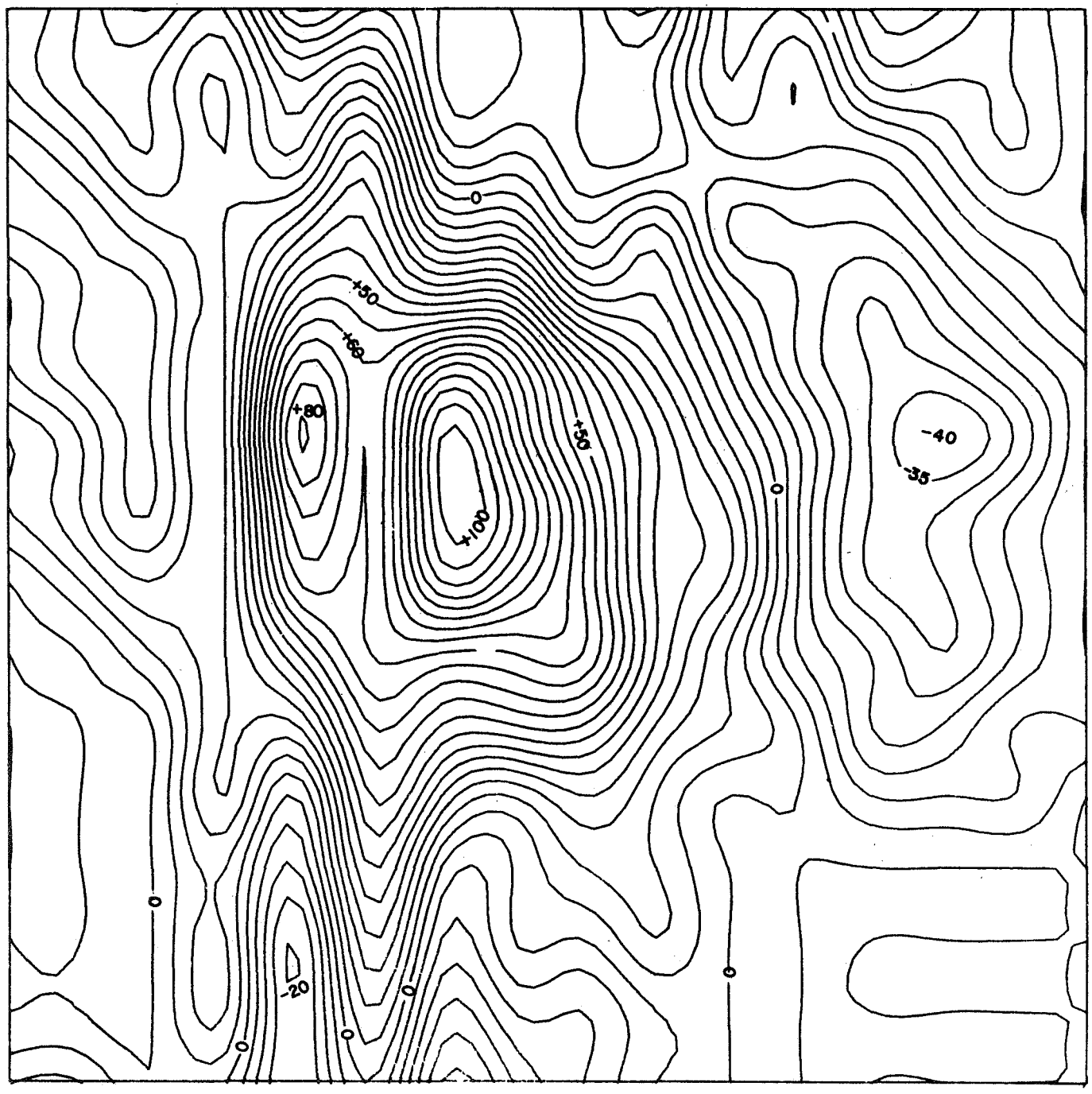

FIG. 2

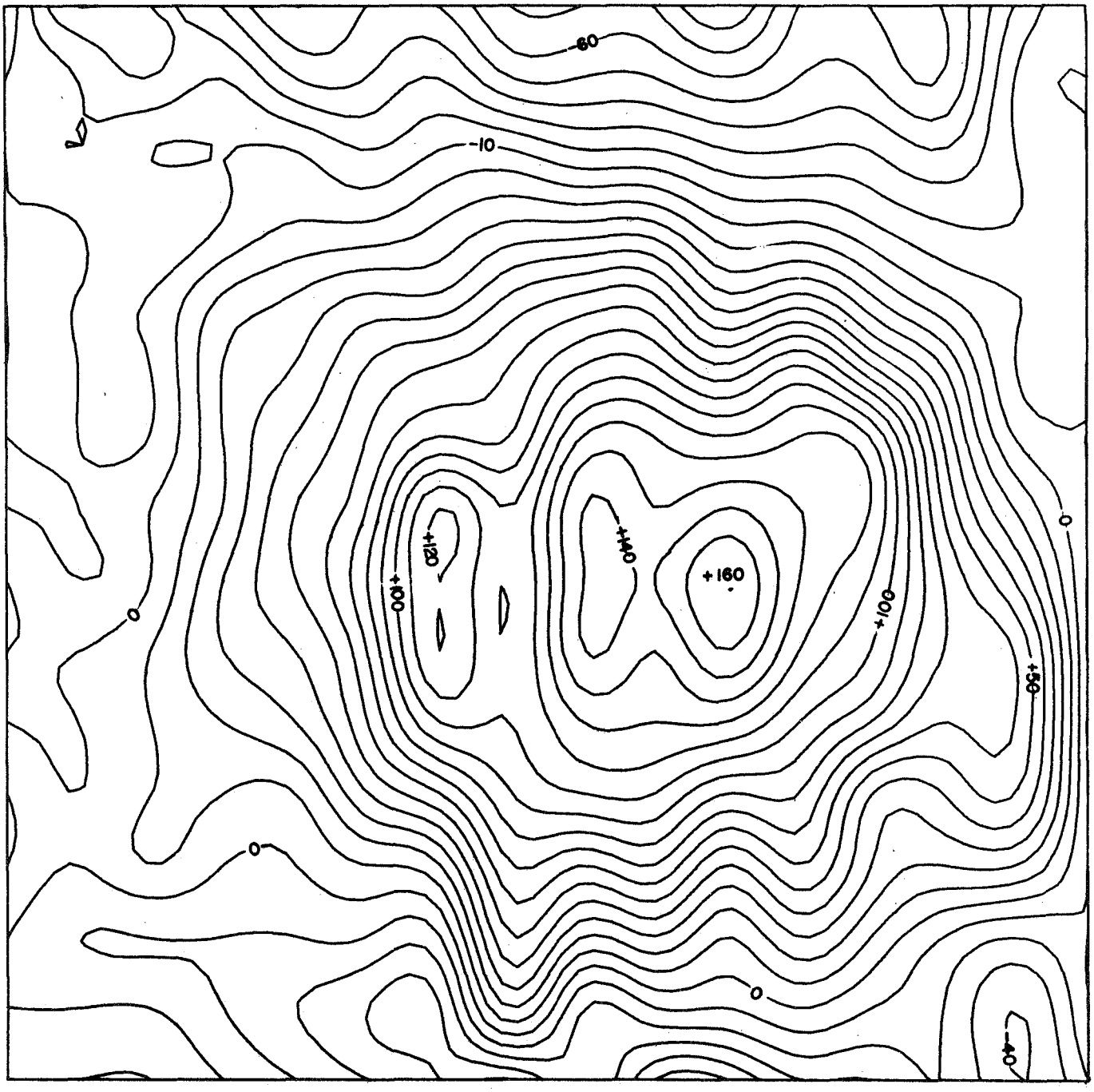

FIG. 3

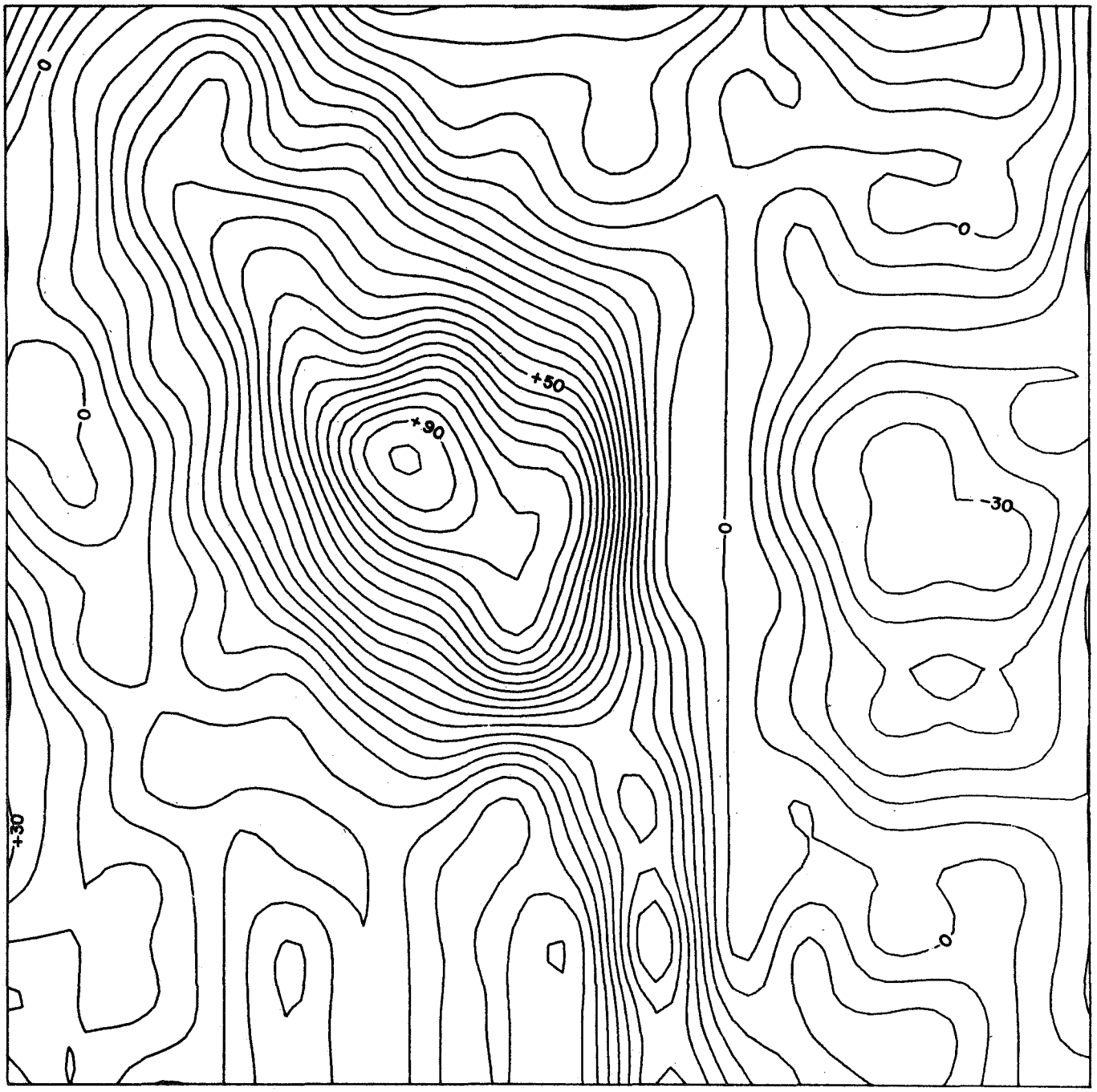

FIG. 4

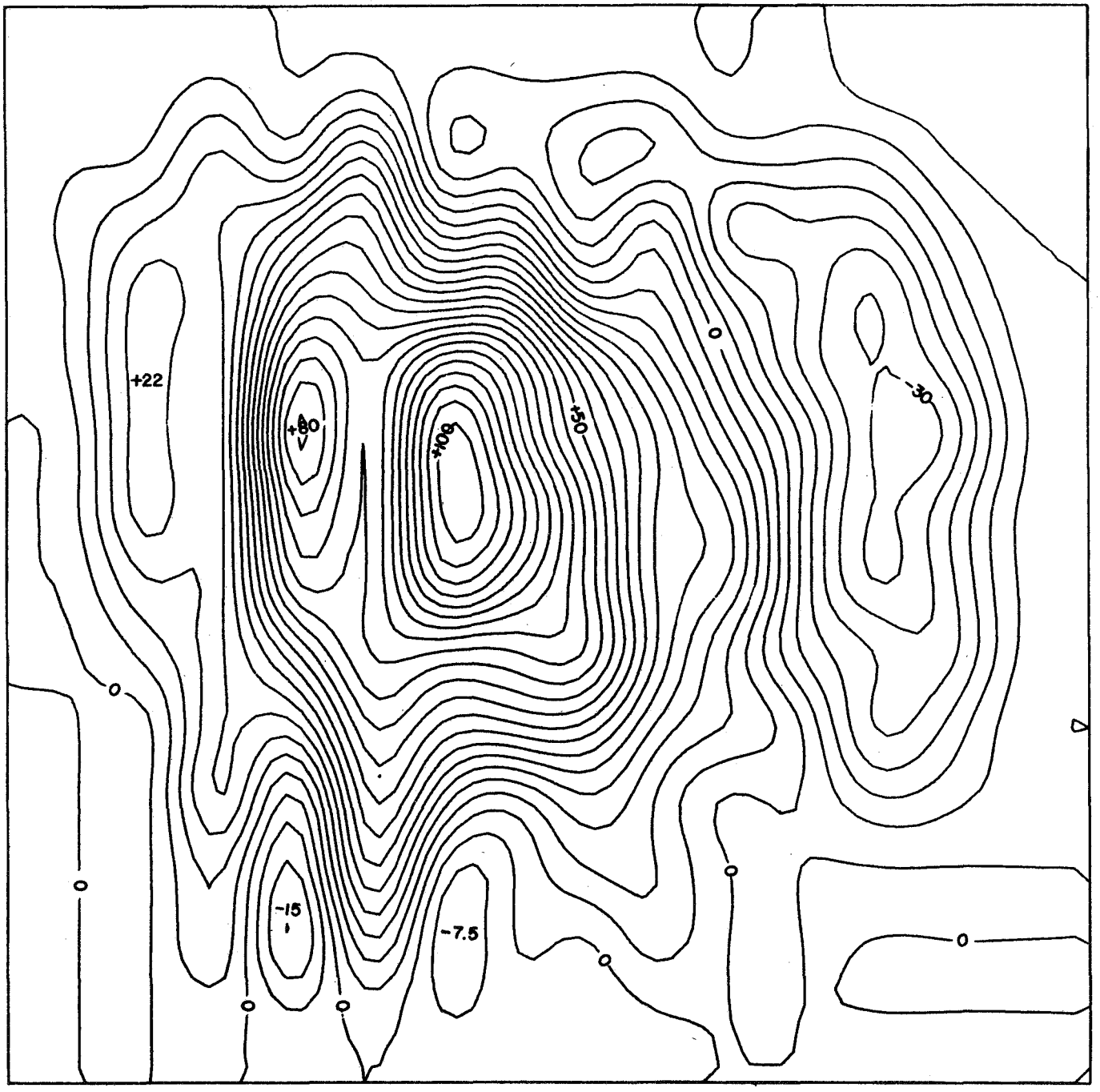

FIG. 5

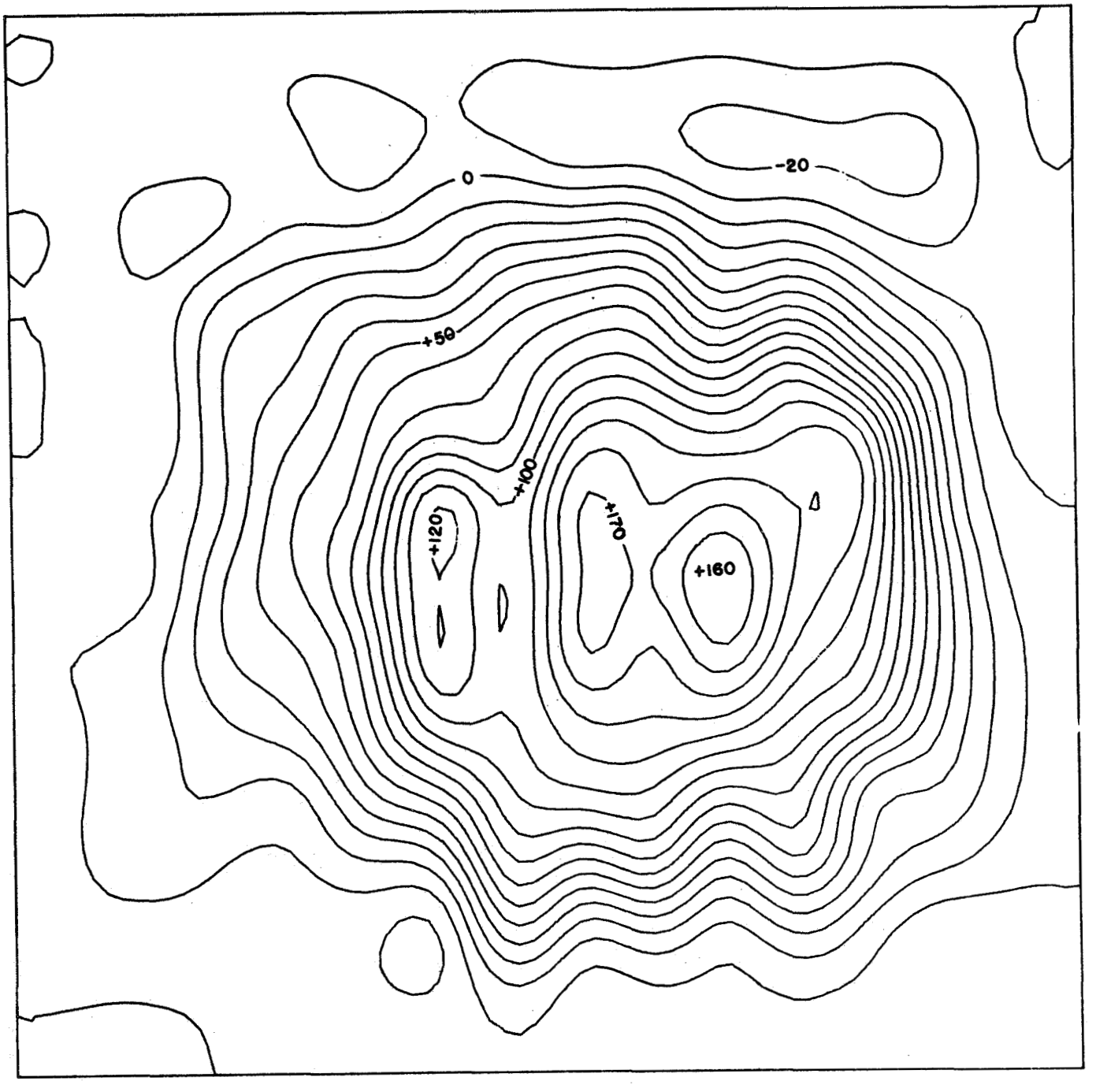

FIG. 6

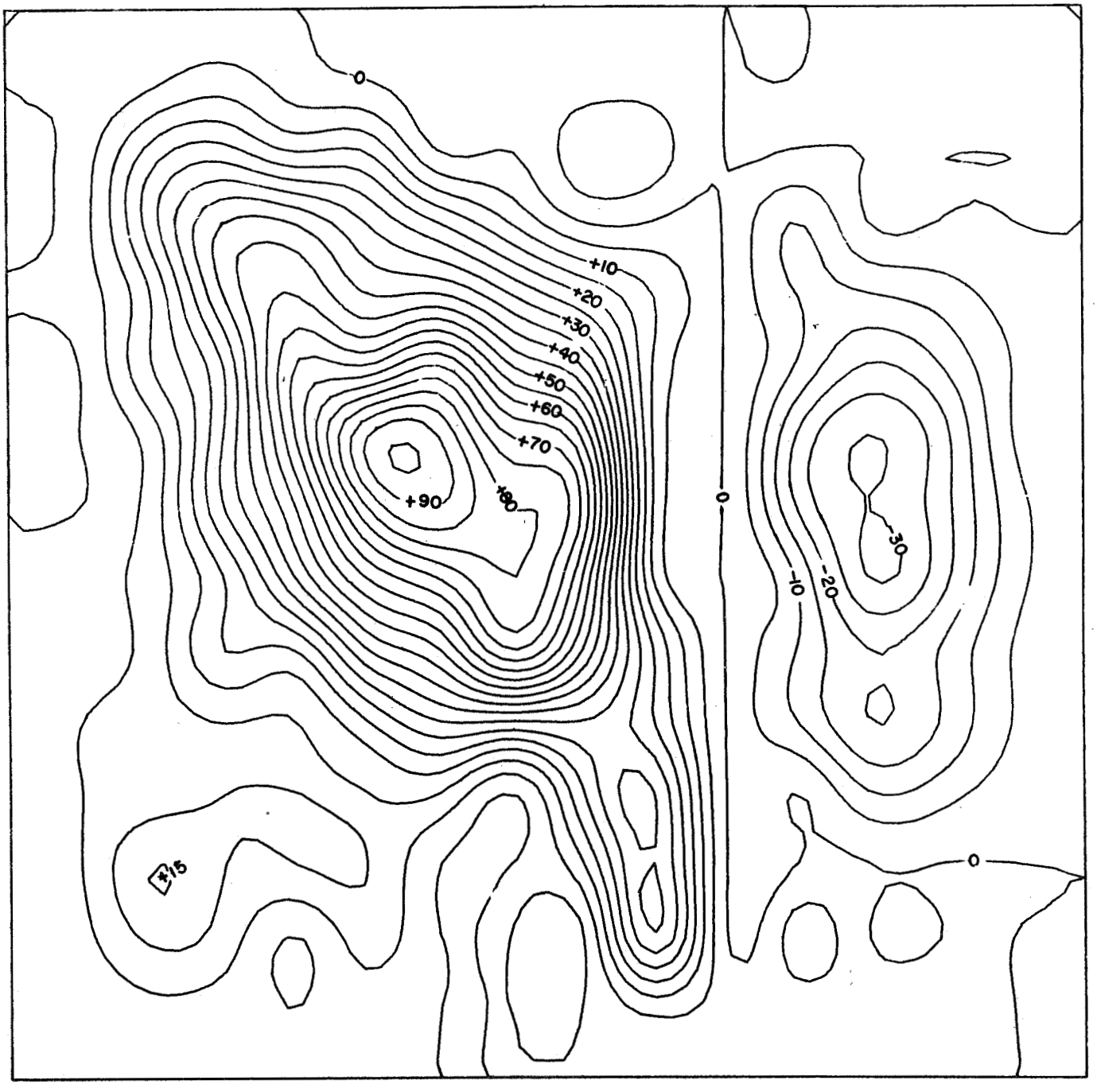

FIG. 7

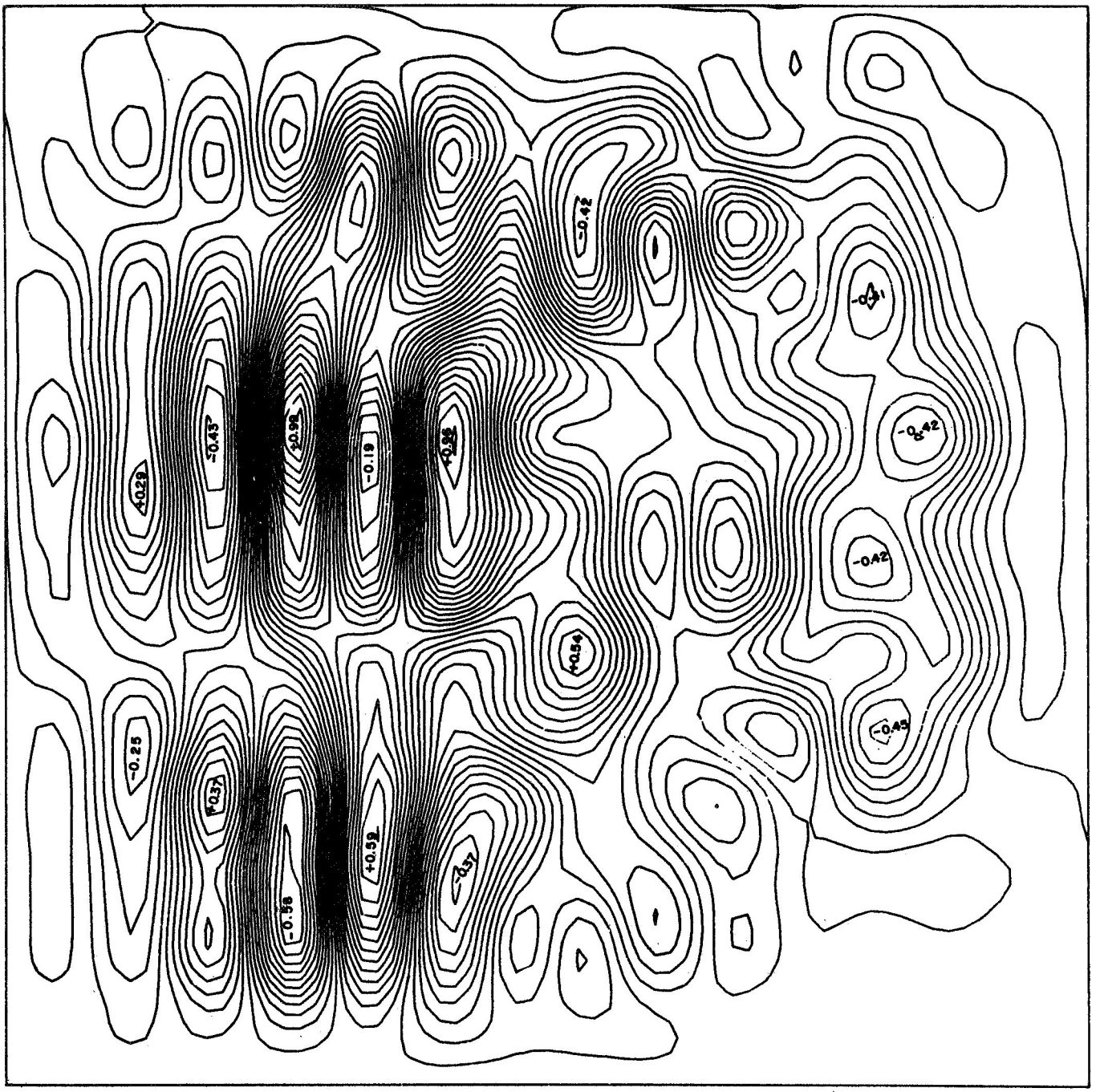
-0.42
-0.41
-0.42
-0.43
+0.29
-0.43
+0.92
-0.19
+0.83
-0.42
+0.54
-0.43
-0.25
+0.37
-0.98
+0.32
-0.37

FIG. 8

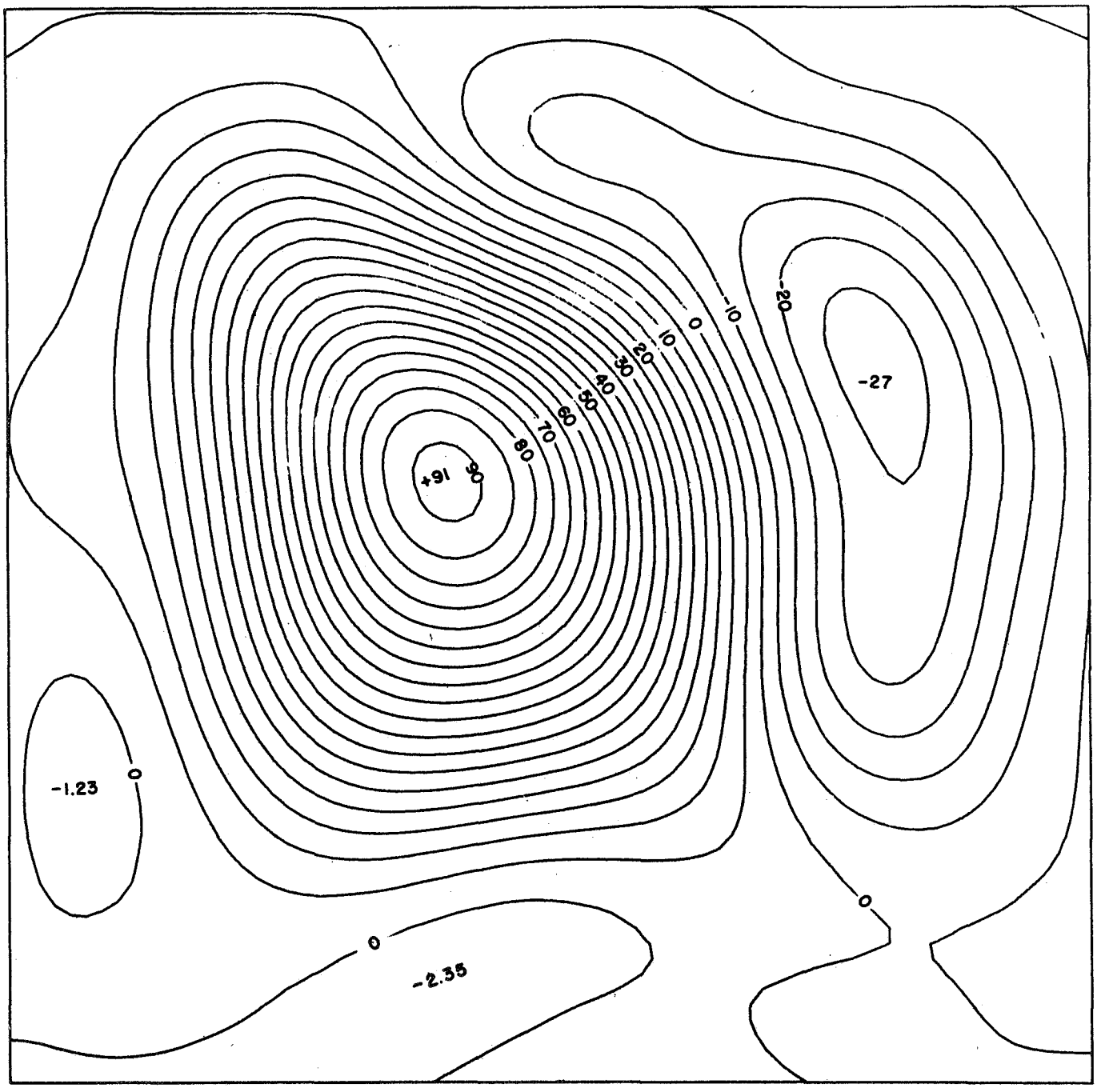

FIG. 9

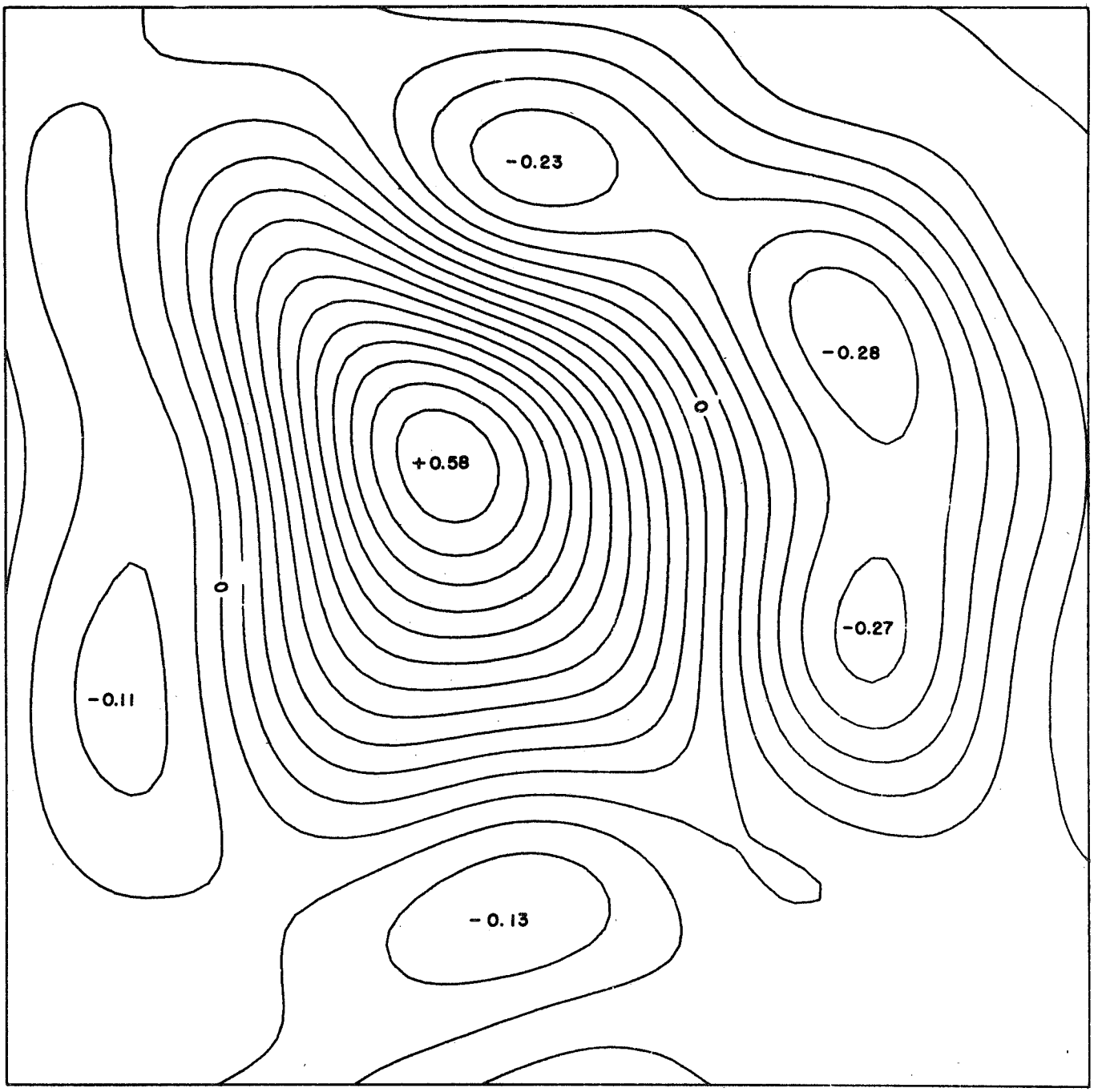

FIG. 10

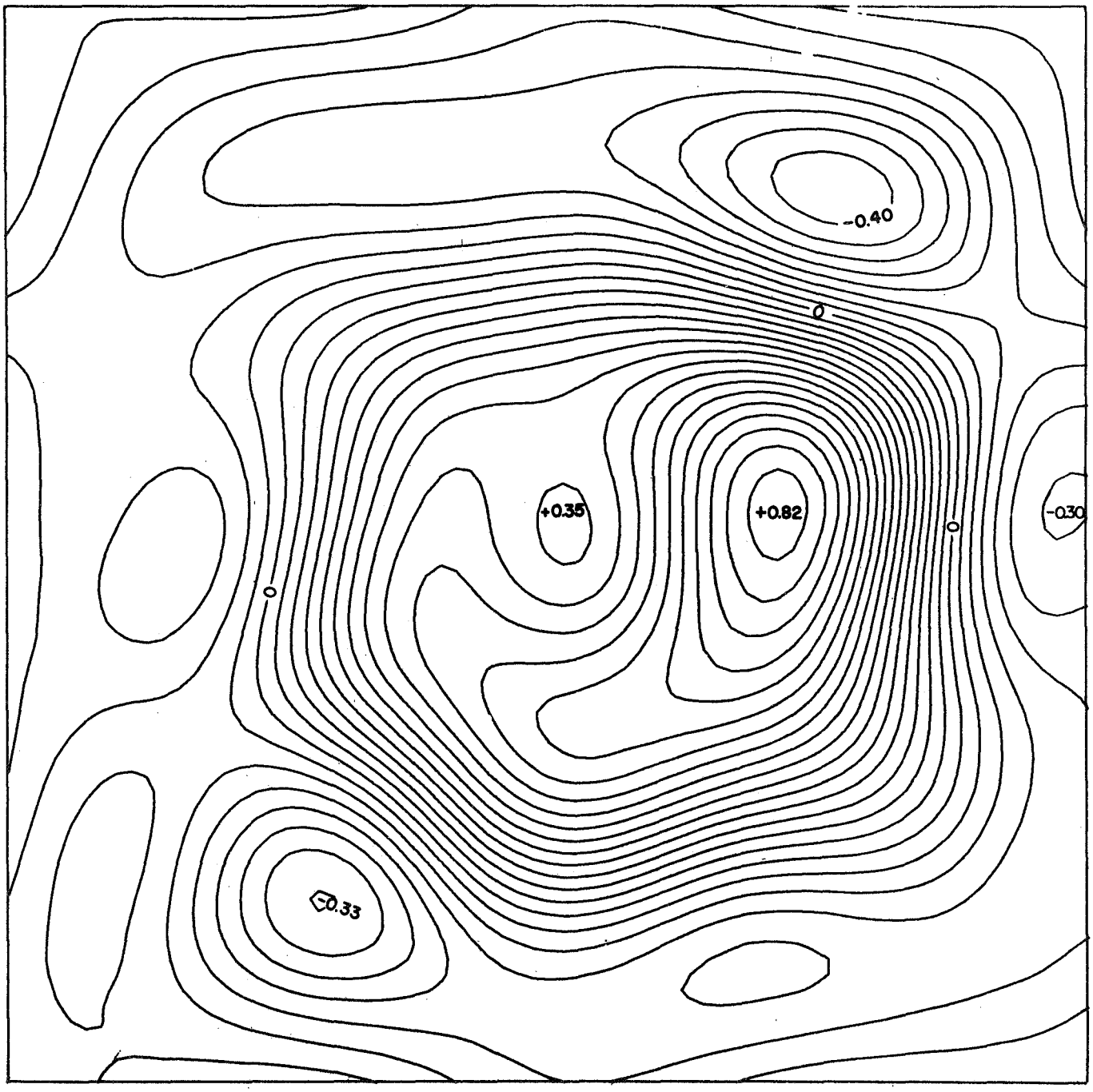

FIG. 11

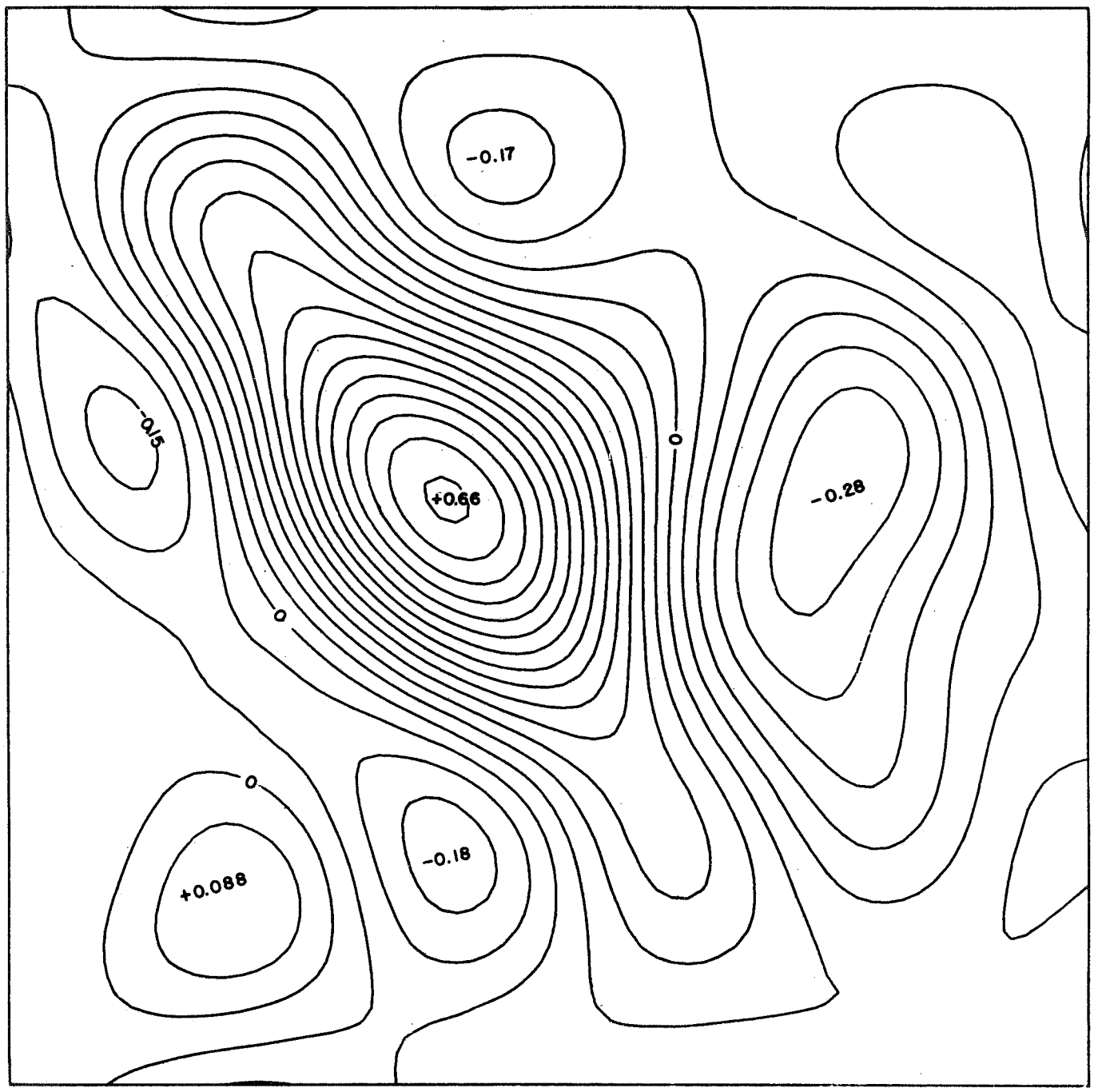

FIG. 12

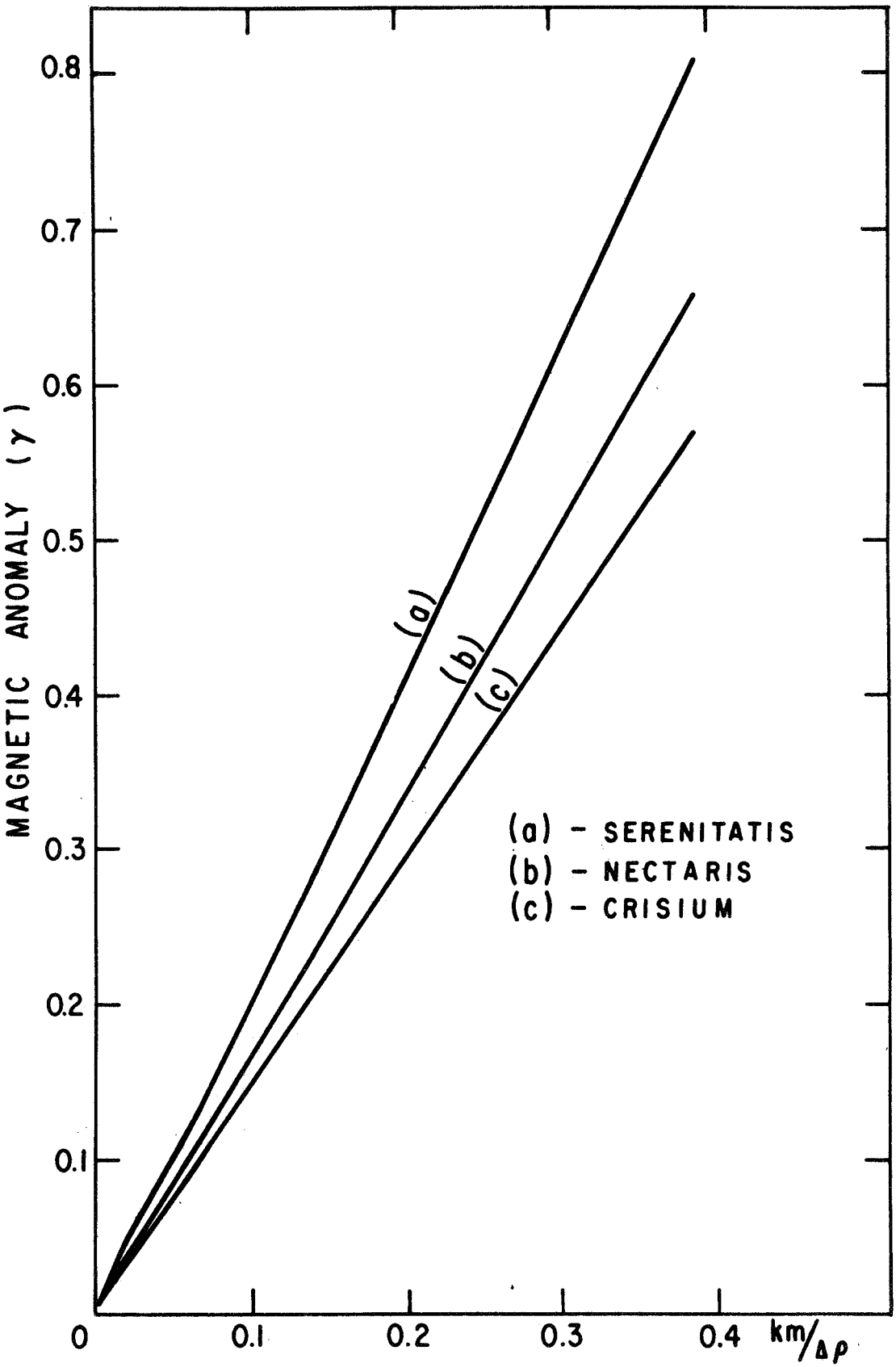
MAGNETIC ANOMALY (γ)
0.8
0.7
0.6
0.5
0.4
0.3
0.2
0.1
0
0.1
0.2
0.3
0.4
km/Δρ
(a)
(b)
(c)
(a) - SERENITATIS
(b) - NECTARIS
(c) - CRISIUM

FIG. 13

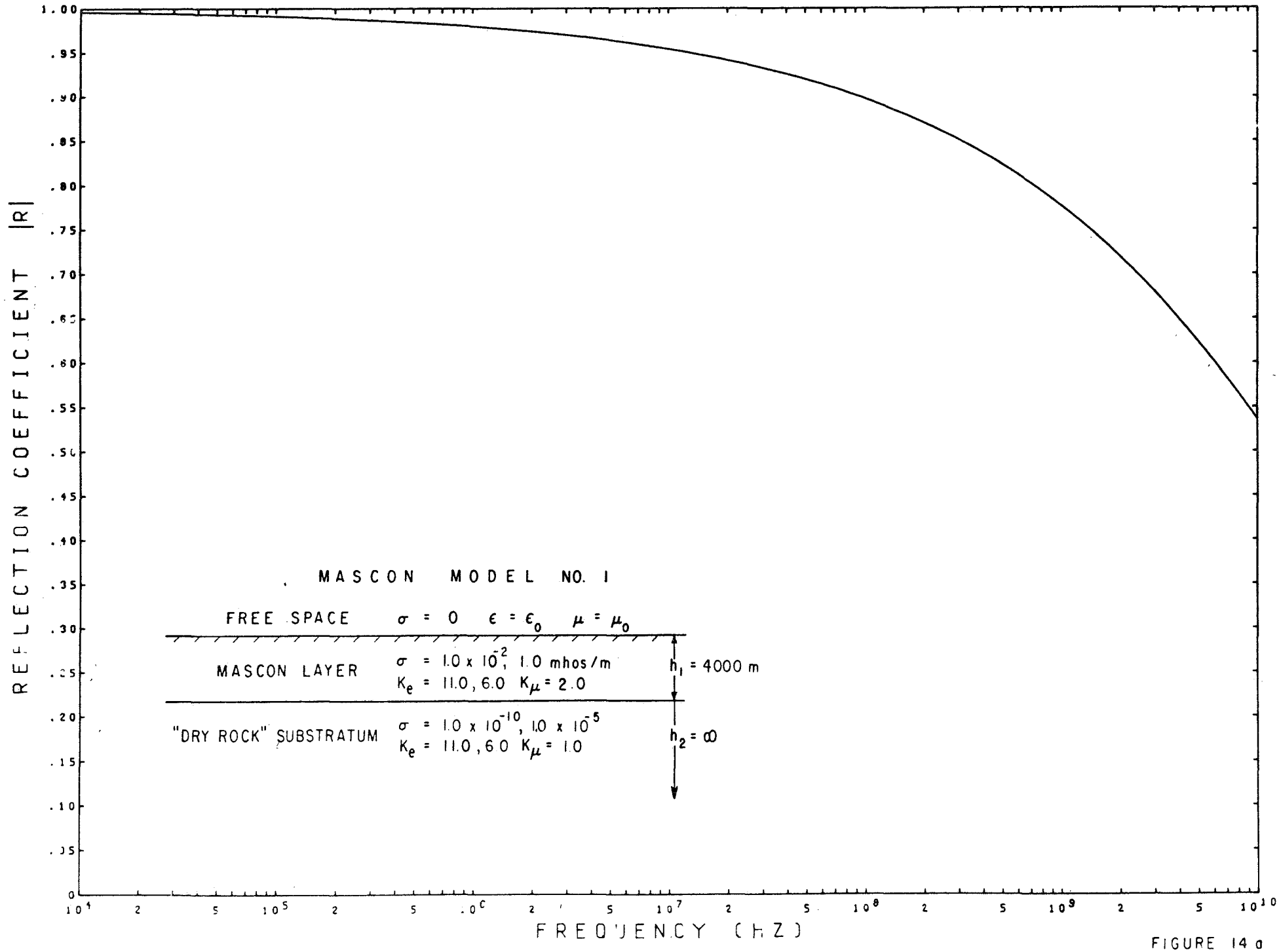
REFLECTION COEFFICIENT |R|
1.00
.95
.90
.85
.80
.75
.70
.60
.55
.50
.45
.40
.35
.30
.25
.20
.15
.10
.05
0
10^4 2 5 10^5 2 5 10^6 2 5 10^7 2 5 10^8 2 5 10^9 2 5 10^{10}
FREQUENCY (HZ)
MASCON MODEL NO. 1
FREE SPACE $\sigma = 0$ $\epsilon = \epsilon_0$ $\mu = \mu_0$
MASCON LAYER $\sigma = 1.0 \times 10^{-2}$, 1.0 mhos/m
$K_e = 11.0, 6.0$ $K_\mu = 2.0$
$h_1 = 4000$ m
"DRY ROCK" SUBSTRATUM $\sigma = 1.0 \times 10^{-10}, 1.0 \times 10^{-5}$
$K_e = 11.0, 6.0$ $K_\mu = 1.0$
$h_2 = \infty$

FIGURE 14 a

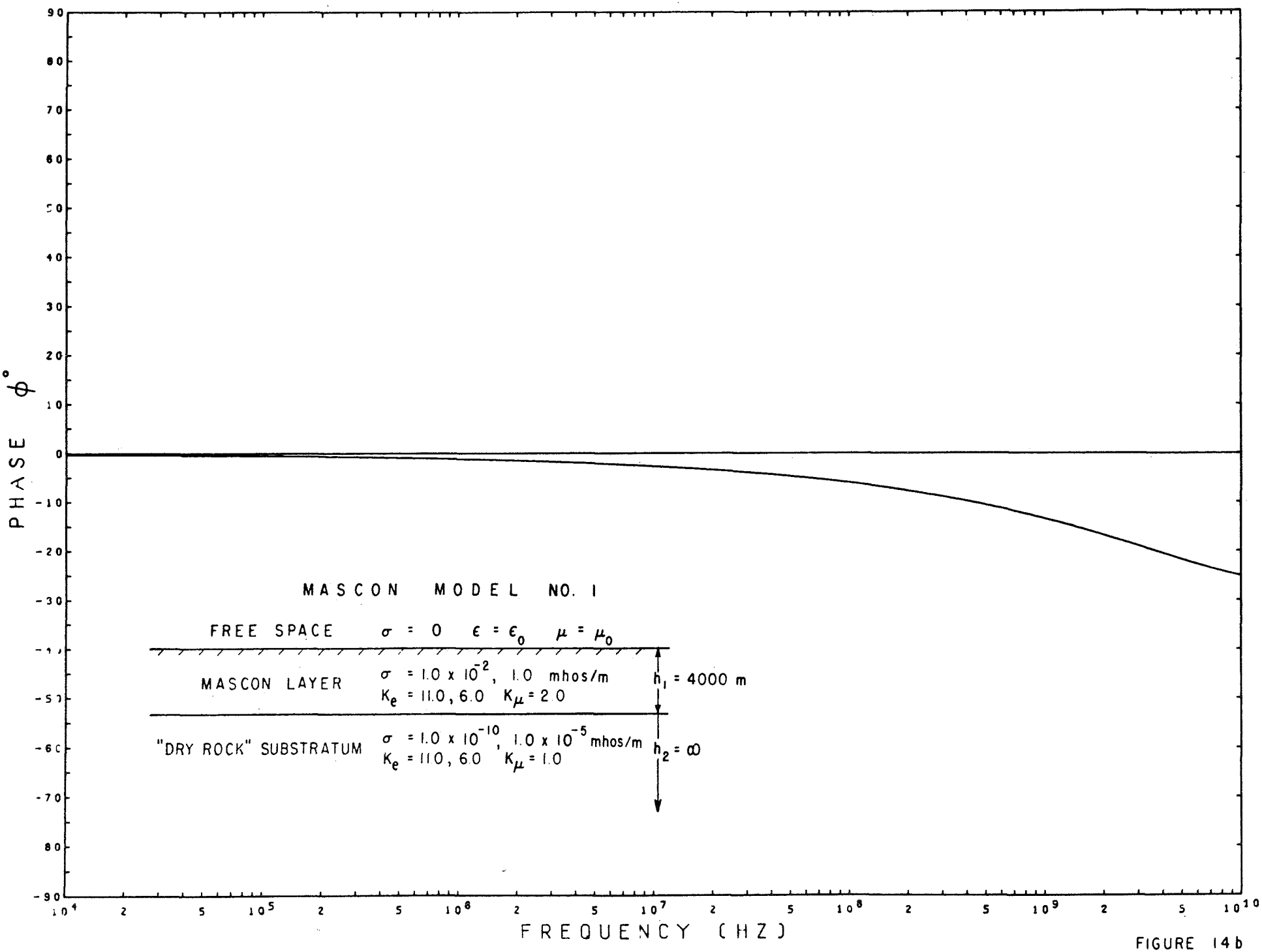
PHASE φ°
90
80
70
60
50
40
30
20
10
0
-10
-20
-30
-40
-50
-60
-70
-80
-90
MASCON MODEL NO. 1
FREE SPACE σ = 0 ε = ε0 μ = μ0
MASCON LAYER σ = 1.0 x 10^-2, 1.0 mhos/m
Ke = 11.0, 6.0 Kμ = 2.0
h1 = 4000 m
"DRY ROCK" SUBSTRATUM σ = 1.0 x 10^-10, 1.0 x 10^-5 mhos/m
Ke = 11.0, 6.0 Kμ = 1.0
h2 = ∞
10^4 2 5 10^5 2 5 10^6 2 5 10^7 2 5 10^8 2 5 10^9 2 5 10^10
FREQUENCY (HZ)

FIGURE 14 b

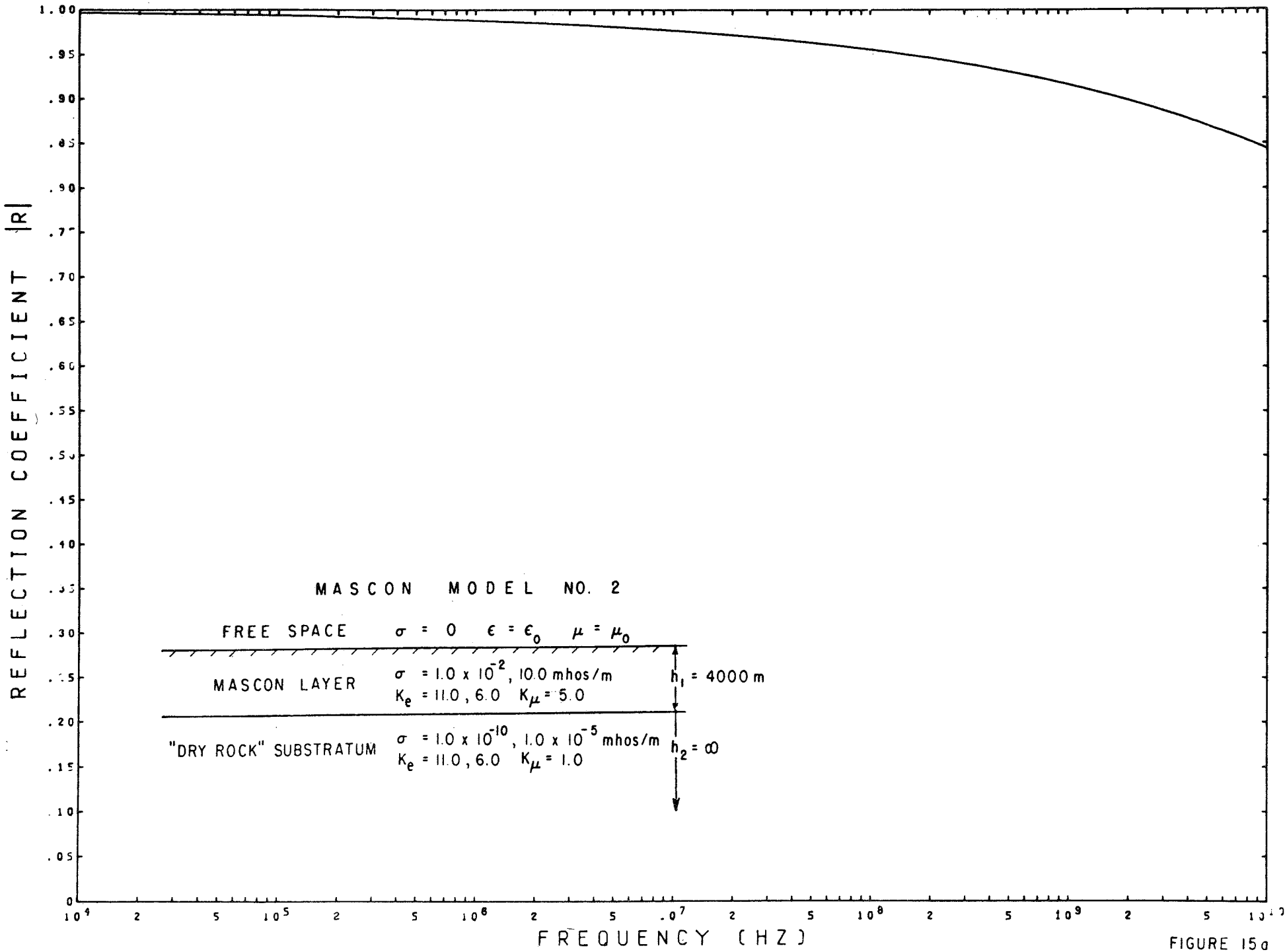
REFLECTION COEFFICIENT |R|
1.00
.95
.90
.85
.80
.75
.70
.65
.60
.55
.50
.45
.40
.35
.30
.25
.20
.15
.10
.05
0
10^4 2 5 10^5 2 5 10^6 2 5 10^7 2 5 10^8 2 5 10^9 2 5 10^{10}
FREQUENCY (HZ)
MASCON MODEL NO. 2
FREE SPACE $\sigma = 0$ $\epsilon = \epsilon_0$ $\mu = \mu_0$
MASCON LAYER $\sigma = 1.0 \times 10^{-2}$, 10.0 mhos/m
$K_\epsilon = 11.0, 6.0$ $K_\mu = 5.0$
$h_1 = 4000$ m
"DRY ROCK" SUBSTRATUM $\sigma = 1.0 \times 10^{-10}$, 1.0×10^{-5} mhos/m
$K_\epsilon = 11.0, 6.0$ $K_\mu = 1.0$
$h_2 = \infty$

FIGURE 15a

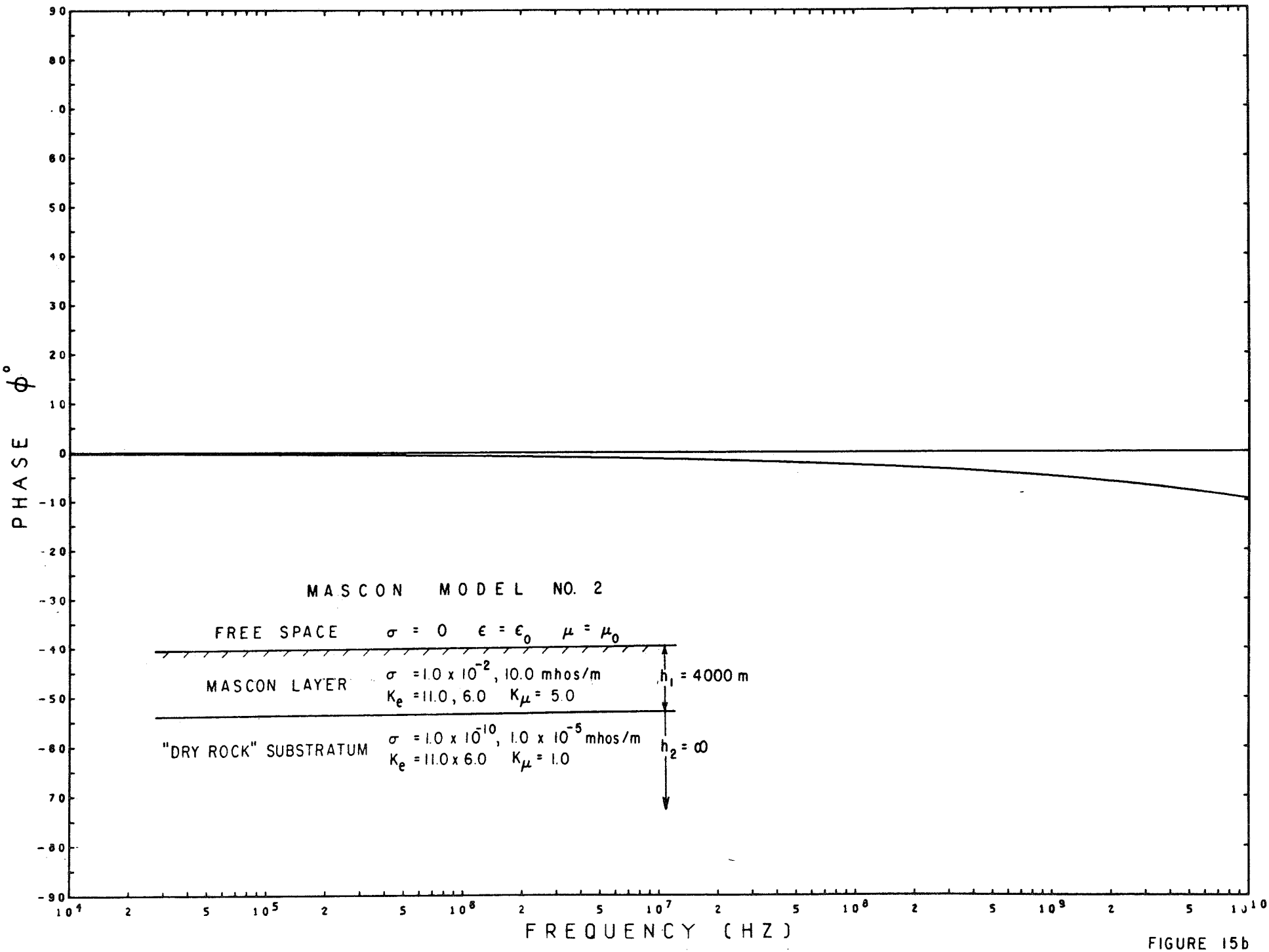
PHASE ϕ°
90
80
70
60
50
40
30
20
10
0
-10
-20
-30
-40
-50
-60
-70
-80
-90
10^4
2
5
10^5
2
5
10^6
2
5
10^7
2
5
10^8
2
5
10^9
2
5
10^{10}
FREQUENCY (HZ)
MASCON MODEL NO. 2
FREE SPACE $\sigma = 0$ $\epsilon = \epsilon_0$ $\mu = \mu_0$
MASCON LAYER $\sigma = 1.0 \times 10^{-2}$, 10.0 mhos/m
$K_e = 11.0, 6.0$ $K_\mu = 5.0$
$h_1 = 4000$ m
"DRY ROCK" SUBSTRATUM $\sigma = 1.0 \times 10^{-10}$, 1.0×10^{-5} mhos/m
$K_e = 11.0 \times 6.0$ $K_\mu = 1.0$
$h_2 = \infty$

FIGURE 15b

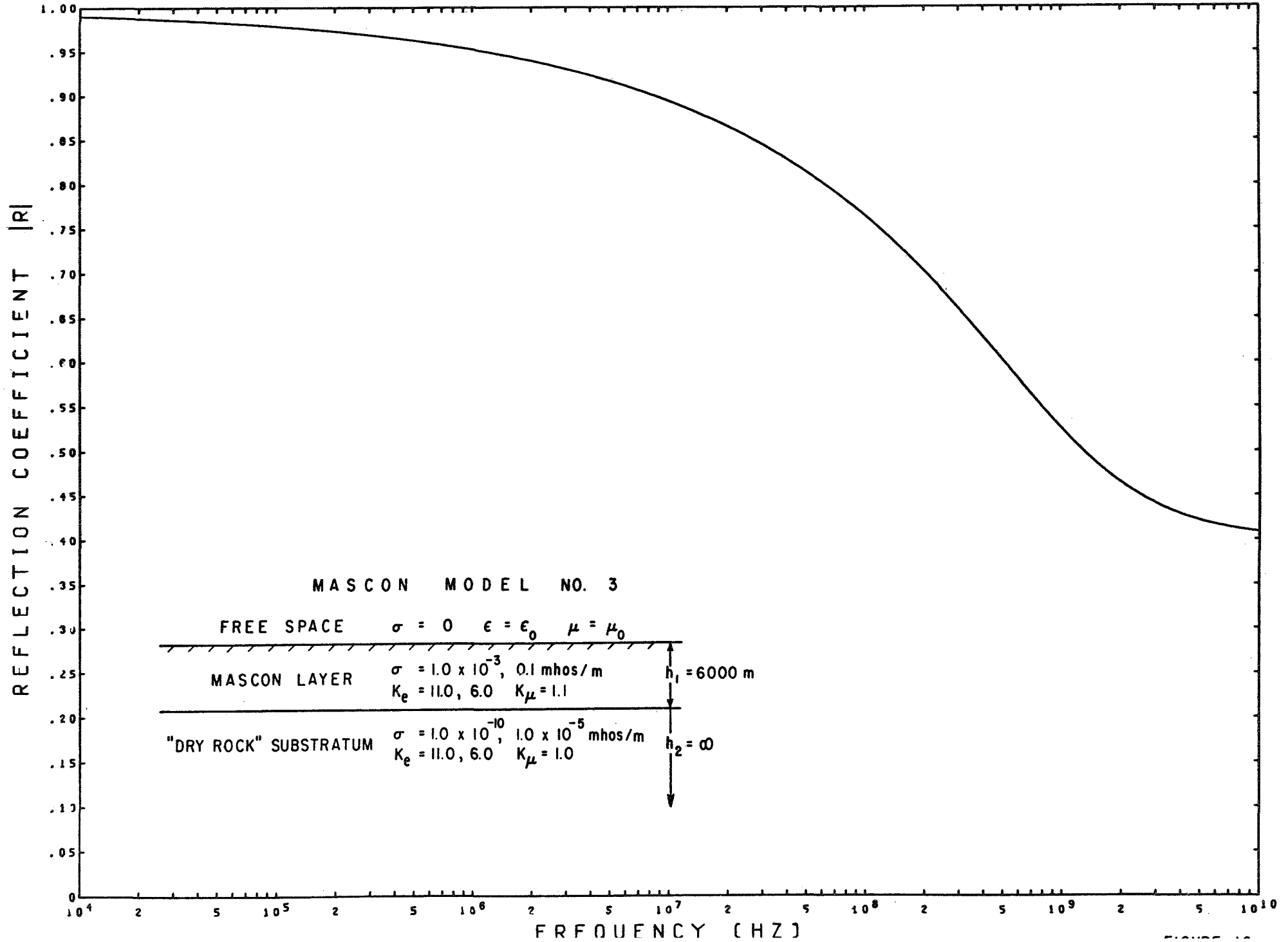
REFLECTION COEFFICIENT |R|
1.00
.95
.90
.85
.80
.75
.70
.65
.60
.55
.50
.45
.40
.35
.30
.25
.20
.15
.10
.05
0
10^4 2 5 10^5 2 5 10^6 2 5 10^7 2 5 10^8 2 5 10^9 2 5 10^{10}
FREQUENCY (HZ)
MASCON MODEL NO. 3
FREE SPACE $\sigma = 0$ $\epsilon = \epsilon_0$ $\mu = \mu_0$
MASCON LAYER $\sigma = 1.0 \times 10^{-3}$, 0.1 mhos/m
$K_e = 11.0, 6.0$ $K_\mu = 1.1$
$h_1 = 6000$ m
"DRY ROCK" SUBSTRATUM $\sigma = 1.0 \times 10^{-10}$, 1.0×10^{-5} mhos/m
$K_e = 11.0, 6.0$ $K_\mu = 1.0$
$h_2 = \infty$

FIGURE 12

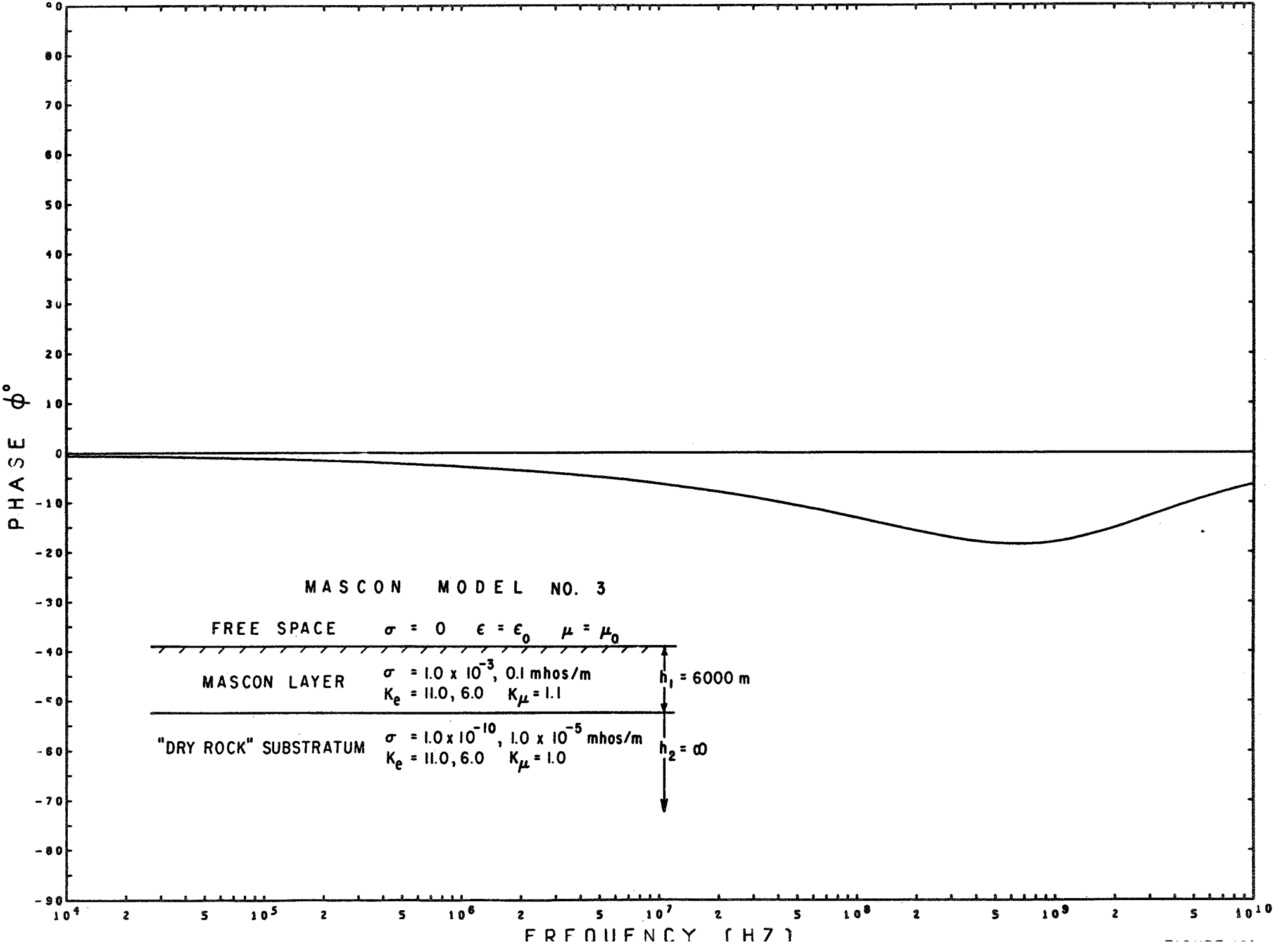
PHASE φ°
0
-10
-20
-30
-40
-50
-60
-70
-80
-90
MASCON MODEL NO. 3
FREE SPACE σ = 0 ε = ε0 μ = μ0
MASCON LAYER σ = 1.0 x 10^-3, 0.1 mhos/m
Ke = 11.0, 6.0 Kμ = 1.1
h1 = 6000 m
"DRY ROCK" SUBSTRATUM σ = 1.0 x 10^-10, 1.0 x 10^-5 mhos/m
Ke = 11.0, 6.0 Kμ = 1.0
h2 = ∞
10^4 2 5 10^5 2 5 10^6 2 5 10^7 2 5 10^8 2 5 10^9 2 5 10^10
FREQUENCY (HZ)

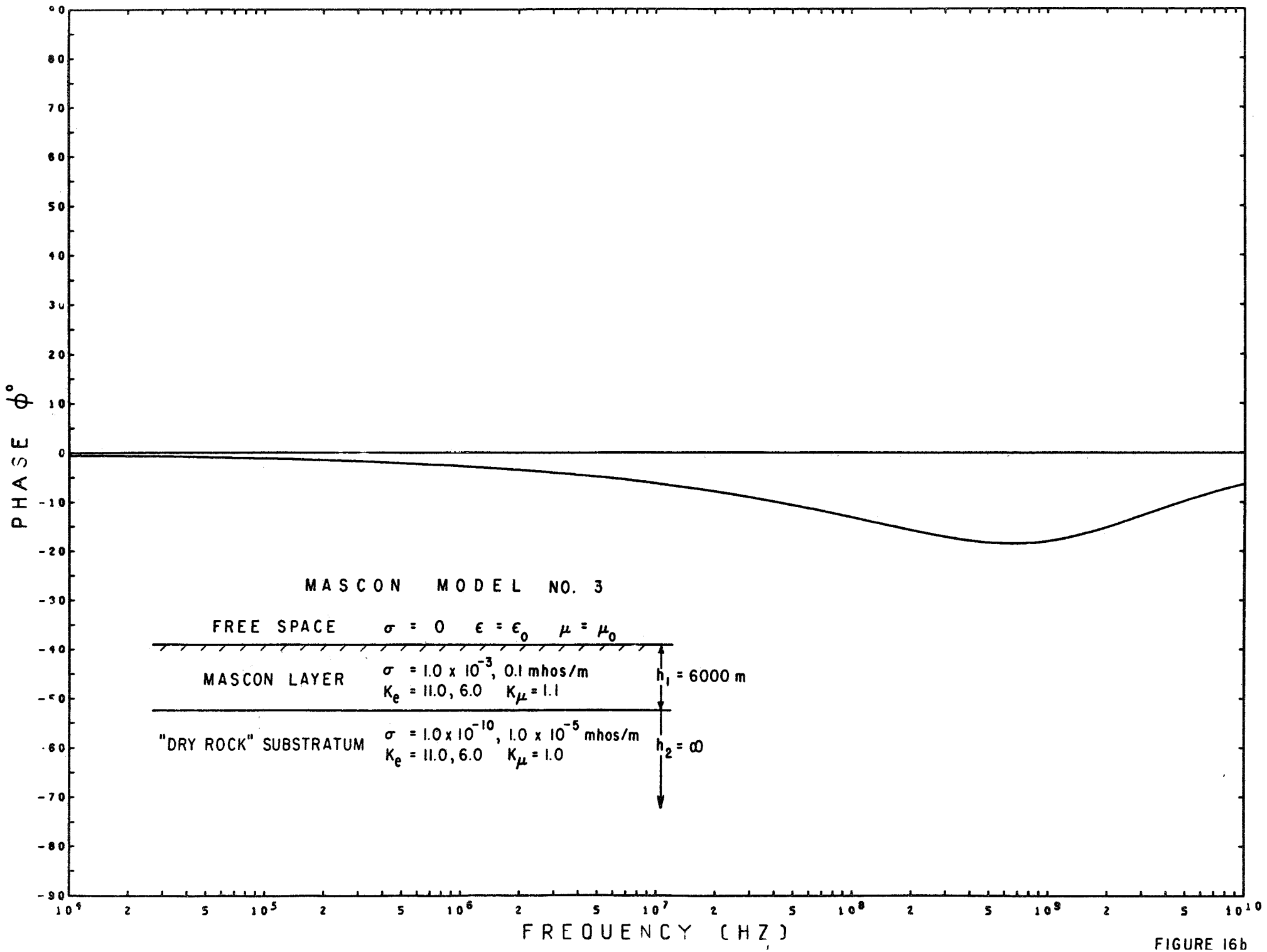
PHASE φ°
0
-10
-20
-30
-40
-50
-60
-70
-80
-90
MASCON MODEL NO. 3
FREE SPACE σ = 0 ε = ε0 μ = μ0
MASCON LAYER σ = 1.0 x 10^-3, 0.1 mhos/m
Ke = 11.0, 6.0 Kμ = 1.1
h1 = 6000 m
"DRY ROCK" SUBSTRATUM σ = 1.0 x 10^-10, 1.0 x 10^-5 mhos/m
Ke = 11.0, 6.0 Kμ = 1.0
h2 = ∞
10^4 2 5 10^5 2 5 10^6 2 5 10^7 2 5 10^8 2 5 10^9 2 5 10^10
FREQUENCY (HZ)

FIGURE 16b

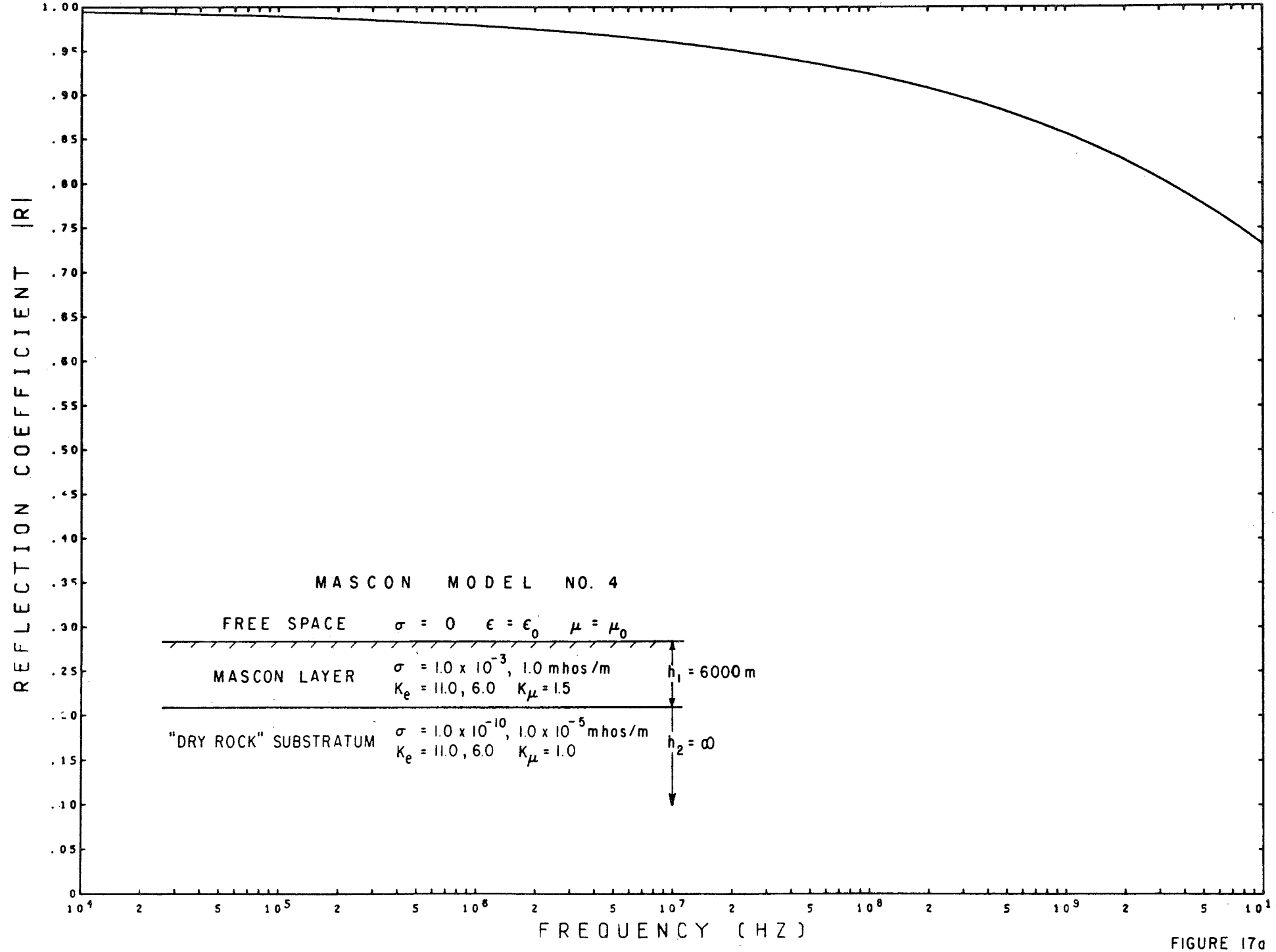
REFLECTION COEFFICIENT |R|
1.00
.95
.90
.85
.80
.75
.70
.65
.60
.55
.50
.45
.40
.35
.30
.25
.20
.15
.10
.05
0
10^4 2 5 10^5 2 5 10^6 2 5 10^7 2 5 10^8 2 5 10^9 2 5 10^{10}
FREQUENCY (HZ)
MASCON MODEL NO. 4
FREE SPACE $\sigma = 0$ $\epsilon = \epsilon_0$ $\mu = \mu_0$
MASCON LAYER $\sigma = 1.0 \times 10^{-3}$, 1.0 mhos/m
$K_e = 11.0, 6.0$ $K_\mu = 1.5$
$h_1 = 6000$ m
"DRY ROCK" SUBSTRATUM $\sigma = 1.0 \times 10^{-10}$, 1.0×10^{-5} mhos/m
$K_e = 11.0, 6.0$ $K_\mu = 1.0$
$h_2 = \infty$

FIGURE 17a

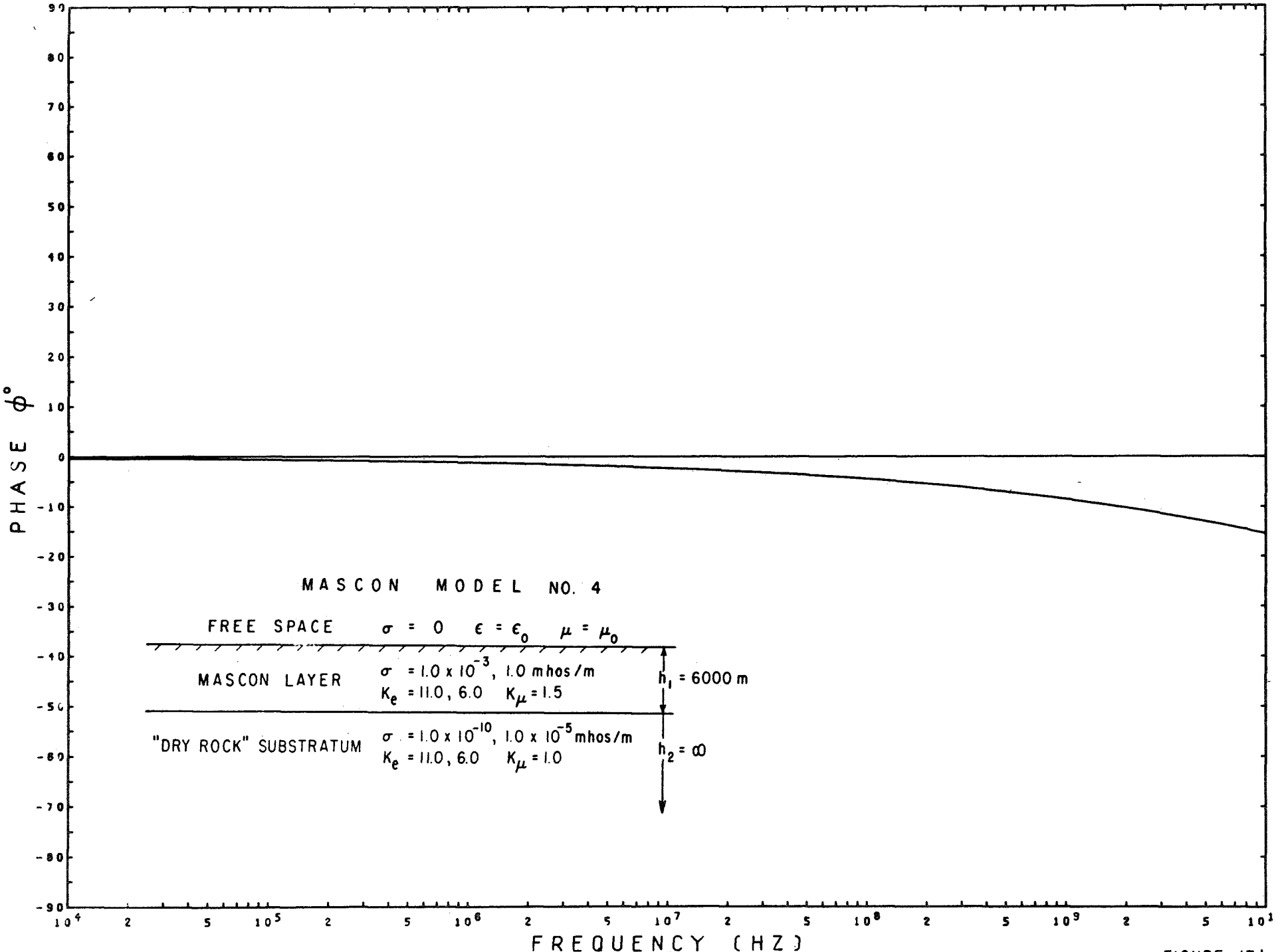
PHASE $\phi°$
90
80
70
60
50
40
30
20
10
0
-10
-20
-30
-40
-50
-60
-70
-80
-90
MASCON MODEL NO. 4
FREE SPACE $\sigma = 0$ $\epsilon = \epsilon_0$ $\mu = \mu_0$
MASCON LAYER $\sigma = 1.0 \times 10^{-3}$, 1.0 mhos/m
$K_e = 11.0, 6.0$ $K_\mu = 1.5$
$h_1 = 6000$ m
"DRY ROCK" SUBSTRATUM $\sigma = 1.0 \times 10^{-10}$, 1.0×10^{-5} mhos/m
$K_e = 11.0, 6.0$ $K_\mu = 1.0$
$h_2 = \infty$
10^4 2 5 10^5 2 5 10^6 2 5 10^7 2 5 10^8 2 5 10^9 2 5 10^{10}
FREQUENCY (HZ)

FIGURE 17b

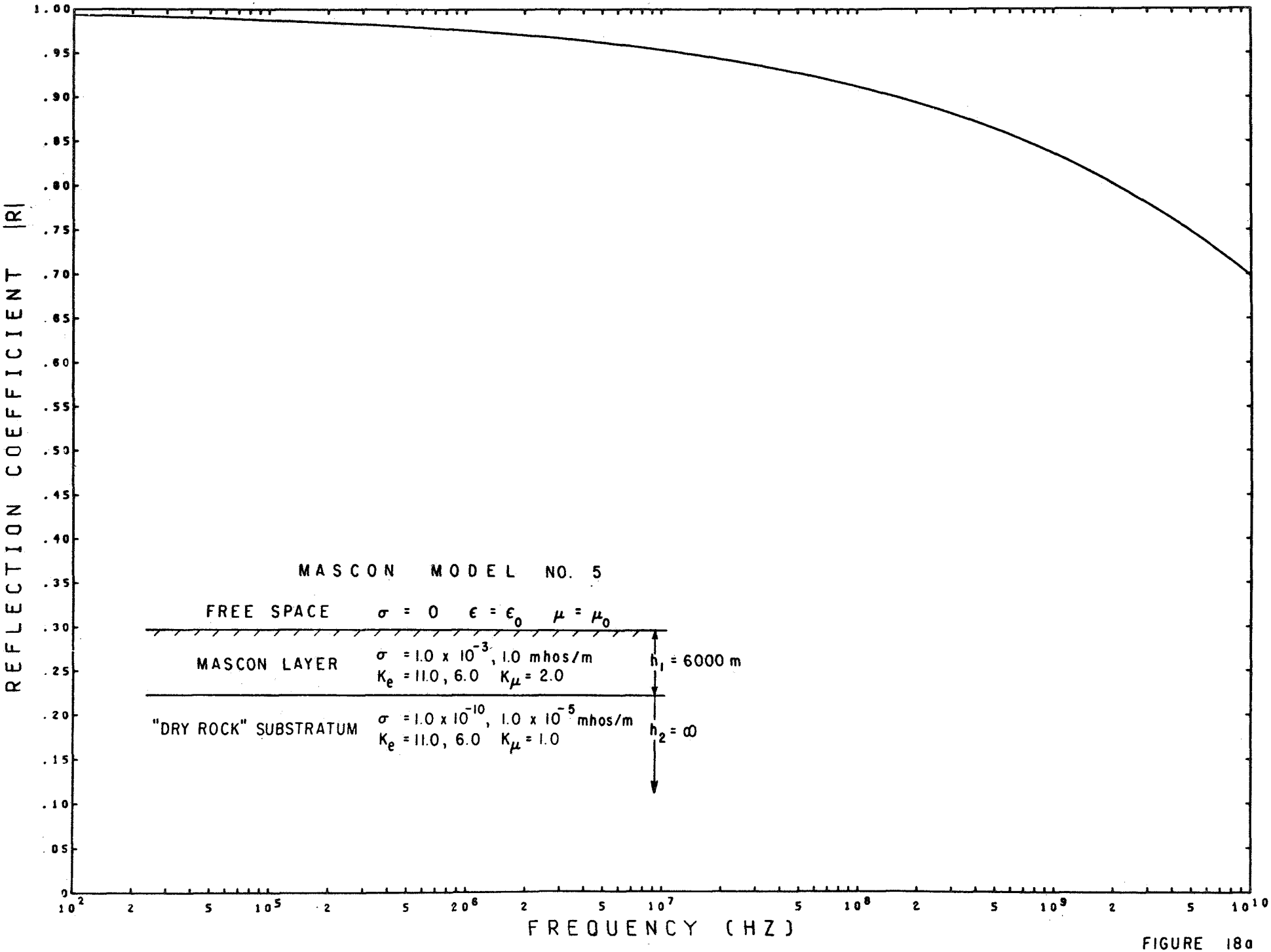
REFLECTION COEFFICIENT |R|
1.00
.95
.90
.85
.80
.75
.70
.65
.60
.55
.50
.45
.40
.35
.30
.25
.20
.15
.10
.05
0
10^2 2 5 10^3 2 5 10^4 2 5 10^5 2 5 10^6 2 5 10^7 5 10^8 2 5 10^9 2 5 10^{10}
FREQUENCY (HZ)
MASCON MODEL NO. 5
FREE SPACE $\sigma = 0$ $\epsilon = \epsilon_0$ $\mu = \mu_0$
MASCON LAYER $\sigma = 1.0 \times 10^{-3}$, 1.0 mhos/m
$K_e = 11.0, 6.0$ $K_\mu = 2.0$
$h_1 = 6000$ m
"DRY ROCK" SUBSTRATUM $\sigma = 1.0 \times 10^{-10}$, 1.0×10^{-5} mhos/m
$K_e = 11.0, 6.0$ $K_\mu = 1.0$
$h_2 = \infty$

FIGURE 18a

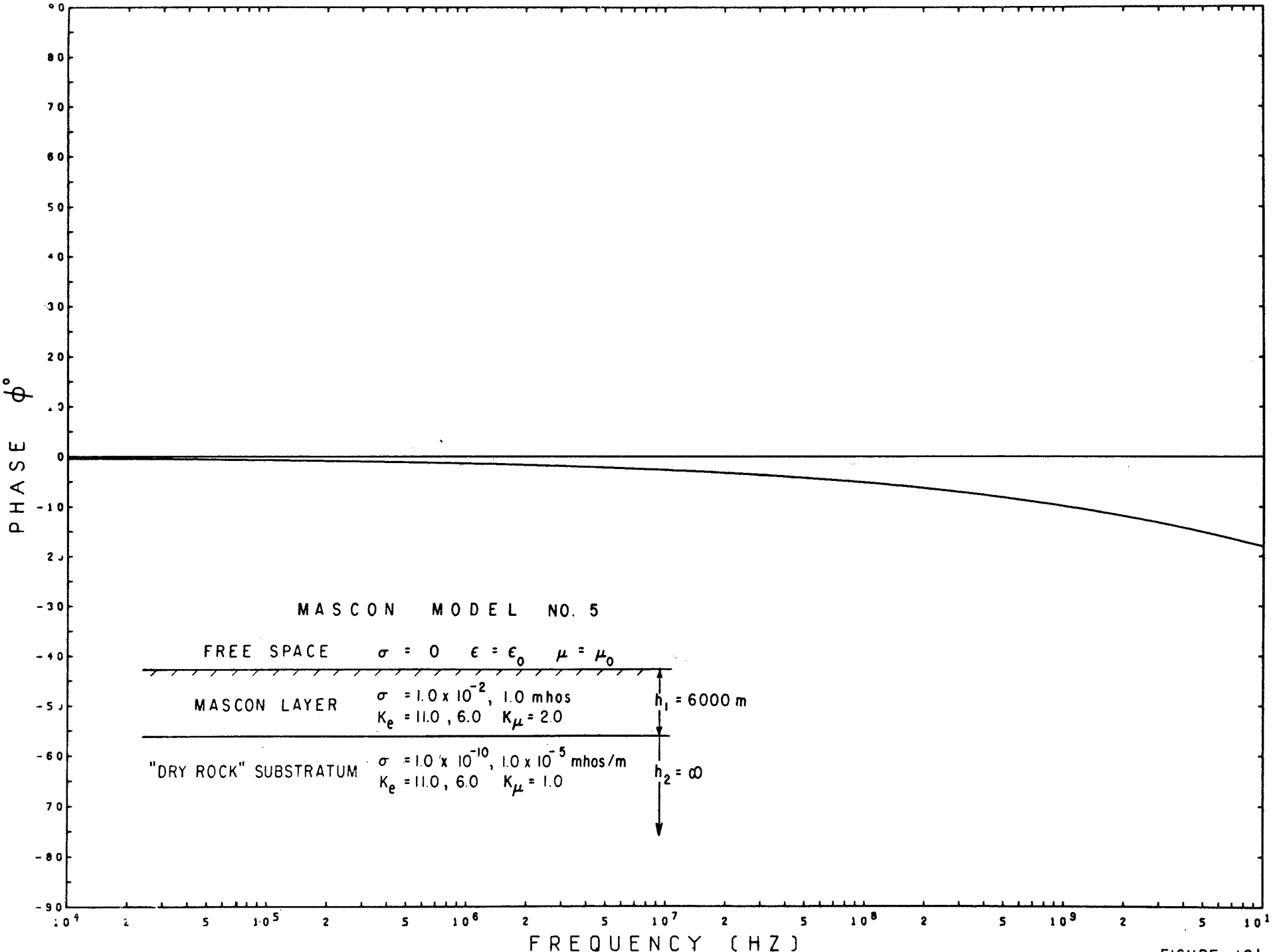
PHASE φ°
FREQUENCY (HZ)
MASCON MODEL NO. 5
FREE SPACE σ = 0 ε = ε0 μ = μ0
MASCON LAYER σ = 1.0 x 10^-2, 1.0 mhos
Ke = 11.0, 6.0 Kμ = 2.0
h1 = 6000 m
"DRY ROCK" SUBSTRATUM σ = 1.0 x 10^-10, 1.0 x 10^-5 mhos/m
Ke = 11.0, 6.0 Kμ = 1.0
h2 = ∞

FIGURE 18b

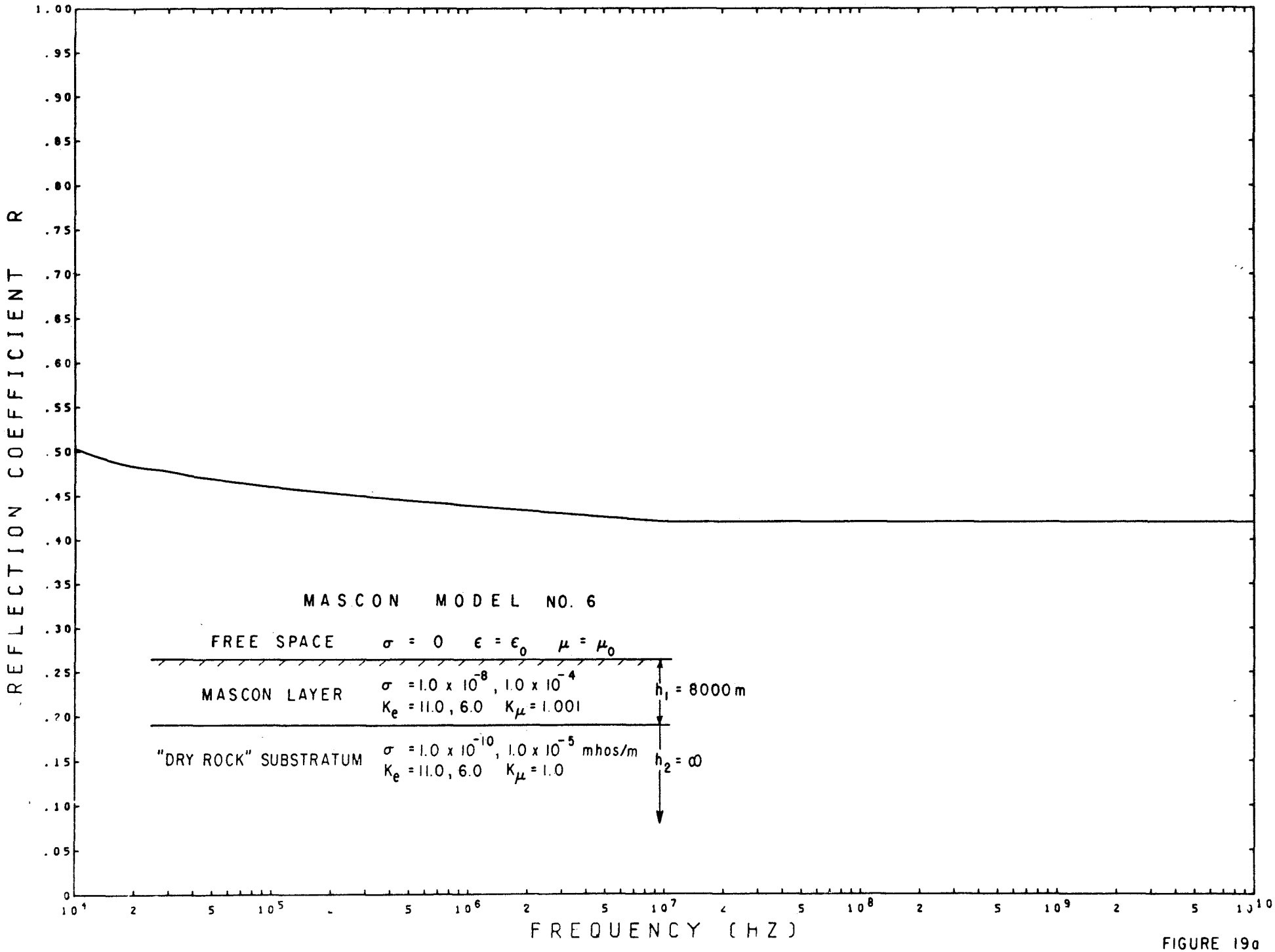
REFLECTION COEFFICIENT R
1.00
.95
.90
.85
.80
.75
.70
.65
.60
.55
.50
.45
.40
.35
.30
.25
.20
.15
.10
.05
0
MASCON MODEL NO. 6
FREE SPACE σ = 0 ε = ε0 μ = μ0
MASCON LAYER σ = 1.0 x 10^-8, 1.0 x 10^-4
Ke = 11.0, 6.0 Kμ = 1.001
h1 = 8000 m
"DRY ROCK" SUBSTRATUM σ = 1.0 x 10^-10, 1.0 x 10^-5 mhos/m
Ke = 11.0, 6.0 Kμ = 1.0
h2 = ∞
10^4 2 5 10^5 5 10^6 2 5 10^7 2 5 10^8 2 5 10^9 2 5 10^10
FREQUENCY (HZ)

FIGURE 19a

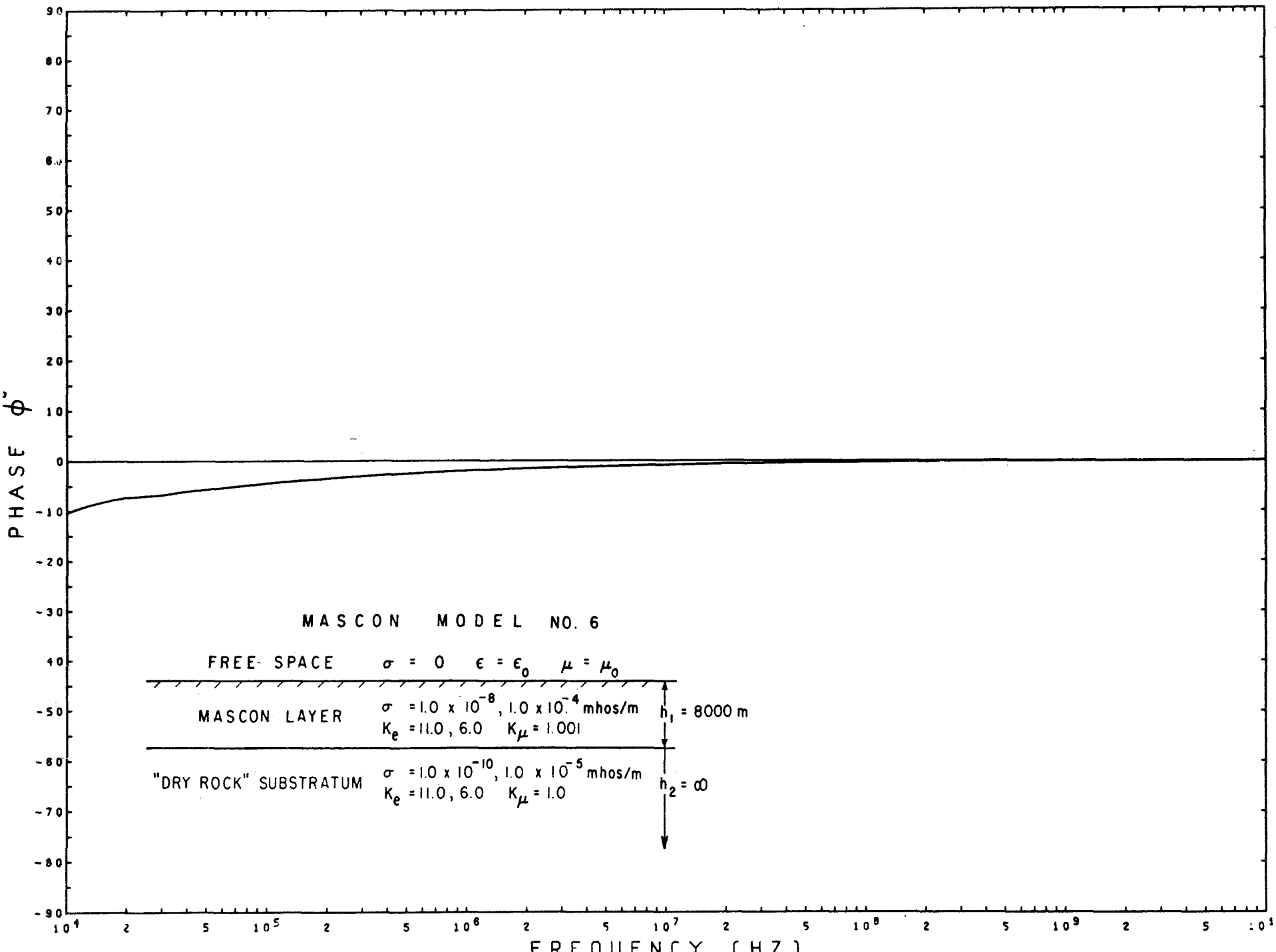
PHASE ϕ°
FREQUENCY (HZ)
MASCON MODEL NO. 6
FREE SPACE $\sigma = 0$ $\epsilon = \epsilon_0$ $\mu = \mu_0$
MASCON LAYER $\sigma = 1.0 \times 10^{-8}, 1.0 \times 10^{-4}$ mhos/m
$K_e = 11.0, 6.0$ $K_\mu = 1.001$
$h_1 = 8000$ m
"DRY ROCK" SUBSTRATUM $\sigma = 1.0 \times 10^{-10}, 1.0 \times 10^{-5}$ mhos/m
$K_e = 11.0, 6.0$ $K_\mu = 1.0$
$h_2 = \infty$

FIGURE 19 b

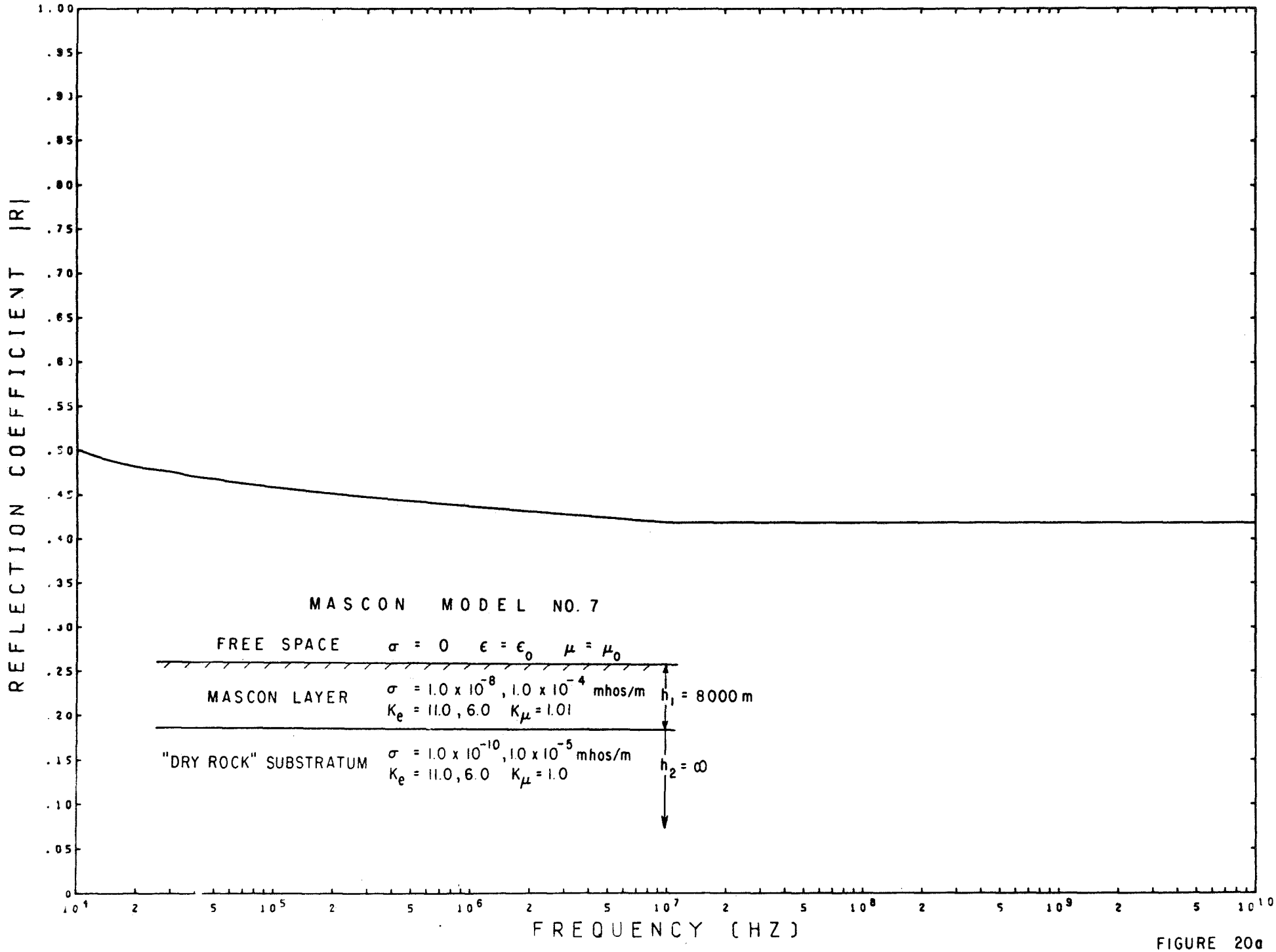
REFLECTION COEFFICIENT |R|
1.00
.95
.90
.85
.80
.75
.70
.65
.60
.55
.50
.45
.40
.35
.30
.25
.20
.15
.10
.05
0
MASCON MODEL NO. 7
FREE SPACE σ = 0 ε = ε0 μ = μ0
MASCON LAYER σ = 1.0 x 10^-8, 1.0 x 10^-4 mhos/m
Ke = 11.0, 6.0 Kμ = 1.01
h1 = 8000 m
"DRY ROCK" SUBSTRATUM σ = 1.0 x 10^-10, 1.0 x 10^-5 mhos/m
Ke = 11.0, 6.0 Kμ = 1.0
h2 = ∞
10^4 2 5 10^5 2 5 10^6 2 5 10^7 2 5 10^8 2 5 10^9 2 5 10^10
FREQUENCY (HZ)

FIGURE 20a

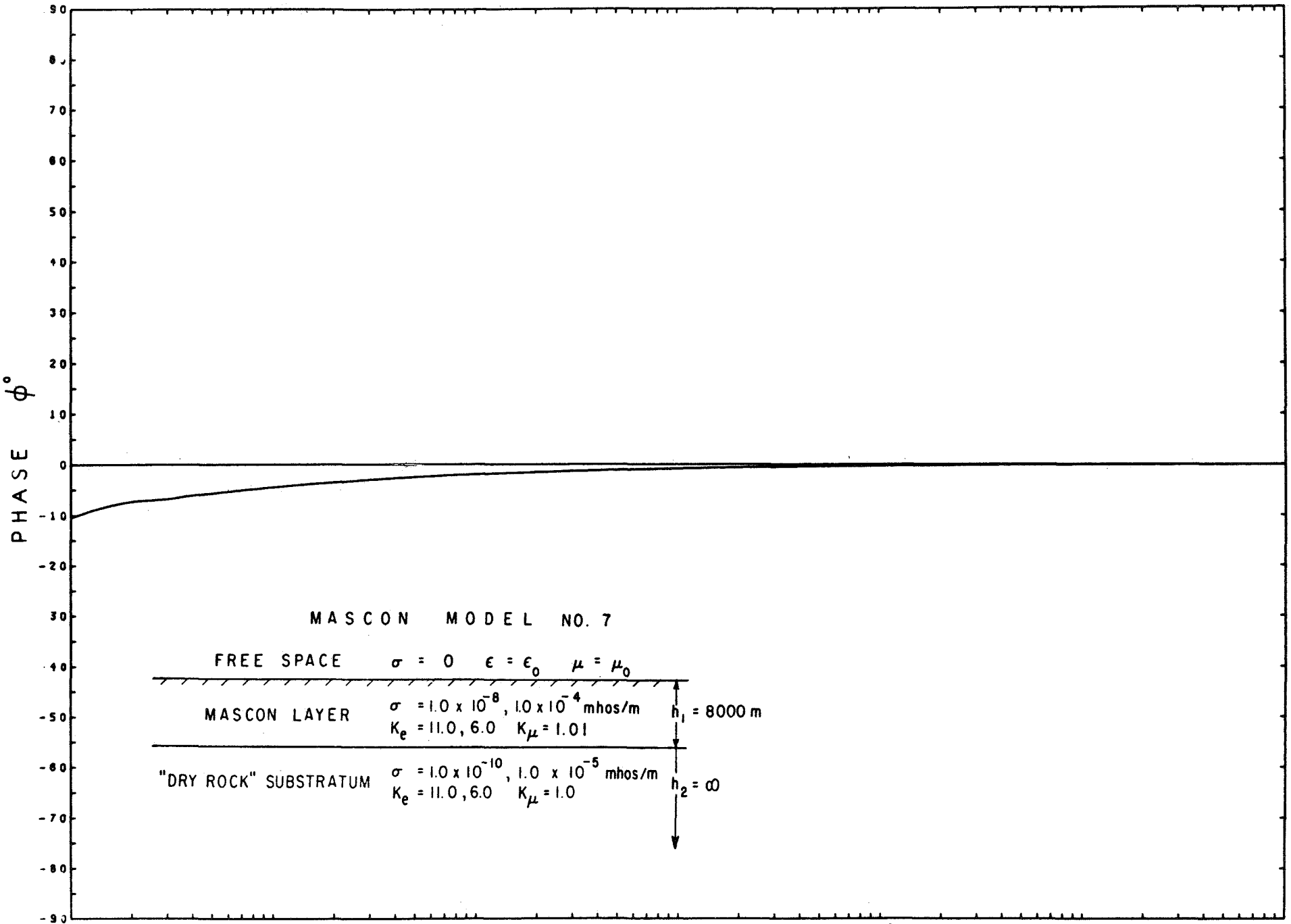
PHASE ϕ°
90
80
70
60
50
40
30
20
10
0
-10
-20
-30
-40
-50
-60
-70
-80
-90
MASCON MODEL NO. 7
FREE SPACE $\sigma = 0$ $\epsilon = \epsilon_0$ $\mu = \mu_0$
MASCON LAYER $\sigma = 1.0 \times 10^{-8}, 1.0 \times 10^{-4}$ mhos/m
$K_e = 11.0, 6.0$ $K_\mu = 1.01$
$h_1 = 8000$ m
"DRY ROCK" SUBSTRATUM $\sigma = 1.0 \times 10^{-10}, 1.0 \times 10^{-5}$ mhos/m
$K_e = 11.0, 6.0$ $K_\mu = 1.0$
$h_2 = \infty$
10^4 2 5 10^5 2 5 10^6 2 5 10^7 2 5 10^8 2 5 10^9 2 5 10^{10}
FREQUENCY (HZ)

FIGURE 20b

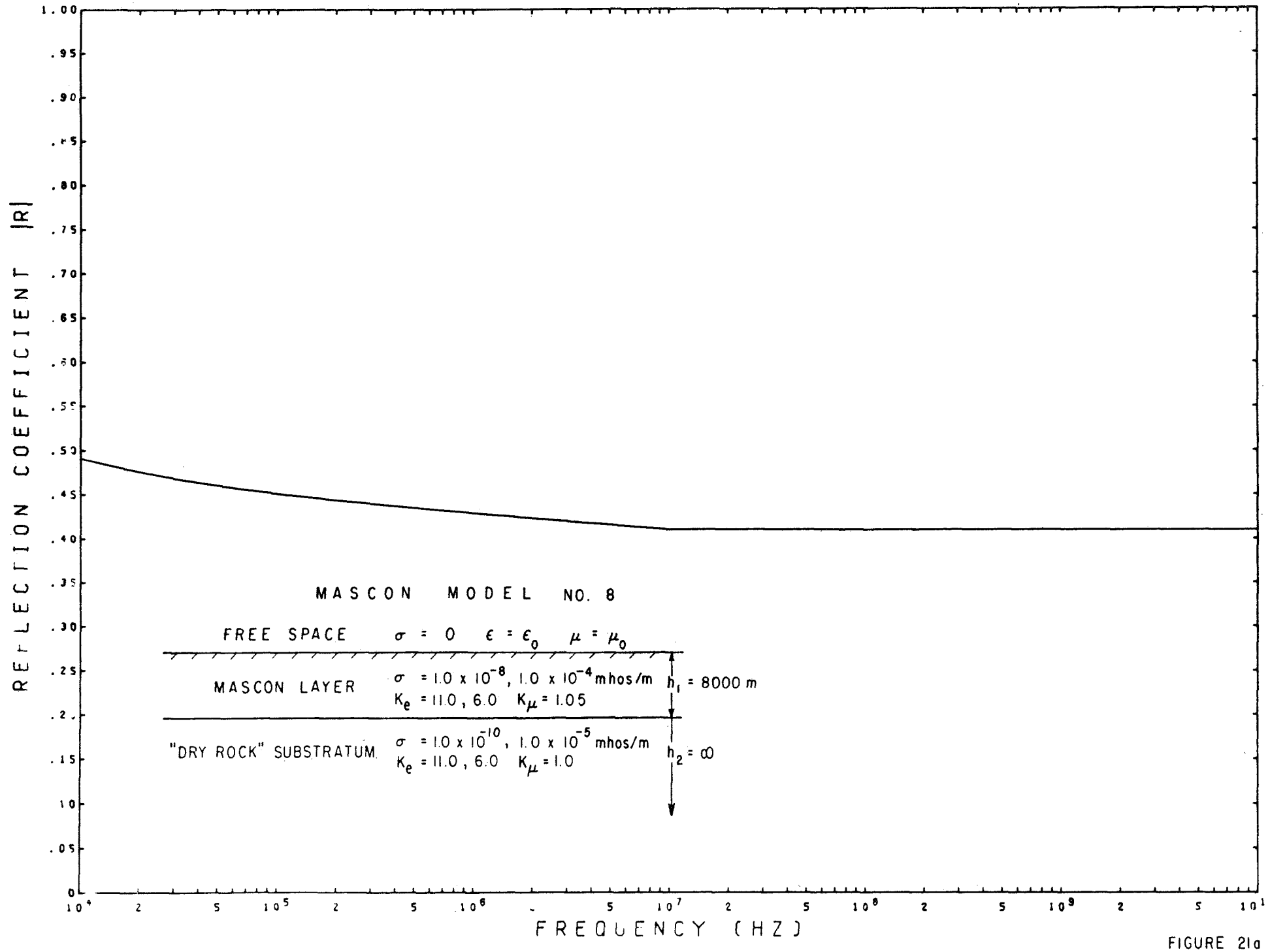
REFLECTION COEFFICIENT |R|
1.00
.95
.90
.85
.80
.75
.70
.65
.60
.55
.50
.45
.40
.35
.30
.25
.20
.15
.10
.05
0
MASCON MODEL NO. 8
FREE SPACE σ = 0 ε = ε0 μ = μ0
MASCON LAYER σ = 1.0 x 10^-8, 1.0 x 10^-4 mhos/m
Ke = 11.0, 6.0 Kμ = 1.05
h1 = 8000 m
"DRY ROCK" SUBSTRATUM σ = 1.0 x 10^-10, 1.0 x 10^-5 mhos/m
Ke = 11.0, 6.0 Kμ = 1.0
h2 = ∞
10^4 2 5 10^5 2 5 10^6 5 10^7 2 5 10^8 2 5 10^9 2 5 10^10
FREQUENCY (HZ)

FIGURE 21a

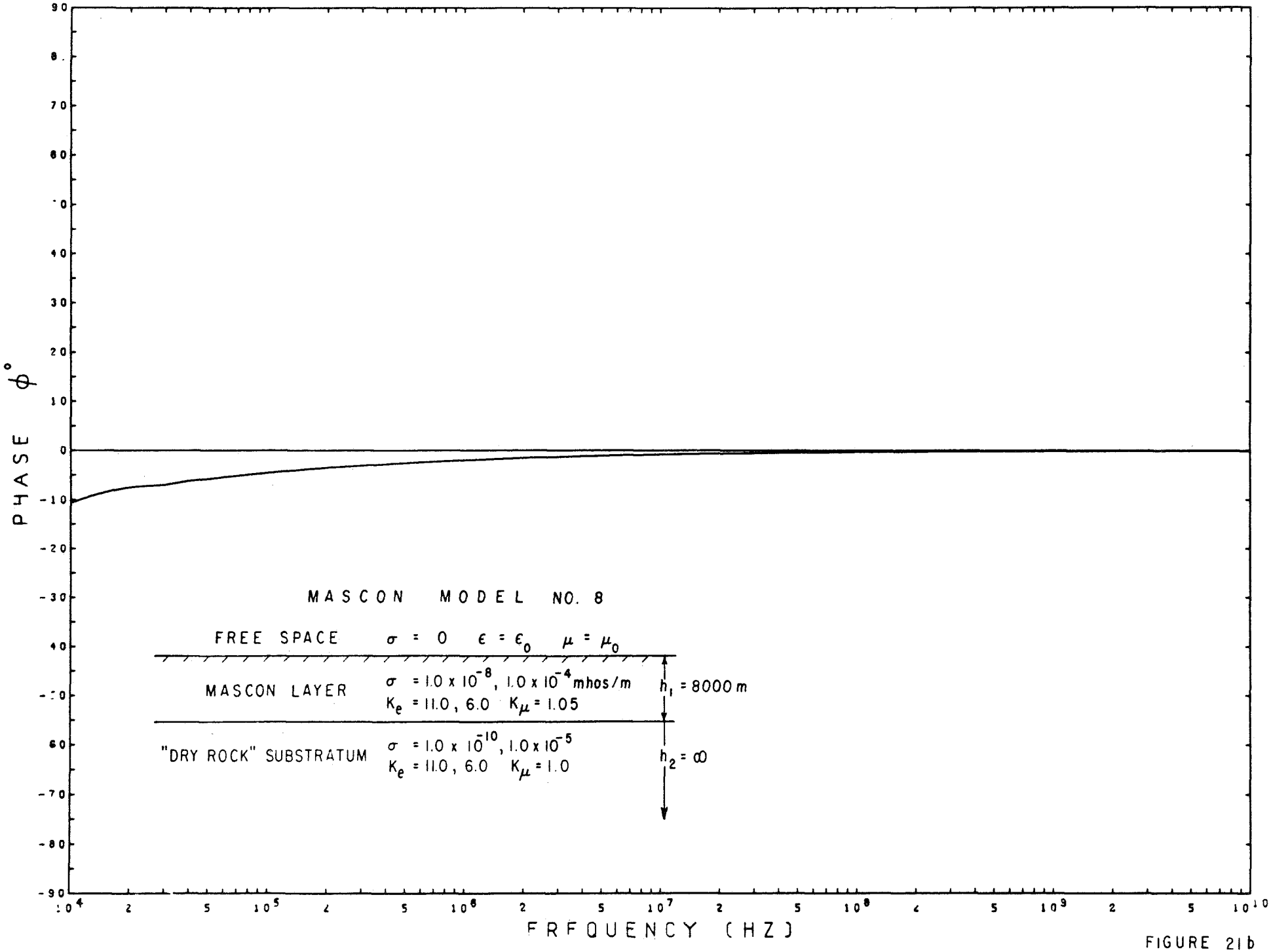
PHASE φ°
90
80
70
60
50
40
30
20
10
0
-10
-20
-30
-40
-50
-60
-70
-80
-90
MASCON MODEL NO. 8
FREE SPACE σ = 0 ε = ε0 μ = μ0
MASCON LAYER σ = 1.0 x 10^-8, 1.0 x 10^-4 mhos/m
Ke = 11.0, 6.0 Kμ = 1.05
h1 = 8000 m
"DRY ROCK" SUBSTRATUM σ = 1.0 x 10^-10, 1.0 x 10^-5
Ke = 11.0, 6.0 Kμ = 1.0
h2 = ∞
10^4 2 5 10^5 2 5 10^6 2 5 10^7 2 5 10^8 2 5 10^9 2 5 10^10
FREQUENCY (HZ)

FIGURE 21b

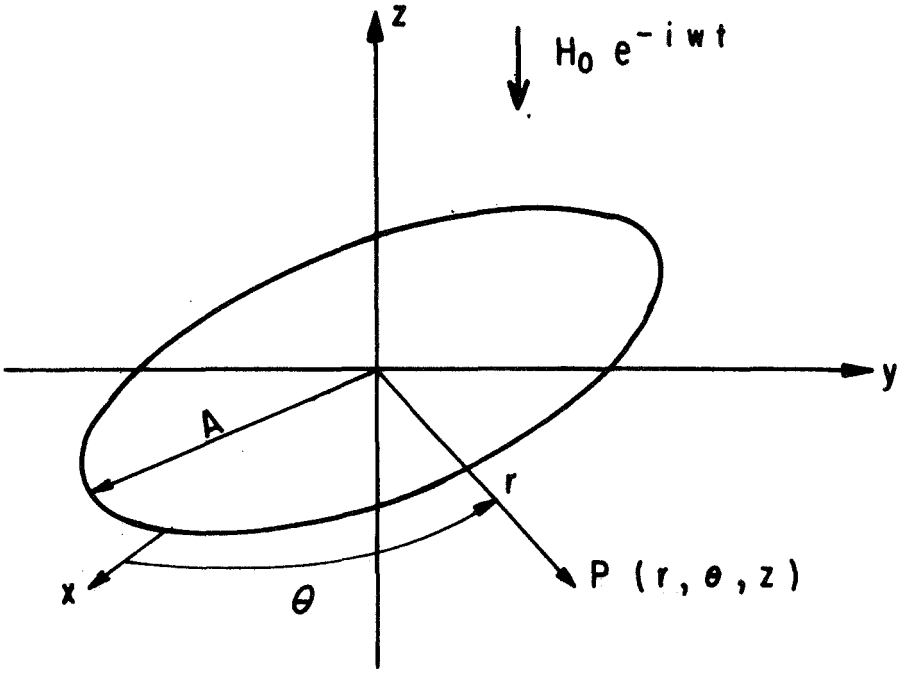

FIG. 22 A PERFECTLY CONDUCTING, INFINITESIMALLY THIN DISK OF RADIUS "A" IN A UNIFORM HARMONICALLY VARYING FIELD, FREQUENCY ω; $r^2 = x^2 + y^2$.

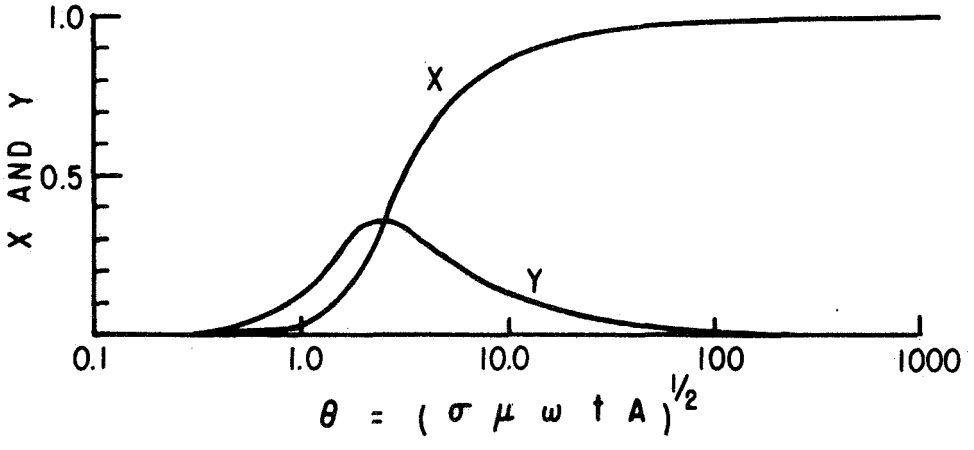

FIG. 23 ESTIMATED IN-PHASE X AND QUADRATURE Y RESPONSE OF A DISK IN A UNIFORM FIELD AS FUNCTIONS OF THE INDUCTION NUMBER θ

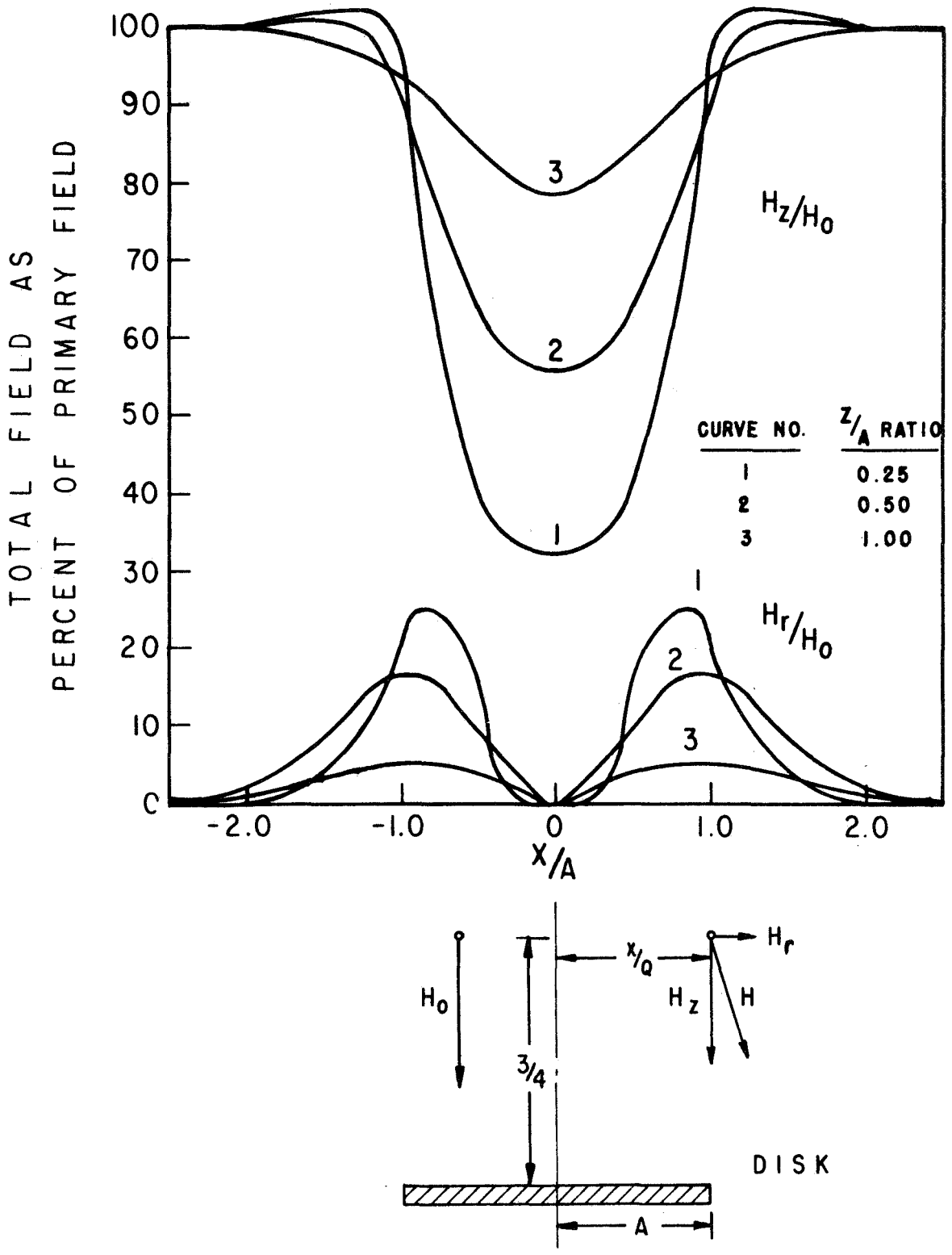

FIG. 24 FIELD COMPONENTS H_z/H_0 AND H_r/H_0 OVER HORIZONTAL DISK AS PERCENT OF NORMALLY INCIDENT PRIMARY FIELD.

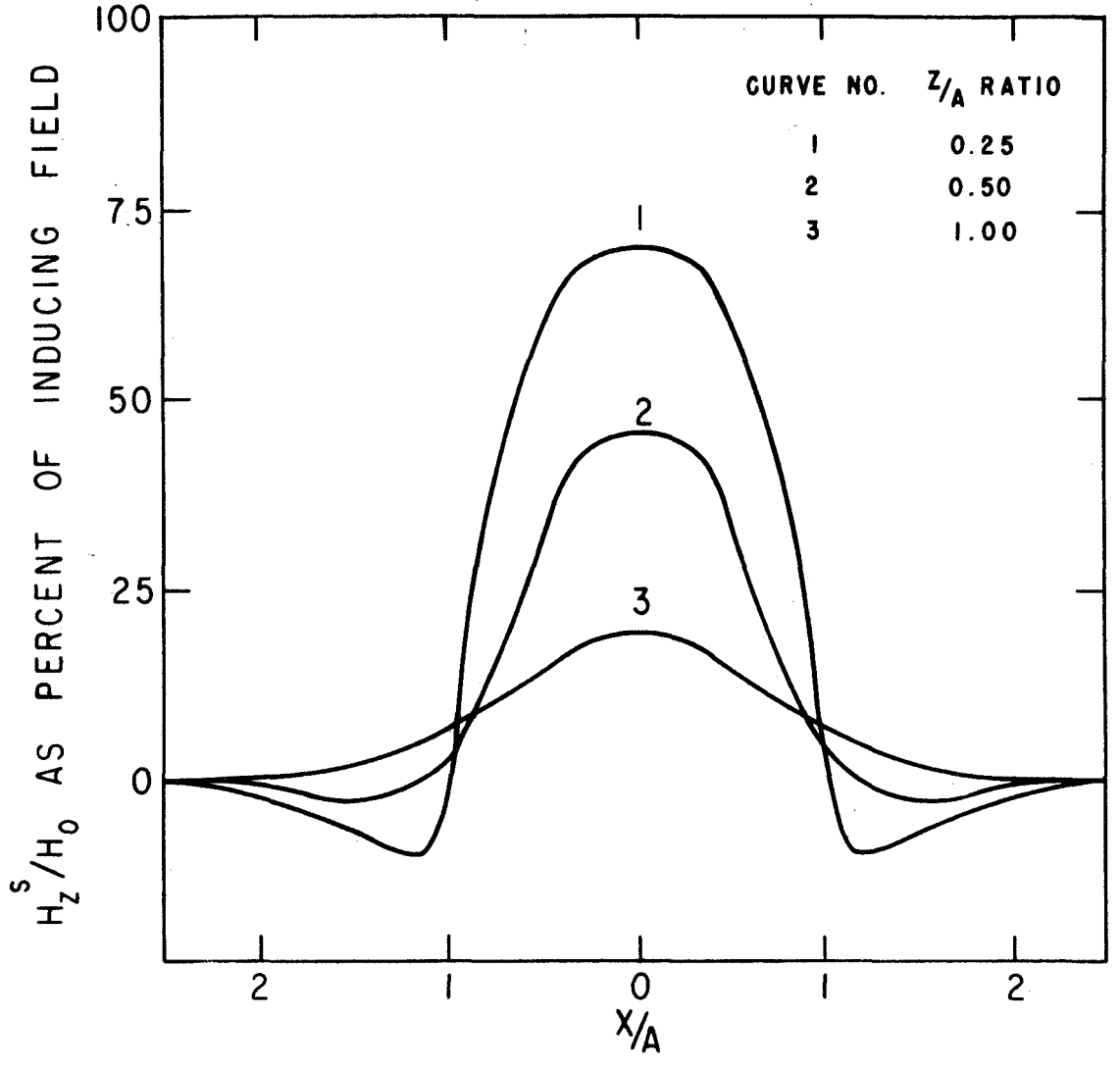

FIG. 25 SECONDARY VERTICAL MAGNETIC FIELD AS PERCENT OF INDUCING FIELD. Z/A IS VERTICAL OBSERVATION DISTANCE NORMALIZED TO DISK RADIUS AND X/A IS NORMALIZED TRAVERSE DISTANCE.

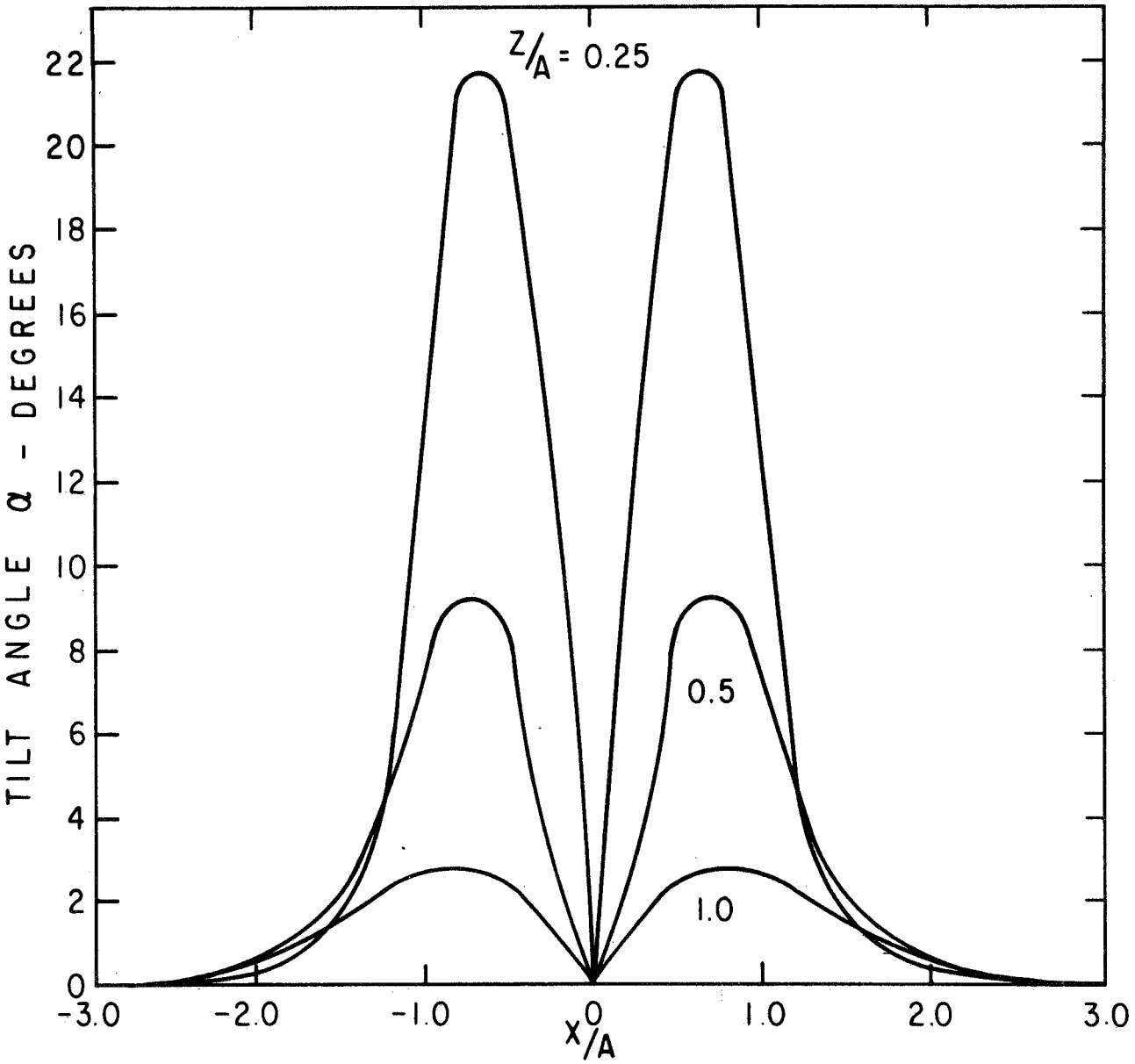

FIG. 26 TILT ANGLE PROFILES OVER HORIZONTAL DISK IN NORMALLY INCIDENT PRIMARY FIELD.

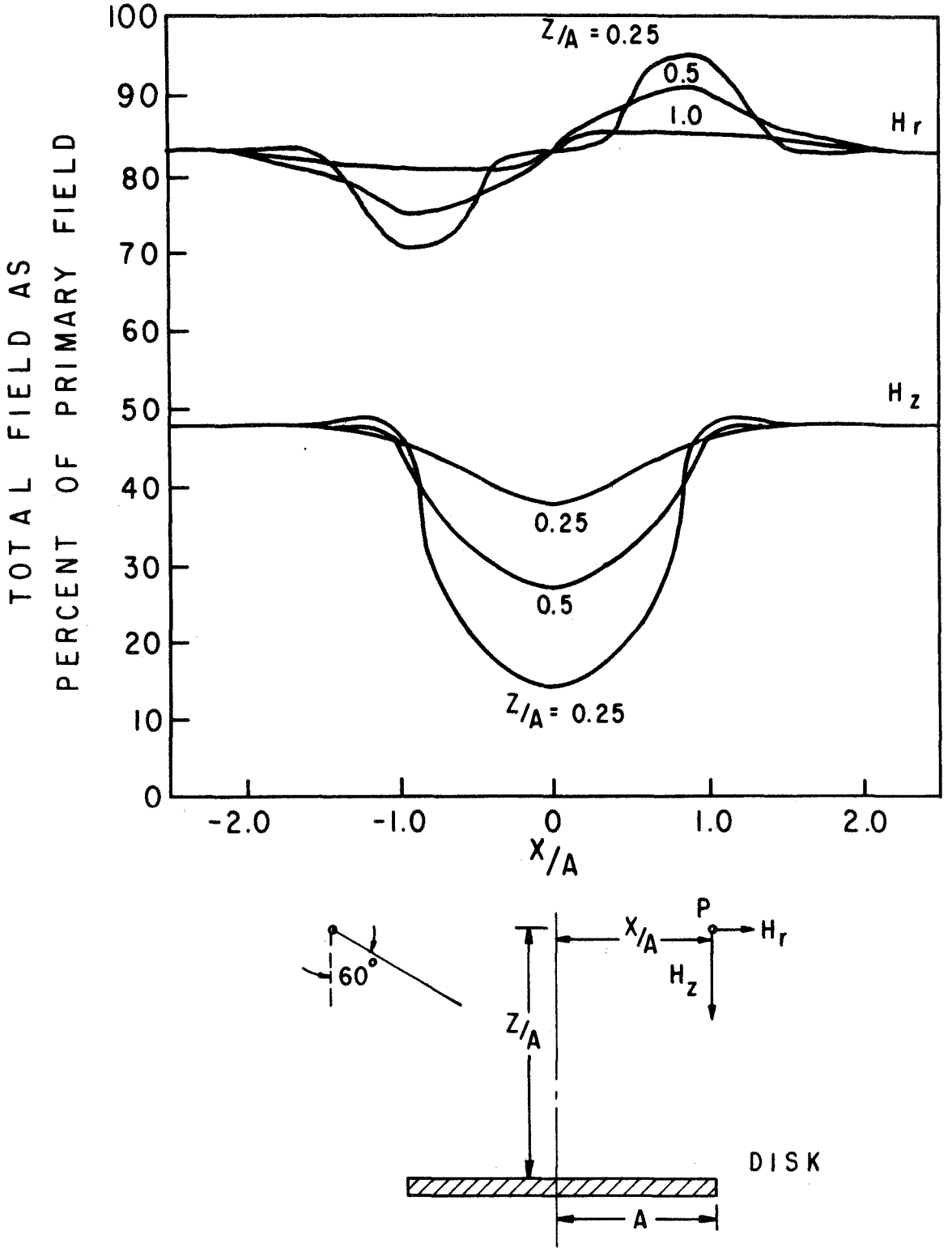

FIG. 27 FIELDS ABOUT A HORIZONTAL DISK IN HARMONICALLY VARYING MAGNETIC FIELD, ANGLE OF INCIDENCE EQUAL TO 60° IN X-Z PLANE.

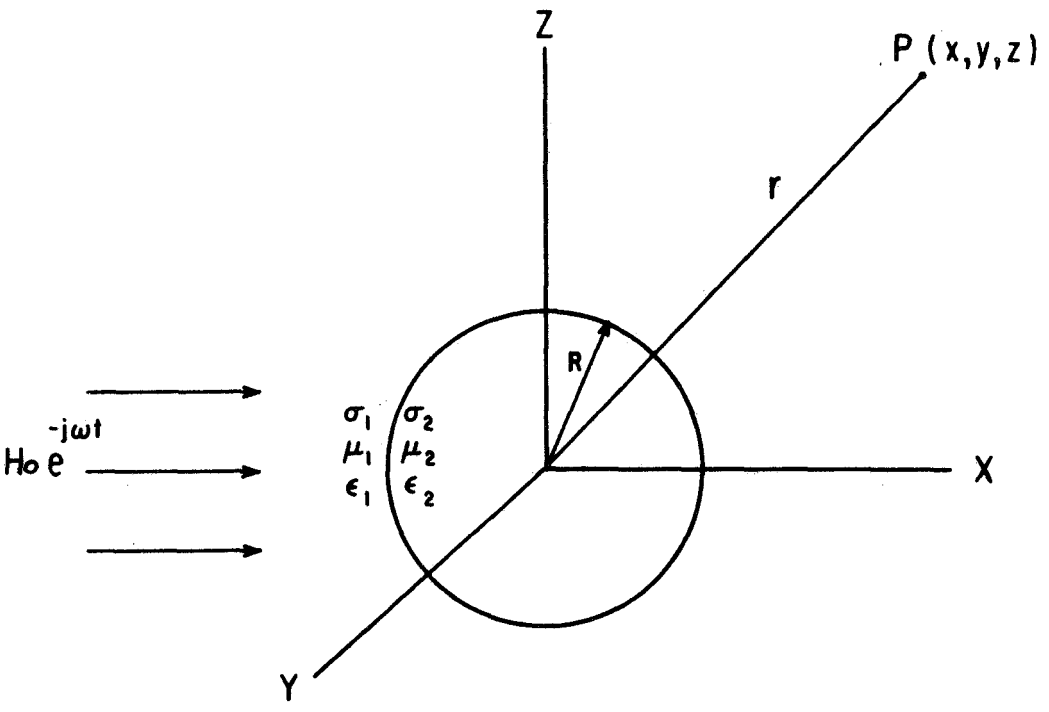

FIG. 28 A CONDUCTIVE, PERMEABLE SPHERE IN A WHOLE SPACE IN A UNIFORM TIME - VARYING MAGNETIC FIELD.

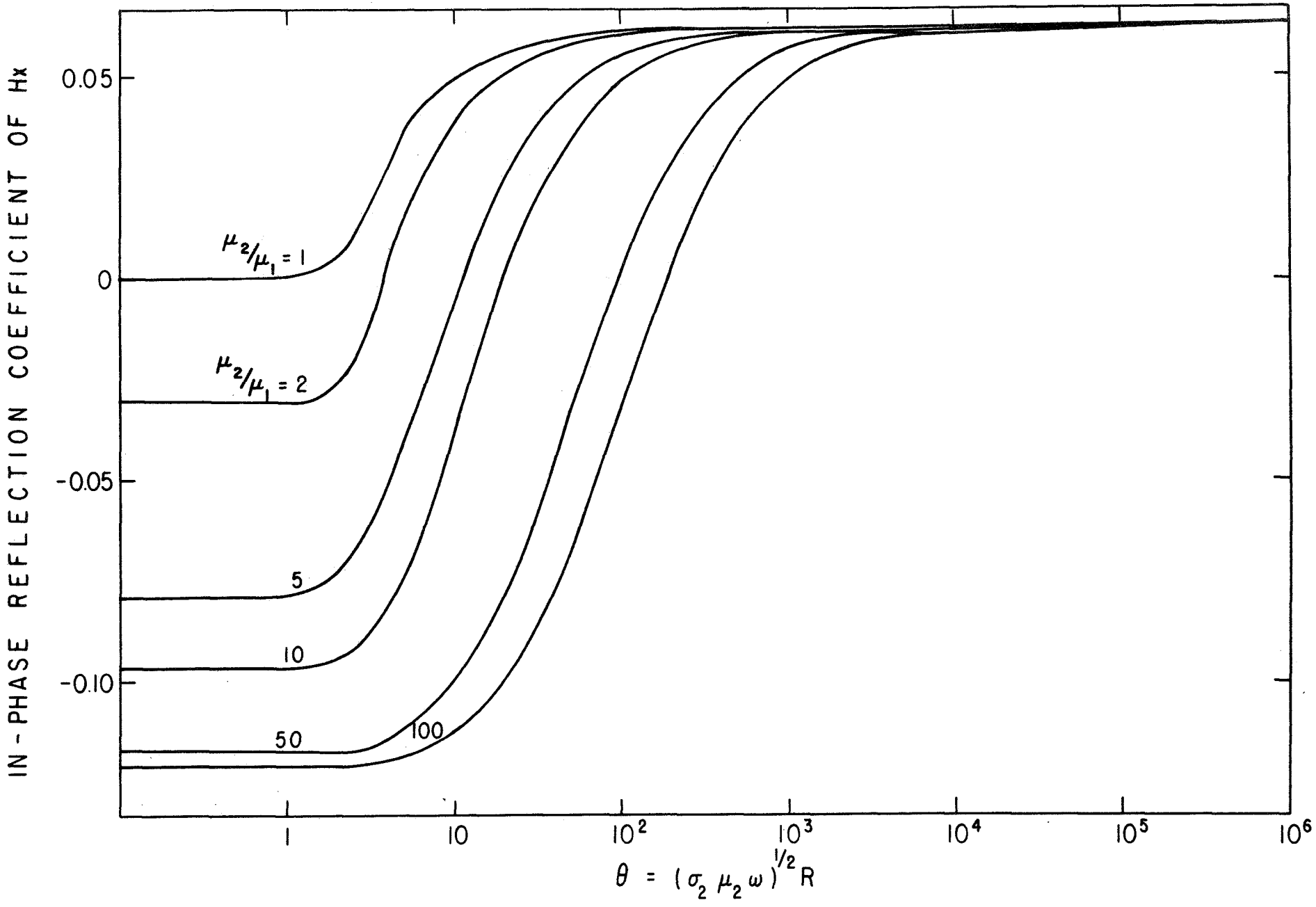

FIG. 29 IN-PHASE COMPONENT OF THE REFLECTION COEFFICIENT AT THE LUNAR SURFACE OVER A SPHERICAL MASCON

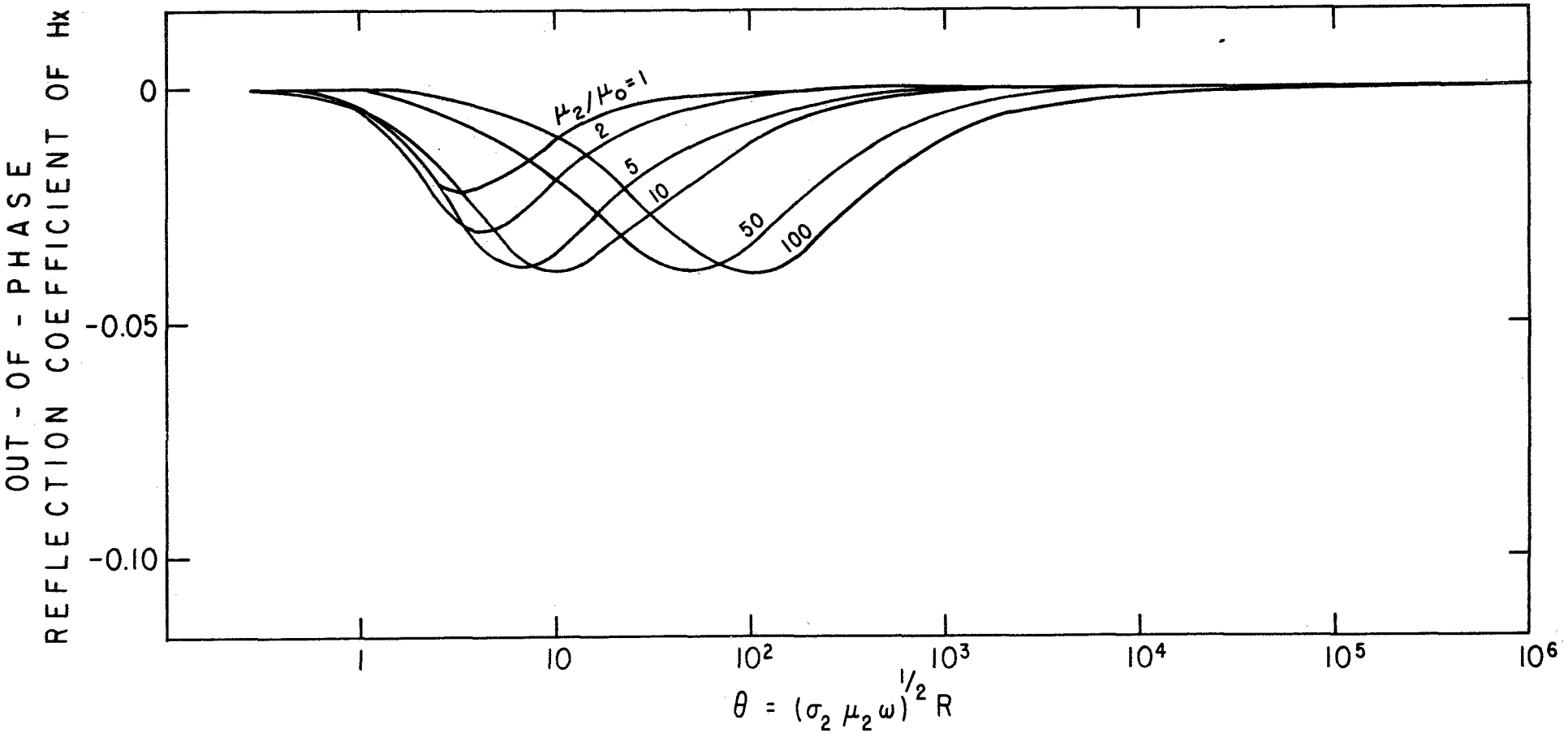

FIG. 30 OUT-OF-PHASE COMPONENT OF THE REFLECTION COEFFICIENT AT THE LUNAR SURFACE OVER A SPHERICAL MASCON